MACHINE LEARNING-BASED FRAMEWORK FOR REMEDIAL CONTROL ACTION PREDICTION USING WIDE-AREA MEASUREMENTS IN INTERCONNECTED POWER SYSTEMS

A Thesis Submitted to the
College of Graduate and Postdoctoral Studies
In Partial Fulfillment of the Requirements
For the Degree of Doctor of Philosophy
In the Department of Electrical and Computer Engineering
University of Saskatchewan
Saskatoon

By

Soheil Naderi

PERMISSION TO USE

In presenting this thesis/dissertation in partial fulfillment of the requirements for a Postgraduate degree from the University of Saskatchewan, I agree that the Libraries of this University may make it freely available for inspection. I further agree that permission for copying of this thesis/dissertation in any manner, in whole or in part, for scholarly purposes may be granted by the professor or professors who supervised my thesis/dissertation work or, in their absence, by the Head of the Department or the Dean of the College in which my thesis work was done. It is understood that any copying or publication or use of this thesis/dissertation or parts thereof for financial gain shall not be allowed without my written permission. It is also understood that due recognition shall be given to me and to the University of Saskatchewan in any scholarly use which may be made of any material in my thesis/dissertation.

Requests for permission to copy or to make other uses of materials in this thesis/dissertation in whole or part should be addressed to:

Head of the Department of Electrical and Computer Engineering
57 Campus Drive
University of Saskatchewan
Saskatoon, Saskatchewan (S7N 5A9)
Canada

OR

Dean
College of Graduate and Postdoctoral Studies
University of Saskatchewan
116 Thorvaldson Building, 110 Science Place
Saskatoon, Saskatchewan (S7N 5C9)
Canada

DISCLAIMER

The use and reference of MATLAB, IEEE systems, Power factory (Digsilent), and GAMS were exclusively created to meet the thesis and/or exhibition requirements for the degree of Doctor of Philosophy at the University of Saskatchewan. Reference in this dissertation to any specific commercial products, process, or service by trade name, trademark, manufacturer, or otherwise, does not constitute or imply its endorsement, recommendation, or favoring by the University of Saskatchewan. The views and opinions of the author expressed herein do not state or reflect those of the University of Saskatchewan and shall not be used for advertising or product endorsement purposes.

ABSTRACT

Growing demand for power systems, economic, and environmental issues, lead to power systems operating close to their stability margin. Power systems are always exposed to disturbances, leading to either instability or cascading outages and blackouts in the worst cases. Although numerous methods have been proposed since 1920 to prevent disturbances, instability and blackout still exist. Among all the instabilities, the fastest occurring one is rotor angle instability or transient instability. Since this instability happens in a fraction of a second, time must be considered in designing remedial control actions (RCAs). Different types of remedial control actions have been proposed in the past, but due to the lack of time consideration in their design, they are not practical for those cases quickly lead to transient instability. Additionally, pre-planned remedial control actions have been employed to overcome time limitations, but they are not able to cover most of the possible scenarios that may occur in the power system. Based on the literature done for this research, predicting remedial control actions has not been implemented yet. This study presents an innovative idea to predict remedial control action schemes that are able to include time limitations and cover possible scenarios properly. There are numerous challenges to consider in performing such a method, such as remedial control actions selection, implementation, practical aspects, and wide-area measurement systems (WAMS). In this study, the different parts of the framework are discussed in detail and implemented.

Based on the above discussion, first, an optimized artificial neural network (ANN) is implemented to make a comprehensive framework that can predict a proper remedial control action to prevent cascading outages and blackouts. The different steps of the framework are predicted using this comprehensive algorithm. A micro model strategy has been employed, which builds a model for each line separately. This micro model decreases prediction complexity and increases the prediction accuracies of the modules. The common RCAs, including controlled islanding, load shedding, and generator rejection, are implemented in this research project.

To address controlled islanding prediction, in the first step, using voltage data, the stability status was predicted. In the second step, a new method to identify coherent groups of generators was developed, and based on that method; the coherency patterns have been predicted. In the third step, a combination of islanding and load shedding is selected as a control action, and a mixed-

integer linear programming (MILP) method is designed to compute islands, the amount of load shedding, and load buses. Since the load shedding prediction has two aspects and it is a very challenging problem, a new concept called the specific set of loads (SSLs) had been proposed to simplify this issue. Finally, the islanding and load shedding patterns are predicted. The framework was tested via the IEEE 39 bus system and 74-bus Nordic power system, and the results show the effectiveness of the framework.

To implement generator rejection prediction, the bus voltage data are used to predict the stability status. Next, the critical generators are predicted. Then, using the equal area criterion, the amount of generator rejection for each critical generator is calculated, and the patterns are extracted. Finally, the number of generator rejections is predicted using the dataset and designed ANN. The performance of the generator rejection prediction framework is tested via the IEEE 9-bus system and 74-Bus Nordic power network.

ACKNOWLEDGEMENT

First and foremost, I am deeply grateful to God Almighty for giving me the knowledge, ability, and opportunity to undertake this research study and to complete it satisfactorily. Without his blessings, this achievement would not have been possible. Moreover, my deepest gratitude to everyone who helped me complete my PhD in any form, and even if your name is not in this acknowledgement due to length constraints you are definitely in my mind and soul.

I would like to express my sincere gratitude to my supervisors Prof. Tony C.Y. Chung for his support throughout my Ph.D. program. Also, I would like to thank the University of Saskatchewan and more specifically the Electrical and Computer Engineering Department for providing the opportunity and resources required to complete my PhD. Special thanks go to the members of my Advisory Committee for their insightful comments and suggestions.

Many thanks to my friends, especially Alireza Zangouie, Mojtaba Abdolahnezhad, Masoud Javadi, Mahdi Mazhari, Mansour Moradi for their help, motivation, and friendship during my PhD program.

On a personal level, I owe my deepest gratitude to my parents, Asa'd and Fatemeh, as words can never express the amount of support that they provided me throughout the years. Also, the gratitude is extended to my love, Zahra, for her continuous support in all aspects of my life. In addition, I thank all my siblings, Parsa, Mohammad, and Maryam each one of you helped me in a unique way and it is my honor to mention each one of you by name.

Finally, I would like to thank prof. Tony C.Y. Chung for financially supporting my PhD. The thanks are also extended to NSERC, SaskPower, and the University of Saskatchewan.

DEDICATION

This PhD is dedicated to my parents, Asa'd and Fatemeh, and my lovely wife, Zahra.

TABLE OF CONTENTS

TABLE OF TABLES

TABLE OF FIGURES

ABBREVIATIONS

RCA	Remedial Control Actions
$WAMS$	Wide Area Measurement Systems
ANN	Artificial Neural Network
$MILP$	Mixed Integer Linear Programming
SSL	Specific Set of Loads
PMU	Phasor Measurement Units
GPS	Global Positioning System
TEF	Transient Energy Function
UEP	Unstable Equilibrium Point
BCU	Binary Controlled Unstable Equilibrium Point
EAC	Equal Area Criterion
$SIME$	Single Machine Infinite Bus
DT	Decision Tree
SVM	Support Vector Machine
$LSTM$	Long-Short Term Memory
CNN	Convolutional Neural Network
$ASVM$	Aggressive Support Vector Machine
$CSVM$	Constructive Support Vector Machine
SPS	Special Protection Scheme
$HVDC$	High Voltage Direct Current
$OMIB$	One Machine Infinite Bus
NLP	Non-linear Programming
$IEEE$	Institute of Electrical and Electronics Engineers
$FSCEC$	First Swing Constraint Emergency Control
DAE	Differential Algebraic Equations
OSI	Outage Sensitivity Index
$ROCOF$	Rate of Change of Frequency
AC	Alternate Current

DC	Direct Current
PCA	Principle Component Analysis
QR	Quantile Regression
$OBDD$	Order Binary Decision Diagram
$SCIC$	Spectral Clustering Control Islanding
TVC	Threshold Value Constraint
MMS	Micro Model Set
$CBRDE$	Collaborative Binary-Real Differential Evolution
LM	Levenberg Marquardt
OPF	Optimal Power Flow
DPL	Digsilent Programming Language
$PFCs$	Post Fault Cycles
$EEAC$	Extended Equal Area Criterion
CM	Critical Machine
NM	Non-critical Machine
CGP	Critical Generator Pattern

NOMENCLATURE

Ω^{TL}	Set of transmission lines
Ω^{L}	Set of loads
Ω^{G}	Set of generators
Ω^{B}	Set of all buses
$\{\cdot\}^{pref}$	Pre-fault values
$\{\cdot\}^{postf}$	Post-fault values
N_{ij}^{U}	Number of unstable scenarios for line ij
N_{ij}^{S}	Number of generated scenarios for line ij
N_{ij}^{CP}	Number of coherency patterns for line ij
M_{ij}	Parameter representing the criticality value of line
LC_{ij}	Parameter representing the criticality label of line ij
S_{G-F}	Sensitivity of different generators to fault location
N^{G}	Number of generators
X_F	Integer number showing the fault occurrence in a transmission line
$S^{l}(t)$	Binary string for determining active and inactive neurons in the l^{th} ANN and t^{th} generation
$W^{l}(t)$	Weight connection including weight and bias in the l^{th} ANN and t^{th} generation
N^{P}	Population of the trained ANN
w_i	i^{th} weight of connection in the ANN
B_i	i^{th} bias of nodes in the ANN
X_P	Input vector of the ANN
H_P^{L}	Hidden layer output of the l^{th} ANN
O_P^{L}	Output layer of the l^{th} ANN
D^{L}	Diagonal matrix of S^{l} for the l^{th} ANN
G/B	Conductance/susceptance matrix
Y	Admittance matrix
M_i	Inertia constant of generator i

D_i	Damping factor of generator i
C_i	Center of coherent group i
α_i	Penalty factor for load shedding of the load at bus i
β_{ij}	Penalty factor for line ij
RC_i	Ramping cost for generator i
$A^{con-dis}$	Connectivity and dis-connectivity matrix
$\Delta\delta_k^{max}$	Maximum rotor angle difference for the k^{th} scenario.
δ_{Gi}	Rotor angle of generator i
V_{Gi}	Voltage magnitude of generator i
ω_i/ω_0	Speed of the i^{th} generator/ synchronous speed
V_i	Voltage magnitude of bus i
γ_k	Stability status of scenario k
U_{ij}	Binary variable showing the connectivity status of line ij
Pf_{ij} /Qf_{ij}	Active/reactive power flow from bus i to bus j
θ_{ij}	Voltage angle difference between buses i and j
Pe_i	Electrical power of generator i
Pm_i	Mechanical power of generator i
E_i	Terminal voltage of generator i
P_{Gi}^{nom}	Nominal active power of generator i
P_{Gi}/Q_{Gi}	Active/reactive power of generator i
P_{Li}	Active load demand at bus i
$\Delta P_{Gi}^{+/-}$	Generation increment/decrement of generator i after islanding
ΔP_i^{shed}	Load shed at bus i
M_i	Inertia coefficient of i^{th}generator
M_{CM}	Inertia coefficient of critical machines
M_{NM}	Inertia coefficient of non-critical machines
δ_{CM}/δ_{NM}	Equivalent rotor angle of critical/non-critical machine
A_{acc}	Acceleration area
A_{dcc}	Deceleration area

η_i	Stability margin of i^{th} scenario
δ_0	Rotor angle of SMIB at the fault moment
δ_{cl}	Rotor angle of SMIB at the moment of clearing the fault
δ_u	Rotor angle of SMIB at the instability moment
δ_{GR}	Rotor angle of SMIB at the moment of applying RCA
$\delta_{u'}$	Datapoints index
$A_{dec_{new}}$	Deceleration area after applying RCA
ΔP_m	Required amount of generator rejection to stabilize the scenario
β	Penalty factor related to the stability margin
MMS_{i_C}	The class of i^{th}micro model
N_i^{CGP}	Number of critical generator pattern of i^{th}micro model
$\Delta P_{G_i}^{trip}$	Amount of generator rejection of i^{th} generator

1 INTRODUCTION

1.1 General context

The power system is one of the greatest interconnected dynamic networks in the world, created by humans. The integrated dynamics, time-varying elements, and nonlinearity nature of power systems make their operation and control processes complex and challenging. Ensuring secure and stable operation of the network is one of the significant challenges that power engineers encounter [1]. Due to the growing demand, economic reasons, environmental issues, and grid integration of new technologies, including renewable energies, power systems are being operated close to the stability margins [2]. Therefore, modern power systems are more prone to lose their stability following a disturbance.

Power systems have always been subjected to small disturbances such as load variation and large disturbances such as generator loss or transmission line loss. These faults and disturbances can affect power system stability. Power system stability describes the ability of a power network to maintain a stable status during normal conditions and to return to a new stable operating point following a disturbance [3]. There are different types of instability and disturbance characteristic, one or a combination of the instability issues can emerge when the system encounters a disturbance. Power system stability is considered as a single problem; however, because of the high dimensionality and complexity of stability problems, it is necessary to make simplifying assumptions to analyze specific types of problems using an appropriate degree of detail for system representation and appropriate analytical techniques. Analysis of stability, including identifying key factors that contribute to instability and implementing methods for improving stable operation, is greatly facilitated by the classification of stability into appropriate categories [4]. According to the Institute of Electrical and Electronics Engineers (IEEE) and International Council on Large Electric Systems (CIGRE) report, power system stability issues can be classified in the following diagram. In the following paragraphs, different types of stability are explained in detail.

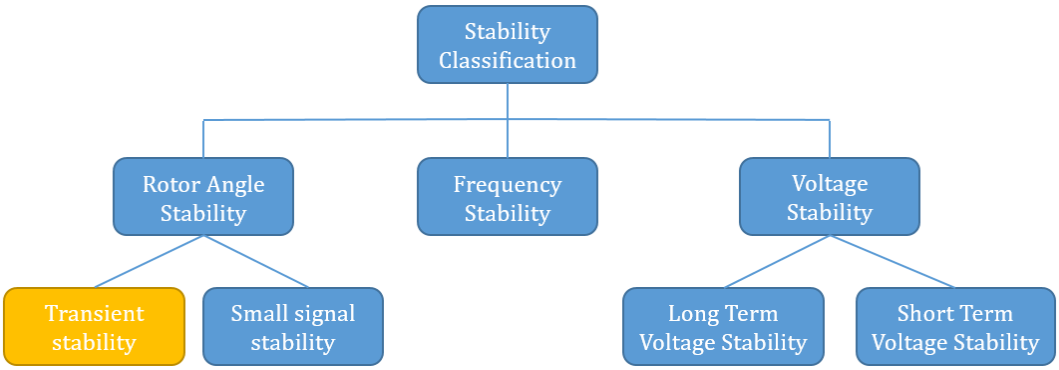

Figure 1-1. Classification of power system stability [3].

Rotor angle stability refers to the ability of synchronous generators of a power system to keep their synchronism after encountering a disturbance. This type of stability depends on the ability of synchronous generators to maintain equilibrium between electromagnetic and mechanical torque. Loss of synchronism can occur, whether between one machine and the rest of the network or between a group of generators [5]. According to the severity of faults, the rotor angle stability is categorized into two subcategories, including 1) Small signal rotor angle stability, which is studying the ability of the power network to maintain synchronism under small disturbance. Since the disturbance is sufficiently small, the linearization of power system equations is allowed to analysis of this type of stability. 2) Large-disturbance rotor angle stability or transient stability evaluates the power network's ability to maintain synchronism when subjected to a severe disturbance. The system response involves large excursions of generator rotor angles and is influenced by the nonlinear power-angle relationship [5].

Voltage stability refers to the power system's ability to maintain buses' voltage in the acceptable range. When an increase in reactive power injection at any system bus leads to a voltage drop at the same bus, the system considered to be voltage unstable. If the voltage for significant parts of the power system is unacceptably low, the voltage will collapse [3].

Frequency stability refers to the ability of a power system to maintain a steady frequency following a severe system upset resulting in a significant imbalance between generation and load. It depends on the ability to maintain/restore equilibrium between system generation and load, with minimal unintentional loss of load. Maintaining real-time balance between generation and load is

of paramount importance, because frequency instability leading to devastating consequences, such as unintentional load shedding and machine damage [3].

The above-mentioned types of instability or combinations of those can affect power systems, leading to cascading failure or blackouts in severe cases. In the 20th century, in many cases, transient instability due to large disturbances led to large blackouts, which have had large social and economic impacts. The below table shows significant large blackouts during the 21st century. In addition, the details of each blackout are represented [6]–[10].

Table 1-1. Large blackouts and their impacts in 21st century

Location	**Year**	**Time (h)**	**Loss of Load(GW)**	**Population affected(million)**
USA-Canada	2003	2 - 48	61.8	55
Italy	2003	12	26	56
Indonesia	2005	7	-	100
Brazil-Paraguay	2009	6	24	60
India	2012	15	48	620
Turkey	2015	8	25	70
South Australia	2016	3-24	2.9	-
Texas (USA)	2021	72-336	34	29

As shown in table 1-1, numerous blackouts are still occurring in different areas, albeit many methods and techniques are proposed to prevent these catastrophic results. It is worth mentioning that these blackouts result in huge power interruptions and losses of billions of dollars to both utilities and consumers. Moreover, they lead to negative social impacts such as an increased crime rate, which cannot be quantified in dollars [11]. Therefore, preventing blackouts is still one of the important challenges in modern power systems, which needs to be addressed [12]. In this regard, the factors that lead to blackouts should be studied. In addition, the proper control and protection schemes should be designed to deal with this issue and save power systems from these negative results.

There are different reasons for occurring blackouts. One quickest phenomenon leading to blackouts is rotor angle instability (transient instability). Transient instability occurs when a power

system is exposed to a large disturbance, and it happens in less than 1 second [13]. The time limitation and non-linear dynamics of power systems make transient stability analysis more challenging. Therefore, determining transient instability and designing fast and accurate control actions or protection schemes is of paramount importance.

The last control actions or protection schemes that can save the power system before cascading failure or blackout are called remedial control actions (RCAs) or emergency control actions. RCAs take a set of corrective actions, including generator rejection, fast valving, controlled islanding, load shedding, etc. [2] to maintain stability and system integrity. Designing an optimal and quick RCAs calculation is challenging and needs to be studied.

1.2 Wide Area measurement systems (WAMS)

In the past, unavailable and insufficient real-time data to monitor the state of the power system was a big challenge. In addition, the integration and complexity of power systems make events grow into wide-area phenomena, which local measurements cannot monitor. However, thanks to the phasor measurement units (PMUs) and wide-area measurement systems (WAMS), this issue has been largely facilitated in modern power systems. The WAMS system can collect time-labeled data to monitor the power system online and provide information to prevent instability and blackouts [14]–[16].

PMUs are collecting data from different parts of power systems. These devices measure the electrical waves on the power grid using a common time source for synchronization. This process makes it possible for the real-time measurement from various power grid points to be synchronized. PMUs were first developed at Virginia Polytechnic Institute and State University (Virginia Tech) in 1988 and use signals from the Global Positioning System (GPS) to achieve a synchronization accuracy of 1 μs [17]. The format of the data files created and transmitted by commercially available PMUs is presently governed by the Institute of Electrical and Electronics Engineers (IEEE) standard and PMU, which is an open-source platform that encourages research into further synchrophasor algorithm development [18].

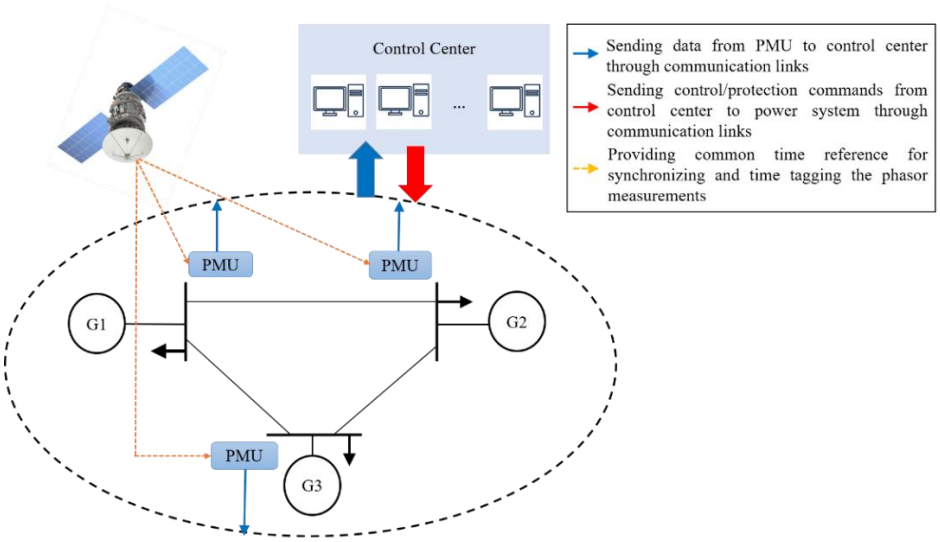

Figure 1-2. Schematic to show the WAMS application in power system

The data, which is the fundamental requirement to perform the WAMS function, can be collected from different parts of the power system using PMUs [19]. Moreover, the process of WAMS is represented in the above figure. The collected data, along with their time tags, are gathered from PMUs, and those data will be synchronized using GPS. To send the raw data to the control center, the communication links are accessible. The control center will do data processing. Based on the WAMS application, the decisions will be made to operate the power network safely and securely. The necessary control signal and protection signal will be applied to the power system through communication links.

The sum of the times demanded to render PMU data toward the system or regional control center and the time needed for transferring commands to control devices is referred to as the communication delay or latency. This time delay depends on the communication system loading, which is a feedback control loop, diminishes the effectiveness of the control system and may even result in complete system instability [20]. Accordingly, it is of critical importance to consider the latency during the controller design process. The approximate latency for different types of technologies is represented in table 1-2.

Table 1-2. Latency communication in different types of communication link [21].

Communication Link	Associated delay(ms)
Fiber-optic Link	100-150
Digital microwave link	100- 150
Power line carrier	150- 350
Telephone lines	200- 350
Satellite link	500- 700

One of the most important challenges to centralized control and protection of power systems is the communication delays. Regarding the above table, sending data from the PMUs to the control center and from the control center to the actuator takes at least 300ms. Considering PMU's state estimation and phasor calculation, the approximated time delay in the WAMS process will be around 400 ms, which necessarily should be considered when designing and applying control actions in power systems. If the delays are not considered while designing wide-area applications in power network, the protection/control actions might lead to adverse results.

1.3 Problem Statement and research gap

As discussed earlier, transient instability occurs quickly and causes cascading outages and blackouts in severe conditions. Since 1920 different protections and control schemes have been implemented to decrease the effects of this kind of instability so that interconnected power systems can be operated in secure and safe conditions. However, blackouts and cascading outages still occur. As it is mentioned, one of the main reasons of blackouts is related to those scenarios that quickly evolving into transient instability [22]–[24].

There are some cases that lead to transient instability in less than 500 ms [24]. In addition, The communication delays, including latencies for sending the data from the PMUs to the control center and delays for sending the control commands to the relays and switches, are assumed to be around 18-24 cycles or equivalently 300-400 ms for 60 Hz frequency. If the communication delays are subtracted from the (fault clearance time ~ instability moment) time interval, the available time for performing a control or protection scheme will be extremely limited. Therefore, it is clear that any control or protection scheme should be determined within a reasonable amount of time

necessarily lower than the available time to ensure the triggered control can effectively prevent transient instability in the system.

The common control schemes to prevent transient instability and blackouts are remedial control actions (RCA). Three RCAs, including controlled islanding, load shedding, and generator tripping, are the most common and challenging strategies that have drawn the attention of engineers and researchers for decades. These RCAs are inherently costly processes, and they impose a cost on the power systems. However, these processes are able to protect the network from blackouts when they are designed and implemented accurately. Developing a proper RCA is a time-consuming optimization process. However, the available time to calculate and perform RCAs is limited. Therefore, previous RCAs performing calculations and optimization and they are not practical for those cases quickly evolving into transient instability. Additionally, existing RCAs based on estimation and approximations are fast but those are not accurate and optimal RCA.

The RCA prediction, which is fast and accurate, is proposed to address the aforementioned drawbacks of the previous methods. It has the potential to save power networks even in those cases quickly, leading to transient instability.

1.4 Research Objectives

The main objective of this research is to predict fast and optimal remedial control actions to prevent transient instability in power systems. The aim of this Ph.D. study can be apportioned to

- Conduct a literature review on transient stability assessment
- Conduct a comprehensive literature review on remedial control action schemes
- Propose a micro model strategy to cover credible scenarios, reduce prediction complexity and increase accuracy
- Propose a method to enhance and improve the accuracy of the coherent generators prediction problem
- Develop a highly accurate framework to predict islanding and load shedding in real-time

- Design a framework to predict optimal generator rejection to prevent transient instability

1.5 Thesis contributions

To achieve the aforementioned objectives, a summary of contributions is presented in this section. The details of contributions are further elaborated in the thesis chapters.

1) A micro model-based strategy is proposed to independently consider credible scenarios for each transmission line. Instead of generating a bulk dataset for the whole system, which results in a large number of possible output scenarios, reasonable portions of the offline dataset are used to develop prediction models for each single facility using the micro model strategy. The proposed approach reduces the prediction complexities and increases the prediction accuracy.
2) A time-varying algorithm is developed to identify the coherency patterns based on the instability moment. The proposed method aims to minimize the number of generator groups for each unstable scenario, leading to fewer RCAs, less load shedding, and higher prediction accuracy compared to existing works.
3) A novel real-time islanding and load shedding prediction framework is proposed to prevent transient instability following the occurrence of fault events. As a trade-off between event-based and response-based methods and considering the time limitation, the proposed framework can efficiently respond to unforeseen scenarios and protect the network against events evolving into fast transient instability. In the case of post-fault instability prediction, the proposed framework predicts and triggers proper RCAs before the loss of synchronism by doing fast predictions rather than time-consuming calculations.
4) A new online generator rejection prediction framework is proposed to prevent transient instability following a disturbance. The proposed method can trigger proper RCAs before the loss of synchronism by performing very fast predictions rather than time-consuming calculations.
5) For training the machine learning models in the offline stage of the proposed framework, a heuristic optimization model considering the full dynamic model of the power network is proposed to assign the optimal amount of generator rejection to critical generators and maximize the stability margin with high accuracy.

1.6 Thesis organizations

The thesis is organized into six chapters as follows.

- Chapter 1 is introduced the transient instability as one of the main factors of blackouts, the importance and application of PMUs and WAMS are discussed in study of blackouts. The issues and challenges of preventing blackouts and transient instability using RCAs is briefly discussed. Also, the main contributions of this study are explained.
- Chapter 2 discusses literature review of transient stability assessment. In addition a comprehensive literature review of different remedial control actions and their advantage and disadvantages are expressed.
- Chapter 3 introduces the micro model strategy in detail. It also presents the scenario generation process and employed classifier.
- Chapter 4 introduces the first framework to predict islanding and load shedding. It discusses offline and online stages of different framework modules, including 1) stability prediction module 2) coherency prediction modules 3) RCA prediction modules in detail. Also, the proposed framework results are illustrated for two test systems consisting of IEEE 39-bus system and 74-bus Nordic power system.
- Chapter 5 shows the second presented framework to predict generator rejection. It discusses offline and online parts of different modules for this framework including 1) stability prediction module 2) critical generator prediction module 3) RCA prediction module in details. The results for two test systems including IEEE 9-bus system and 74-bus Nordic power system are shown.
- Chapter 6 summarizes the thesis, expresses its conclusions, and provide the research area for future work.
- Appendix I, includes the detail information for different used test systems
- Appendix II, includes the list of publications and permission letters from co-authors

2 TRANSIENT STABILITY ASSESSMENT AND REMEDIAL CONTROL ACTIONS: LITERATURE REVIEW

2.1 Introduction

This chapter reviews the existing methods for transient stability assessment with their pros and cons. It provides a brief background related to the power system operating condition and different power system states. In addition, existing remedial control actions (RCAs) for preventing transient instability are explained in detail. Also, the advantages and disadvantages of previous RCAs are discussed. Since the main focus of this research is islanding, load shedding, and generator tripping, a comprehensive review is performed on these RCAs.

2.2 Transient stability assessment

Generally, stability is defined as one of the properties of a power system that enables it to operate in an equilibrium point under normal conditions and regain a new equilibrium operating point after an incident in which the power network encounters a disturbance. As it is mentioned, modern power systems are operating with tighter security and stability margins according to economic and environmental issues. Among different types of stability, transient stability or rotor angle stability is the quickest type that occurs when a power system is exposed to a large disturbance and happens in less than one second [22], [23], [25].In addition, some scenarios lead to transient instability in less than 500 ms. In [24], bulk scenarios are generated for different test systems, and the results show some cases are losing their synchronism in less than 500 ms (Figure2-1). Thus, fast instability detection is critical, and it allows more time to perform proper remedial control actions. Furthermore, fast detection of instability prevents unintentional islanding, cascading failure, and blackouts. Numerous methods have been proposed to assess and predict the transient stability status of power systems. Generally, there are three basic categories for transient stability analysis.

1) Time-domain simulation
2) Direct methods or Energy function methods
3) Machine learning-based prediction method

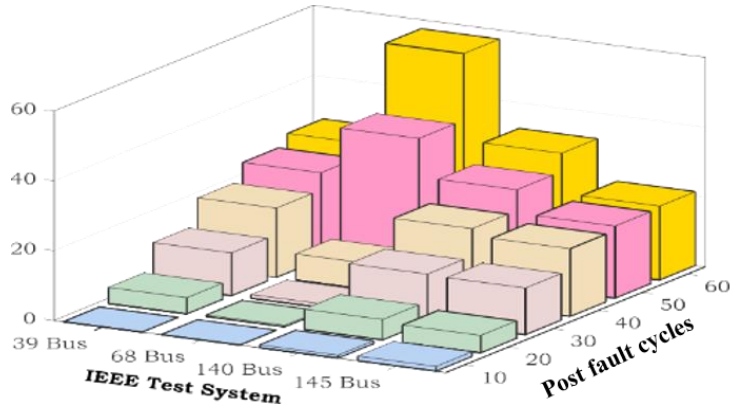

Figure 2-1. Percentage of unstable cases that lose synchronism in different post-fault cycles for various standard power networks [24].

2.2.1 Time-domain simulation

This method is known as one of the most reliable techniques for assessing power system stability [25]. In this method high-order differential-algebraic equations are used to represent power system dynamic models and are solved at each instant of time. In these methods, power system stability is assessed by monitoring the evolution of generator rotor angles and other system variables with respect to time in the post-fault period. For a stable system, machine rotor angles stabilize to a new equilibrium state. However, the machine rotor angles diverge in an unstable system [26]. Existing mainstream commercial power system simulation software capable of carrying out reliable simulations include Power world, PSCAD, AU-Power Lab, ETAP, Power-Factory, and PSS/E. This approach requires accurate information about the network configuration, while a heavy computational burden confines its application for online purposes [27].

2.2.2 Direct methods or energy function methods

TEF (Transient Energy Function) method is another stability analysis approach. These methods use kinetic and potential energies constructed by Lyapunov theory to evaluate transient stability status at the end of the disturbance without explicit integration of differential equations [27]. There are three basic direct methods: (a) lowest energy unstable equilibrium point [28], (b) potential energy boundary surface method [29], and (c) controlling u.e.p. method [30].TEF methods are not time-consuming and perform well at computation speeds compared to time-domain approaches. Despite the promising technique for computing stability margin, direct

methods suffer from two main limitations [26]: (1) it is difficult to find an appropriate Lyapunov function for a detailed multi-machine power system, and (2) defining practical stability domain is difficult. Due to these limitations, many researchers consider direct methods to be impractical. Nonetheless, recent developments of the BCU (Boundary controlling unstable equilibrium point) method can efficiently compute the controlling u.e.p. and now it may emerge as a practical tool for solving large-scale transient stability assessment problems [31], [32].

A hybrid method also combines the strength of both time-domain and direct methods to evaluate transient stability. Time-domain characteristics helps the hybrid method to consider any stability scenario on power system. In this method, the actual system trajectory is computed using time-domain simulation then the stability index, which is transient energy margin, is estimated. There are two main types of hybrid methods. The first type considers a Lyapunov function constructed for the multi-machine power systems and is computed along the multi-machine trajectory using step-by-step time-domain simulation results [33]. In this method, it is difficult to find an appropriate stability limit. In the second type, the one-machine equivalent is constructed from the multi-machine system, and the stability margin is calculated using the equal-area criterion (EAC) [26]. The SIME (Single Machine Equivalent) method belongs to the latter family. The use of EAC greatly simplifies the task of determining stability limits for the one-machine equivalent method.

2.2.3 Machine learning-based methods

There are numerous types of machine learning algorithms such as Decision Tree (DT), Artificial Neural Networks (ANN), Support Vector Machine (SVM), and ensemble learning that have been applied to analyze and predict the transient stability status of power systems. Due to the rapid progress in machine learning and artificial intelligence, these methods are widely used in power systems. Additionally, using WAMS in power systems created possibilities to explore stability prediction tools that support close to real-time decision-making [34].

Contrary to the above-mentioned time-domain and energy function methods, data-driven methods are model-free and evaluate transient stability as a pattern classification problem. Transient stability prediction is a binary classification (0 means stable and 1 means unstable). The main aspects of a pattern classification problem include data pre-processing, feature selection, offline training, and online rule extraction [35]. The machine learning engine learns the mapping relationship between targets (i.e., stability status) and input data used in the training stage. Then

the performance of the trained model will be evaluated using test data. Finally, the stability status of the new inputs can be predicted using the trained model. Generally, the data-driven methods are categorized into four main classes: artificial neural network (ANN), support vector machine (SVM), ensemble learning, and deep learning. In the following paragraphs, the advantage and disadvantages of these models are summarized.

2.2.3.1 Artificial Neural Network (ANN)

ANNs can be used for function approximation and classification problems. The transient stability assessment is one of the relevant early applications of ANNs [36], [37]. The ANN was employed for transient stability prediction for the first time in [36]. In [37], an ANN was trained to calculate the critical clearing time for different loading conditions in a small power system. Furthermore, in [38], online applications of ANN such as online dynamic security assessment has implemented. The long short-term memory (LSTM) network has been used to develop a temporal self-adaptive transient stability assessment [39]. In addition, convolutional neural network (CNN) and recurrent graph convolutional network have been employed for transient stability assessment in [40], [41], respectively.

Those ANN implementations used off-line generated transient stability data for purposes such as input feature selection, training of an ANN, and performance evaluation tests. It is worth mentioning that the main drawback of an ANN is the slow rate of convergence during the training [38]. The structure of a neural network is illustrated in the following figure.

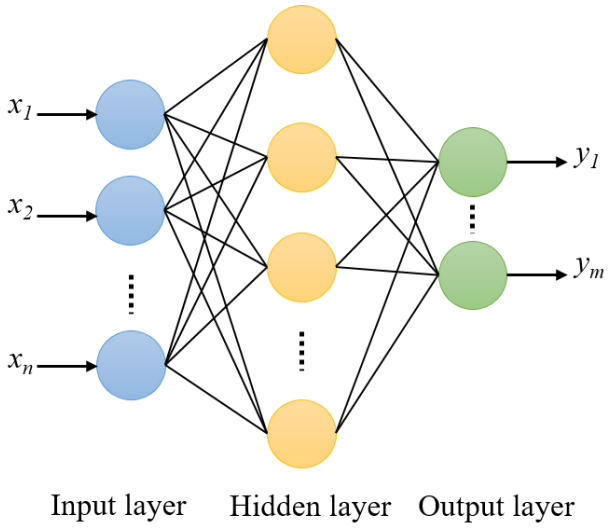

Figure 2-2. Schematic of an artificial neural network with n inputs, one hidden layer, and m outputs

2.2.3.2 Support Vector Machine (SVM)

This method was proposed in 1995 as a new classification method [42]. An SVM model is a representation of the examples as points in space, mapped so that the examples of the separate categories are divided by a clear gap that is as wide as possible. The goal of an SVM classifier is to maximize this gap. New examples are then mapped into that same space and predicted to belong to a category based on the region where they fall [43]. In [44], two improved SVM, including aggressive support vector machine (ASVM) and constructive support vector machine (CSVM), are trained using big data to predict transient stability. In addition, the parameters of multi-layer SVM are optimized using a genetic algorithm for transient stability assessment in the power system [45]. Some applications of SVM for transient stability assessment are reported in [43] and have been proven to provide high accuracy and shorter training time than conventional ANNs and other machine learning-based methods. In addition, SVMs have better generalization ability compared with traditional ANNs [35]. According to these studies, an SVM requires large input data to achieve high accuracy. The SVM structure and its function are shown in figure 2-3.

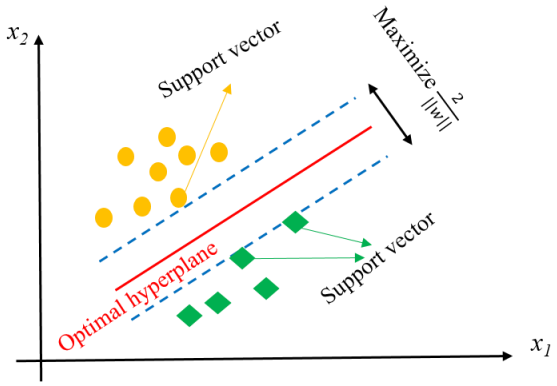

Figure 2-3. Schematic to show the structure of support vector machine classifier

2.2.3.3 Ensemble learning

The main idea behind these methods is to combine multiple learners into a model with more generalization by using different strategies [35]. This method is one of the most efficient and popular methods in classification applications. The implementation of these techniques is easy and fast. Ensemble DTs are commonly used in operation research, particularly in decision analysis, but they are also popular tools in machine learning [46]. After splitting the data in a sequential manner, a DT uses a linear mapping function. The building of decision rules involves determining a threshold margin that accomplishes certain criteria [47]. The random forest, as one of the well-

known ensemble learning methods, has been used in [48] to predict transient stability in power systems. In [49,] a de-noising stacked auto-encoder and voting ensemble classifier is developed to analyze transient stability. An adaptive ensemble learning model based on a decision tree is utilized for dynamic security assessment [50]. Ensemble learning has the potential to solve accuracy fluctuation problems in a single prediction model and enhance the reliability of the prediction model [35]. The figure below shows the structure of random forest, which is an ensemble decision tree.

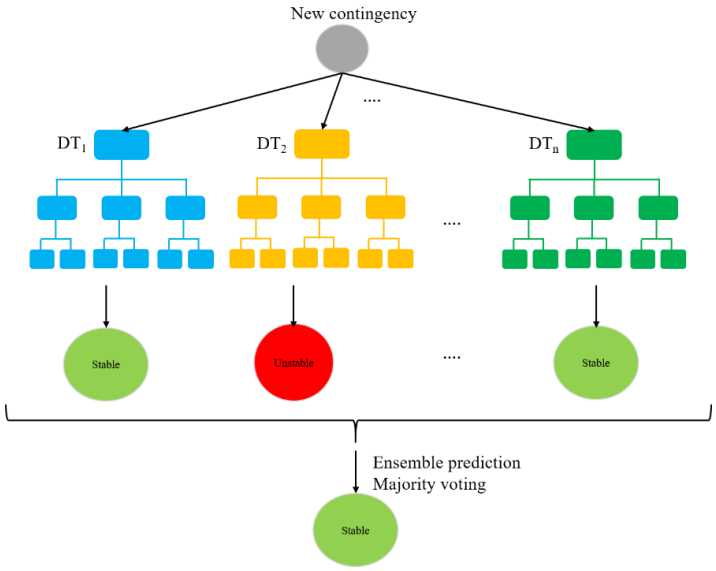

Figure 2-4. The structure of ensemble decision tree to predict the stability status of power system in unforeseen situation

2.2.3.4 Deep learning

In recent years, deep learning methods have been widely used to assess power systems' transient stability [35]. Reference [51] is presented a deep learning prediction model to predict small-signal and transient stability. It employed a deep CNN-based classifier to assess the transient stability status of the power system. Moreover, a deep learning model that uses a stacked auto-encoder is utilized to extract features in [52]. This method is able to increase the prediction accuracy and reduce the computational burden of training. The proposed model that uses deep learning has a great potential to predict transient stability [53]. The structure of a sample deep neural network with three hidden layers, *n* inputs, and *m* outputs is illustrated in the following figure.

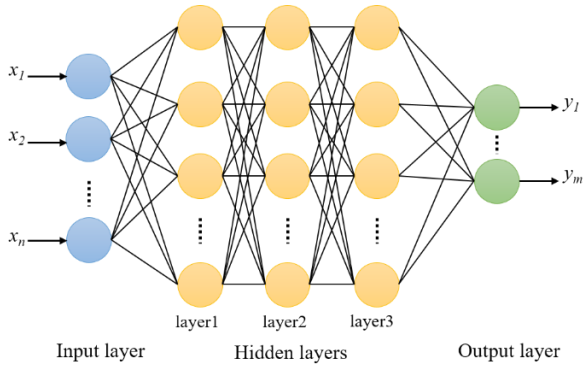

Figure 2-5. The structure of deep neural network with three hidden layers

Above mentioned data-driven approaches have the same process. Implementing a data-driven method to predict transient stability has two stages, including 1) offline training and 2) online prediction. The offline training consists of the scenario generation process, extracting features, training the learning model to find the relationship between inputs and outputs, and testing the trained network. In the online stage, the real-time data are collected from the PMUs, and using the required data and trained network, the stability status of the power network is predicted. The following diagram generally shows the overall process of a data-driven approach [35].

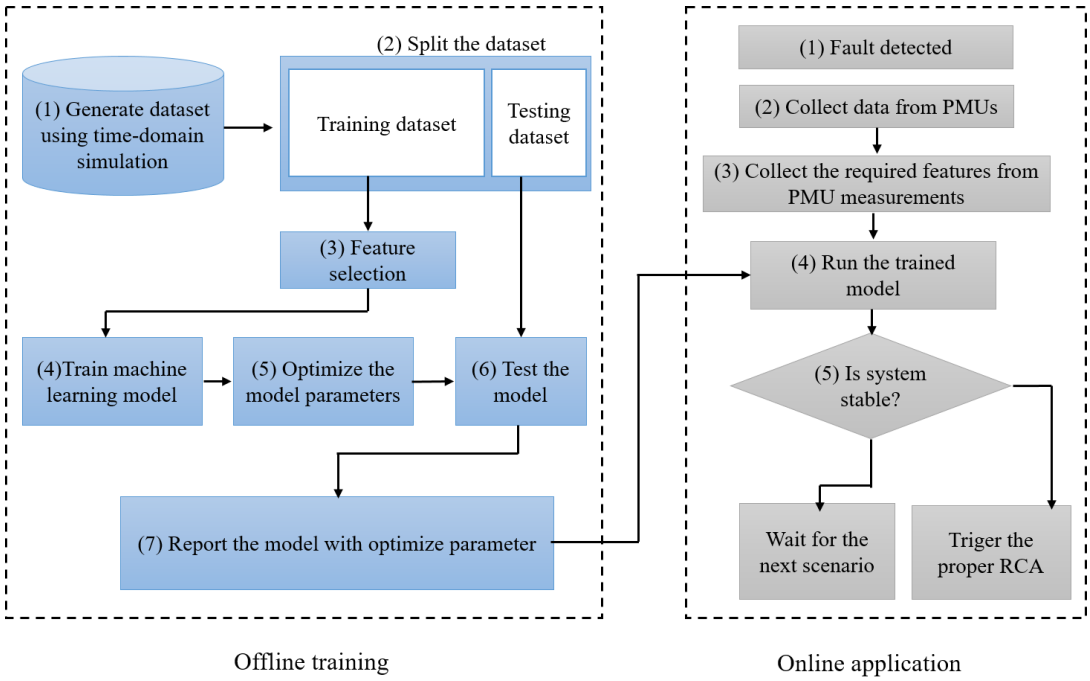

Figure 2-6. Schematic to show the general procedure of a data-driven method for transient stability prediction

2.3 Power system operating states

Power networks are dynamic systems, and their operating states are varied over time. In each operating state, the proper control decision needs to be performed to keep the power system in a secure, reliable, and high stability margin operating condition. Therefore, having an all-inclusive picture of the power system state is of paramount importance [54]. In this regard, different operational states of power system are introduced and explained in the following paragraphs. Figure 2-7 briefly shows these states and the proper control decision in each state.

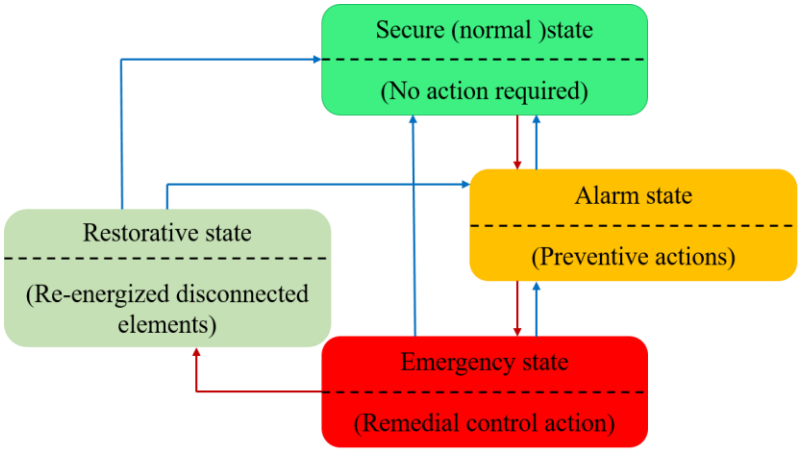

Figure 2-7. Power system operating states and proper action in each state

In normal operating conditions, the system has enough stability margin. In this state, the power system remains intact even after a disturbance. However, growing demand and limitations on building new power plants/ transmission lines due to economic and environmental issues make power system more fragile and remarkably reduce the stability margins. In addition, lots of disturbances stemming from natural, technical, or human agents can put power systems at more risk. If the power system loses the pre-determined stability margin following a disturbance, it will go to the alarm state. If a disturbance occurs in this state, it will lead to the violation of some constraints (i.e. voltage, frequency, etc. may not stay in their acceptable range). Therefore, the operators should take the proper preventive actions such as load shedding [55] and generation rescheduling [56] to increase the stability margin and bring the system back to the secure state. If a severe disturbance occurs before applying preventive actions and while system is in the alarm state, the system will fall into the emergency state. In this state, the equality (i.e., load flow) and inequality constraints (i.e., the system variable should be in the acceptable range) are violated.

Therefore, operators should take fast remedial control actions (RCAs) such as controlled islanding [57], generator shedding [58], or load shedding [59] before losing stability. RCAs are the last resort to save power system stability and prevent a blackout. If the RCAs are not taken in time or fail, the system experiences a cascading failure, partial blackout, or even large blackout due to disturbance severity. After the blackout, the system enters the restorative state. In this state, the different parts of systems that lost their connection to the network, including generators, load, and transmission lines, are re-energized step by step. The system goes to the secure or alarm state depending on the current situation [54]. The main goal of this thesis is to identify the emergency state quickly and design a fast and accurate RCA to prevent transient instability and blackouts.

2.4 Remedial control action schemes (RCAs)

Remedial control action schemes (RCAs) or Special Protection Schemes (SPSs) are actions taken to ensure power system stability and reliability after an instability has been recognized following a large disturbance. RCAs are designed to take a set of corrective actions when abnormal conditions are detected to preserve stability and system integrity [2]. According to this definition, devices and controllers, which act continuously, such as HVDC, and power system stabilizers (PSS), are not remedial control actions. These actions are applied when the system recognizes an abnormal condition in an emergency state. Different types of classifications have been proposed for RCAs based on the RCA characteristics. RCA classification is represented in the following figure.

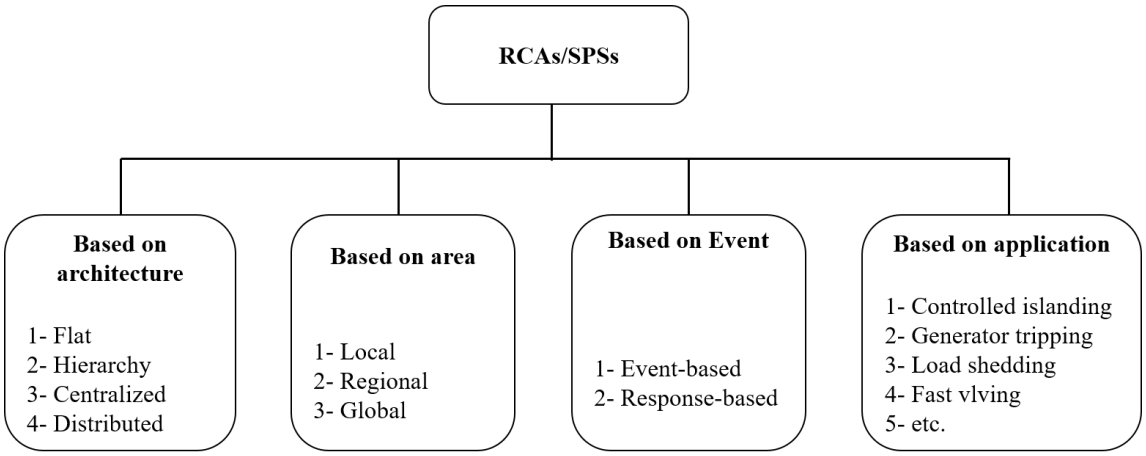

Figure 2-8. RCAs classification based on different criteria [60].

Generally, RCAs are categorized into two main classes: event-based and response-based schemes. Event-based schemes find appropriate RCAs for specific scenarios in offline simulations [61]. The major drawback of event-based methods is that they might be unable to respond to unforeseen events as only a finite number of contingencies are considered [62]. On the other hand, response-based schemes are developed based on phasor measurement unit (PMU) data and compute appropriate RCAs when an unstable situation occurs. Response-based methods are relatively slow and need more time to observe the system's response to a disturbance and determine the proper RCA. Recently, some approaches have combined the event-based and response-based methods to increase the effectiveness under different operating conditions. In [61], an adaptive RCA for different operating points and fault locations is performed. Some researchers have also used a voting system for secure operation. It means that to detect abnormal conditions, multiple criteria are considered, and each one votes to initiate the corresponding RCA.

So far, different types of classification for RCAs have been discussed. Since the focus of this thesis is preventing transient instability, it is important to have knowledge of various types of RCAs, their application, and the implementation strategies in this area of research. The main RCAs for preventing transient instability include 1) fast valving and dynamic braking resistor, 2) generator rejection, 3) controlled islanding, 4) load shedding, and 5) a combination of these methods. A comprehensive literature review has been done in the following sub-sections on this subject.

2.4.1 Fast valving and dynamic breaking resistor

The steam turbine's fast valving is the quick reduction of mechanical power to minimize the acceleration energy of generator which stems from a disturbance near the generator [61]. This method has been known since 1920 and is well-established with its initial implementation in 1927. In [63], the performance of early valve actuation control to enhance the transient stability by reducing the acceleration area and increasing the deceleration area in the $P - \delta$ curve is presented. A complementary technique is a dynamic brake, a resistor that can dissipate high power for a short time. This equipment is able to absorb the excess energy gained by generators during the transient time. The transient stability improvement with the coordinated operation of fast valving and braking resistor has been proposed in [64]. Although the generator tripping can save the power network itself, an excessive amount of generator shedding leads to load shedding and can put the

power system at more risk. Therefore, a combination of fast valving and braking resistor is developed to reduce the amount of generator tripping and prevent transient instability [65]. According to the limitation of braking resistors, such as excessive heat loss temperature rise of resistor along with related problem to fast valving including increased boiler pressure, a coordinated fast valving and braking resistor is proposed in [66] to reduce the mismatch between mechanical and electrical power efficiently. Although fast valving is one of the least expensive RCAs for transient stability improvement, it can cause thermal stress and various mechanical issues. In addition, using a braking resistor near thermal power plants causes stress and negative effects on the turbine shaft [61], [66].

2.4.2 Generator tripping/rejection

Generator rejection is one of the most commonly used RCAs to prevent transient instability [67], [68]. This scheme initiates the outage of accelerated generating units while saving the rest of the generators from the loss of synchronism [69]. Three important factors need to be considered while designing a generator rejection framework, including 1) determining the accurate amount of generator rejection to stabilize the network, 2) identifying the critical generators, and 3) assigning the optimal amount of generator rejection to each critical generator. Several research studies have been conducted for online generator tripping to improve transient stability and prevent blackouts while the power network is encountering a large disturbance. Generally, the previous studies can be categorized into two groups, including energy function-based and optimization-based methods.

The energy function-based methods reduce the complexity of the power network enabling the protection scheme to calculate the amount of generator rejection quickly. These methods are reduced the power system to one machine infinite bus (OMIB) and calculate the amount of generator tripping using the equal-area criterion (EAC). In these methods, first, the system converts into two machines system, which separates critical and non-critical generators. Next, using the equivalent model proposed in [26], two machines system convert to OMIB. According to the equivalent model and energy concept, the stability status and amount of required generator rejection can be calculated using the EAC. The following figure shows the process of generator rejection calculation using EAC. As can be seen in the figure, the A_{acc} is the amount of kinetic energy system gained during the fault. If the $A_{dec}^{(1)}$, which is the amount of energy that system can

dissipate, is less than A_{acc}, the system is unstable, and generator rejection is needed. The $A_{dec}^{(2)}$ is added by generator tripping and prevents transient instability. Several generator rejection schemes in this category are discussed in the following paragraphs.

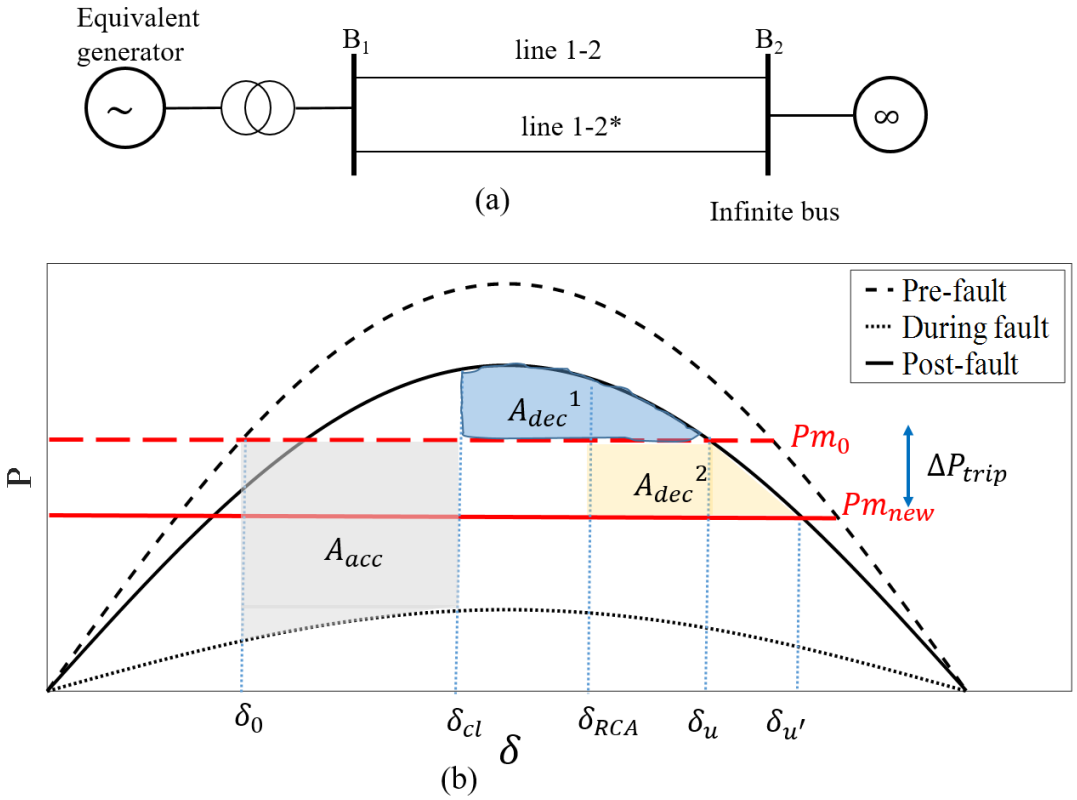

Figure 2-9. Schematic to show (a) single machine infinite bus equivalent system and (b) equal area criterion to calculate the amount of generator shedding

In [70], a combination of load shedding and generator tripping calculation is proposed, which is based on relay setting limited EAC for single machine infinite bus (SMIB) system representation using PMU data. To do so, OMIB equivalent model is formed following the instability detection. Then, the parameters of the OMIB system are estimated using real-time PMU data, and the amount of generator tripping and load shedding are calculated based on power-angle (P–δ) curve estimation. In [67], the virtual load concept is defined as a safety margin for the generator tripping scheme, and an offline look-up table is designed to trip generators for a number of scenarios. Also, the amount of virtual load is calculated at the generation side online to reinforce the pre-determined generator rejection in the look-up table. In [71], the amount of generator

tripping and load shedding has been calculated based on EAC, and a STATCOM has been designed on the generation side to reduce the amount of generation tripping and improve the transient stability. Excessive generation tripping is costly, and it leads to unnecessary load shedding. Therefore, minimizing the amount of generator tipping has been assessed in recent studies [71]. In addition, an energy function-based method is proposed in [72] to quickly identify the critical and non-critical generators and compute the required generation rejection using the relative energy of the equivalent post-fault system. In [59], a combination of load shedding and generator tripping is designed to prevent relay mal-operation and loss of synchronism, respectively. In this scheme, the amount of load shedding and generator tripping are calculated based on critical equivalent acceleration at the clearing time for stable and unstable swings, respectively. In [73], a new index is proposed to determine the stability status of the power system using a two-layer SMIB framework. This method reduces the communicational burden, identifies the critical generators using the largest angle gap, and finally calculates the amount of generator rejection to prevent instability. In [74], a method is proposed to predict transient instability and determine the number of tripped generators using local measurements. This method predicts the stability status by predicting the magnitude of the P–δ curve and determines the number of generators needed to be tripped. Although the aforementioned methods based on energy functions and EAC are fast and can be employed for online applications, approximated models and estimation are used in these models to reduce the computational burden, which affects the accuracy of calculated generator rejection, and the obtained solution might be far from the optimal solution.

Another drawback of the energy function-based methods is that they do not consider the optimal location of generator shedding. Assigning the amount of generator rejection and optimally dividing this amount between critical generators is another important issue that needs to be addressed [72]. The existing methods usually select the sequence of generator tripping based on out-of-step order [59] or energy index [72], [75], [76]. Numerous methods, such as angular separation, generator frequency, kinetic energy, etc., are proposed in the literature to determine critical generators [75], [76]. In [59], relative kinetic energy and absorption capacity of the network are used to identify the critical generators and assign the amount of generator rejection based on their criticality order. In [67], the sequence of generator tripping is determined based on the acceleration energy index of generators.

On the contrary, the optimization-based approaches attempt to calculate the amount of generator rejection accurately because an excessive amount of generator tripping is too costly, and it can also lead to an excessive amount of load shedding and a costly restoration process [67], [71]. In addition, a lower amount of generator rejection might lead to instability and blackout. Therefore, one of the most important research directions in transient stability studies is generator rejection optimization.

In [77], finding the proper RCAs (i.e., a combination of generator tripping and load shedding) is modeled as a large-scale optimization problem to prevent transient instability. This problem is solved using two layers parallel sequential approach. In this regard, sensitivity analysis by using LU-factorization is employed to solve the deferential algebraic equations (DAEs) in the simulation layer. Also, the predictor-corrector interior point method is used to solve the optimization problem, which is a non-linear programming (NLP) problem in the optimization layer. The first swing constrained emergency control (FSCEC) problem is modeled as a large-scale NLP problem with DAEs constraints in [78]. To solve this problem, a parallel reduced-space interior point method (IPM) with orthogonal collocation is employed. To simplify the problem, a two-order generator model is used, which is not realistic. In addition, an open-loop transient stability RCA is proposed in [79] that optimizes the combination of generator shedding and load shedding. Since this problem is computationally expensive, an optimal control method with constraint aggregation is used to reduce the computational burden. Therefore, the problem is converted to a fairly small-scale NLP problem which is solved using the predictor-corrector interior point method. Although lots of numerical and mathematical techniques have been used to solve these large-scale non-linear optimization problems in a fast and efficient way, existing methods are time-consuming and are not suitable for large-scale power systems. Moreover, the optimization-based methods might fail to save even small power systems in those scenarios, quickly evolving into transient instability.

2.4.3 Load shedding

The load shedding schemes are usually applied along with other control actions such as generator tripping and islanding. This scheme initiates load reduction to balance the generation and demand in the power system. It is worth mentioning that load shedding is an optimization problem. The electrical loads have different priorities. In addition, some loads need to be supplied

all the time. Therefore, load shedding schemes are solving an optimization problem and provide two pieces of information: 1) the loads to be shed and 2) the amount of power to be shed at each selected load. Several load shedding schemes are explained in the following paragraphs [80].

The main focus of reference [58] is centralized load shedding optimization based on an online outage sensitivity index (OSI). To solve this optimization problem, this method considers the capacity of renewable energies, excitation of generators, loading of lines, under frequency, and under-voltage relay setting. Unlike previous methods, it does not use ROCOF and power system inertia to calculate the amount of active power deficiency. In this method, the best location to apply load shedding is proposed based on the outage sensitivity index and voltage variation. In [81], a set of contingencies has been applied to IEEE 39 bus system and based on the worst scenario, an RCA is designed to prevent loss of synchronism. Instead of using a look-up table, it predicts the power system state using state estimation and linear interpolation for the near future. Moreover, as a corrective control action, the generation reduction using fast valving or generator tripping is applied, and then load shedding is performed to balance the generation demand in the power system. In [82], fast load shedding is proposed considering wind farm dynamics, voltage variation, and transient performance of power systems. In this regard, the load is prioritized based on load types and these criteria. The novelty of this method is that it considers the contribution of each generator to the dynamic performance of the power system. In [83], multi-stage load shedding is proposed considering the uncertainty of generation loss. The load shedding plan is determined based on dynamic frequency response using a discretized model. In addition, a load shedding prediction approach is proposed in [84] to prevent instability. The heuristic optimization is utilized to find the amount of load shedding and the best location for load shedding in an offline manner. Next, the amount of load shedding is predicted for the unforeseen scenario using the generated dataset and deep learning model. A plethora of strategies have been developed to determine the necessary and optimized amount of load shedding. However, the load shedding should be employed along with other RCAs to prevent transient instability.

2.4.4 Controlled islanding

The islanding is mostly the last resort to prevent a power system from blackout following a large disturbance. In this process, a network will be separated into a number of islands, which have a minimal power imbalance. Since the created islands, compared to the whole system, are

smaller, they can be controlled easier, and it prevents instability propagation in the whole system. A sample islanding strategy is shown in the following figure to show and clarify the principle of islanding strategy. The most important issue in control islanding is separating non-coherent generators and preventing severe power fluctuation on transmission lines by switching off the best lines. Thus, the generator groups' identification is a critical task in islanding problem. Despite identifying generator groups, which is an important issue in islanding, there are two main aspects of the islanding that need to be considered, "where to island and when to island?" Therefore, in this sub-section, different types of methods to identify coherent generators and the islanding methods are reviewed, respectively.

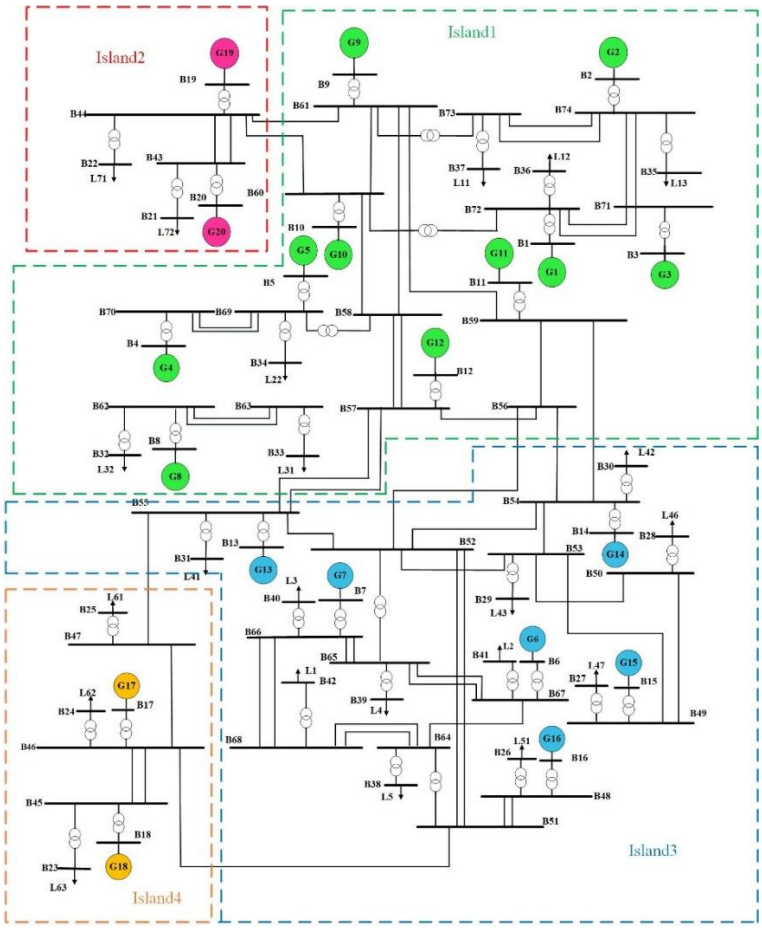

Figure 2-10. Schematic to show the principle of controlled islanding, the Nordic power system is partitioned into 4 islands and coherent generators in each islands are colored using same color

The generator groups' identification is an important part of reduction techniques in the power system. In addition, it is necessary to implement an intentional islanding strategy [85].

Coherent generator identification methods can be classified into two main categories: slow coherency identification and unstable generator grouping [24].

The slow coherency-based methods are one of the most common strategies for generator grouping. In these methods, the generators that fluctuate together in low-frequency mode after a disturbance are known as coherent generators [86], [87]. They are usually based on rotor angles and generators' angular speeds before exceeding the stability limits. For instance, principal component analysis (PCA) [88] and clustering techniques [89] are employed to extract the coherent generators based on slow coherency identification. Moreover, thanks to the artificial intelligence algorithms and PMUs for providing the real-time data, several research works have been carried out for the second category (i.e., unstable generator grouping). These types of methods extract the coherency patterns based on post-fault generators' dynamic response after instability in an offline manner for a large set of scenarios. Then, they employed different learning approaches, such as DT [90], SVM [91], ANN [92], and quantile regression (QR) [24], for pattern prediction.

As it is mentioned, the available time for performing RCAs is limited. Therefore, fast and accurate prediction of coherent generators is crucial for partitioning the power network accurately. Although lots of approaches have been proposed to tackle this problem, existing methods do not have a high accuracy [24]. Therefore, an accurate and fast prediction of coherent generators is one of the hottest research areas, which is evaluated and improved in this study.

Finding the appropriate splitting points for intentional controlled islanding is inherently a large-scale optimization problem, and many approaches are proposed to solve this problem. Generally, these approaches based on objective function in optimization problems can be classified into two main groups: minimizing the power flow disruption and minimizing the power imbalance within islands [93]. Despite defining- the objective function, the islanding problem is a non-deterministic polynomial-time hardness (NP-hard) problem, which means there is no general polynomial-time algorithm to find the optimal solution. In the following paragraphs, a review is performed on the existing methods that solve the islanding optimization problem.

It is worth mentioning that a power network can be represented by an undirected connected and node-weighted graph $G(V, E, W)$ [94]. Where V is a set of nodes and represents the bus in a

power network, E is the set of edges that describe the transmission lines in power systems, and W indicates the power injected into each node. The adjacency matrix of G denote the connections between every two nodes. Therefore, the splitting problem using the graph theory is a search problem that tries to find which edges are best to cut while considering power flow disruption minimization, the operational constraints, and separating the non-coherent generators.

In [95], a system splitting strategy based on graph theory is proposed using an ordered binary decision diagram (OBDD) algorithm. This algorithm searches the whole solution space and finds the best way to partition the network. In this regard, OBDD is performed to reduce the solution space, and then based on the power flow analysis, the best splitting strategy is selected. Reference [57] presented an islanding strategy considering power system restoration constraints, including black-start availability, generation capacity, and observability. This method minimized the power flow disruption using extended mixed-integer linear programming (MILP), one of the most effective methods that can directly find the islands with minimum power flow disruption. It only needs the coherent generators and the state of the power network. In addition, the islanding strategy is described as a graph partitioning problem in [96]. The unique graph-theoretic technique known as spectral clustering controlled islanding (SCCI) is proposed to solve this NP-hard problem. This method minimizes the power flow disruption while ensuring that each island consists of coherent generators and non-coherent generators are disconnected. Since the SCIC can only find the solution for problems with two islands, the recursive bisection is performed to solve the problem for cases with more than two islands. However, these methods are computationally demanding and are not practical in real power systems. In [93], the islanding problem is defined as a linear programming problem. First, a search space reduction is employed to reduce the complexity of the problem. It finds the trees with a minimum number of nodes and makes sure each tree connects all coherent generators. Then the other nodes are assigned to each tree based on operational constraints. Reference [97] is presented an OBDD-based method to find the splitting points considering transient stability constraints. It evaluated whether the determined islanding strategy is feasible and maintains system stability following a small disturbance or not. To do that, it determined a threshold value constraint (TVC) based on offline simulations and checked whether the transient stability constraint was satisfied by the splitting strategy or not.

Contrary to the above-mentioned methods, several research have been proposed to find the splitting point by minimizing the imbalance between generation and demand in each island. The main goal of these strategies is to minimize the amount of load shedding in each formed island. In [98], an optimization based on MILP is proposed to find the islands, amount of load shedding, and generator re-scheduling. These methods consist of two stages, including linear DC power flow to determine the islands and AC optimal load shedding to check the post islanding balance between load and generation in each island. It also evaluates the voltage profile after controlled islanding. In addition, the splitting strategy optimization is modeled as a MILP optimization problem [99]. These methods consider the connectivity and integrity of each island. Also, it evaluated the dis-connectivity of every two islands based on graph theory. The objective function is to minimize the overall amount of load shedding. This method captured multiple optimal solutions, and users can select the appropriate islanding solution with different interests. In [100], a piecewise linear AC power flow is proposed in the islanding model to consider real and reactive power balance at the same time and provide a healthy voltage profile in each island. This linearization also reduces the computational burden in the optimization process significantly. Reference [101] developed a MILP formulation to find the islanding boundary by minimizing overall load shedding under catastrophic events. It linearized swing equations and evaluated frequency stability in resulted islands. Two Fictitious DC power flow is proposed to check the connectivity and dis-connectivity constraints. In addition, the MILP-based islanding is solved using the benders decomposition technique to reduce the computational time [102]. The transient stability constraints are derived offline using equal area criterion to be considered in controlled islanding optimization [103]. Mixed-integer non-linear programming (MINLP) is developed to model the islanding problem with transient stability constraints. Then a linearization is performed and converted the MINLP to MILP. This method minimizes the amount of load shedding and increases the stability margin in resulted islands [104].

2.5 Conclusion

In this chapter, a review is performed to explain different types of transient stability assessment. Among existing methods, machine learning-based methods are very effective for real-time applications due to their fast analysis capability [44]. Moreover, the four main states in a power network are introduced, and the appropriate control action in each state is discussed. Finally,

the RCAs are introduced, and the most practical RCAs to prevent transient stability are discussed in detail. Many studies have been done to propose an accurate and fast RCA for practical and real-time applications in power systems. However, according to the commutation delays and fast dynamics of rotor angle oscillations, there is limited time to compute RCA. Therefore, in this thesis, RCA prediction is proposed to solve this issue.

3 MICRO MODEL STRATEGY AND SCENARIO GENERATION PROCESS

3.1 Introduction

As mentioned, transient instability occurs quickly, and it can lead to cascading outages or blackouts. The existing response-based RCAs might not be practical for those scenarios quickly evolving to transient instability due to communication delays and time limitations. In addition, the event-based methods might be unable to respond to unforeseen scenarios as only a limited number of contingencies are considered in their design. In this regard, the RCA prediction framework is proposed to prevent transient instability following a disturbance. Predicting RCAs for a large power network is a challenging problem. The designed RCA should be fast, accurate, and be able to deal with unforeseen scenarios appropriately. Therefore, to cover credible scenarios, reduce prediction complexities, and increase accuracy, a micro model strategy is employed in which independent models are built for each transmission line of the system. In this chapter, the principle of micro model strategy and bulk scenario generation process is discussed in detail.

3.2 Micro model strategy

The performance of data-driven methods strongly depends on the dataset and selected features. The previous data-driven methods in power systems, including transient stability prediction, coherency prediction, and critical generator prediction methods, generate a large number of scenarios for the whole power network and select a large number of attributes to improve the performance of their methods. This increases the training time and computational burden significantly. In addition, there are numerous coherency, critical generators, and RCA patterns for a large-scale power system that increases the size of solution space for machine learning engines. Therefore, the large set of candidate patterns increases the chance of choosing the wrong pattern and deteriorates prediction accuracy. A micro model strategy is employed to reduce the machine learning engine complexities and improve the prediction accuracy.

In contrast to the previous methods, the proposed framework is designed for individual transmission lines separately, and specific scenarios are generated for individual lines. The main idea behind using the micro model strategy is to run the prediction modules for a much smaller

solution space by predicting among only a finite number of possible patterns. The post-fault dynamic behavior of each micro model set (MMS) follows a certain number of patterns. As a result, the micro model strategy eliminates considering all possible patterns related to all lines in a power system. This strategy makes it easier for the machine learning engine to predict the proper coherency, critical generators, and RCA patterns from a lower number of possible patterns.

Parallel lines are modeled with only one MMS because, in post-fault conditions, each generator exhibits similar dynamic responses for either line. A small power network as a part of a larger power system is shown in figure 3-1 as an example. In this network, TL1-3 and TL*1-3 are considered as one MMS and evaluated using one framework.

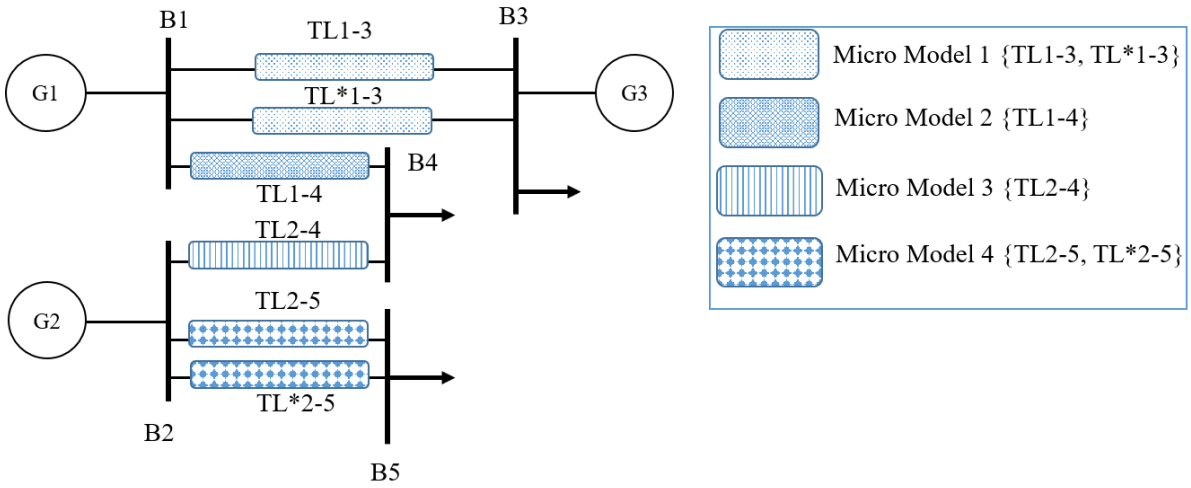

Figure 3-1. Schematic of micro model strategy for an example power network

According to the micro model definition, there are four MMSs for the sample power network shown in figure 3-1. For example, the coherency patterns are extracted for this network. Assume that there are 13 coherency patterns for the whole network. However, each micro model has a few number of coherency patterns. In addition, one of the MMSs only has one coherency pattern, which means there is no need to design a coherency prediction module for that MMS. Therefore, generating the dataset for each MMS individually can reduce the solution space by only considering the finite possible pattern for that specific MMS. A comparison is shown in figure 3-2 to clarify the application of the micro model strategy. For example, assume that a fault has occurred on MMS4, and the micro model strategy is not used. Similar to previous methods, the whole dataset is considered for finding the proper RCA in figure 3-2 (a). In this case, patterns

related to other MMSs (i.e., rectangles, triangles, and circles in figure 3-2) have a chance to be chosen. However, using the micro model strategy and considering a smaller solution space, the probability of choosing patterns related to other MMSs is zero, which significantly increases the accuracy.

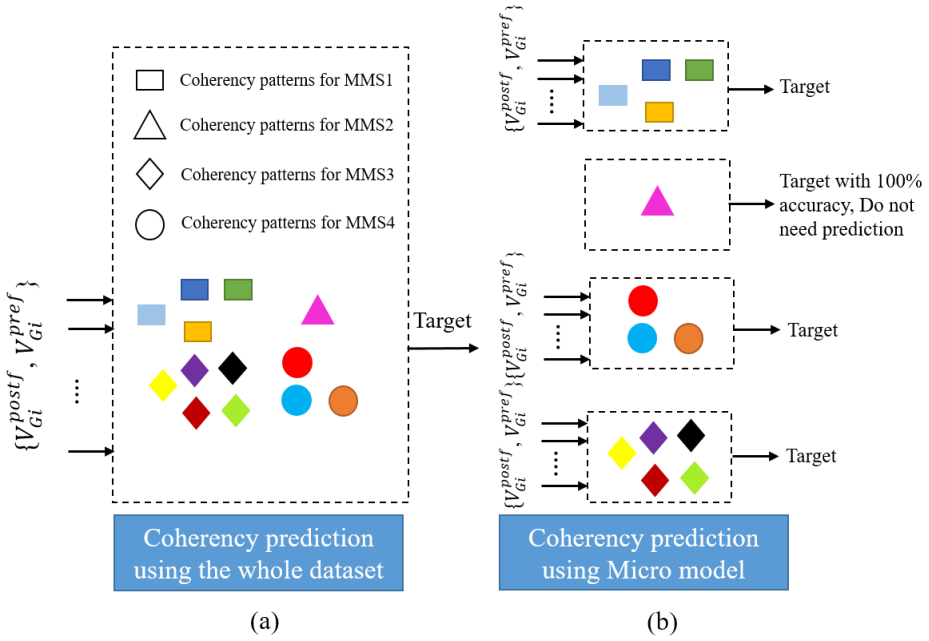

Figure 3-2. Schematic showing the difference between the coherency prediction module of (a) the existing method using the whole dataset predicting all patterns in one module and (b) the proposed framework employing the micro model strategy to reduce the solution space and improve the accuracy.

It is worth noting that the micro model improves the feature selection process by only using the measured data from adjacent buses. For instance, a fault on TL1-3 more significantly affects G1 and G3 than G2. This can be mathematically modeled using a sensitivity matrix as follows:

$$S_{G-F} = [\Delta\delta_G \quad \Delta V_G]^T \tag{1}$$

$$\Delta\delta_{Gi}(X_F) = \delta_{Gi}^{postf}(X_F) - \delta_{Gi}^{pref}(X_F), \quad \forall i \in \Omega^G \tag{2}$$

$$\Delta V_{Gi}(X_F) = V_{Gi}^{postf}(X_F) - V_{Gi}^{pref}(X_F), \quad \forall i \in \Omega^G \ , \ X_F = \{k |\ k \in \Omega^{TL}\} \tag{3}$$

Using (1)-(3), the effective features (i.e., voltage angle and voltage magnitude of certain buses) for scenarios related to each transmission line are extracted and used to train the machine learning engines. The micro model strategy reduces the number of features by using the most effective features from adjacent buses for each MMS.

3.3 Bulk scenario generation

In a dynamic study of a power system, many parameters such as load demand, power generation, network configuration, line power flows, location and duration of faults, types of contingencies, etc., are subject to change over time and affect real-time control and operation of the power system. For transient stability analysis, the main parameters are fault location, fault duration, system loading, and types of contingencies.

Generally, there are three common types of contingencies in a power network including; 1) fault occurs without any outage, 2) fault occurs while one element (i.e. transmission line, generator, or transformer) are not in service (N-1 contingency), and 3) fault occurs while two elements of power network are out of service (N-2 contingencies). The outages can occur because of periodic maintenance or operation failure. Although the occurrence of other types of contingencies (i.e., N-3, N-4, etc.) is possible, they happen in rare cases, and those types of contingencies are not considered in this study. In the scenario generation process, the cases include 70%, 20%, and 10% for these three types of contingencies, respectively. Therefore, Line switching which always occur in power systems are considered in scenario generation process.

As discussed, three parameters consist of fault time duration, fault location, and system loading, which have more impact on the transient stability study. Since the probability of occurring a fault on different parts of a transmission line locations is equal, the location of the fault on each transmission line is selected randomly based on a uniform distribution function in the scenario generation process (i.e., the fault can occur in different parts of the line from 0.05 to 0.95 of line length). In contrast, other parameters, including fault duration time and system loading, are changed randomly based on the normal distribution function. The detail of the above-mentioned parameters range and share of cases in the scenario generation process for each MMS is illustrated in table 3-1.

This research studies three networks, including the IEEE 9-bus system, IEEE 39-bus system, and 74-bus Nordic power network. Depending on the power network size, different number of scenarios are generated for each micro model for various networks.

The number of scenarios are determined based on trial and error for each network to cover all possible patterns. Next, the number of MMS for each system is determined, and the scenario

generation process is performed for each network. In the following paragraphs, the studied networks are introduced.

Table 3-1. Scenario generation process for individual micro model

Parameters	Share of cases involving fault without outage	Share of cases involving fault with N-1 contingency	Share of cases involving fault with N-2 contingency
- Clearing time (30-350 ms)	70 %	20 %	10 %
- Loading (65-130%)			
- Fault location (0.05-0.95 pu)			

3.3.1 IEEE 9-bus system

The IEEE 9-bus system has 3 generators, 6 transmission lines, 9 buses, and 3 loads. The single line diagram of this network is shown in figure 3-3. Since there is no parallel transmission line in this network, the number of MMS are equal to number of transmission lines. Therefore, there are 6 MMSs in this system. To cover credible scenarios for this network, 2000 cases are generated for each MMS. A six-order model is adopted for the synchronous generators. All of the generators are equipped with an automatic voltage regulator (AVR) of IEEET1 type, and an IEEEG1 governor. The π model is used for modeling the AC transmission lines.

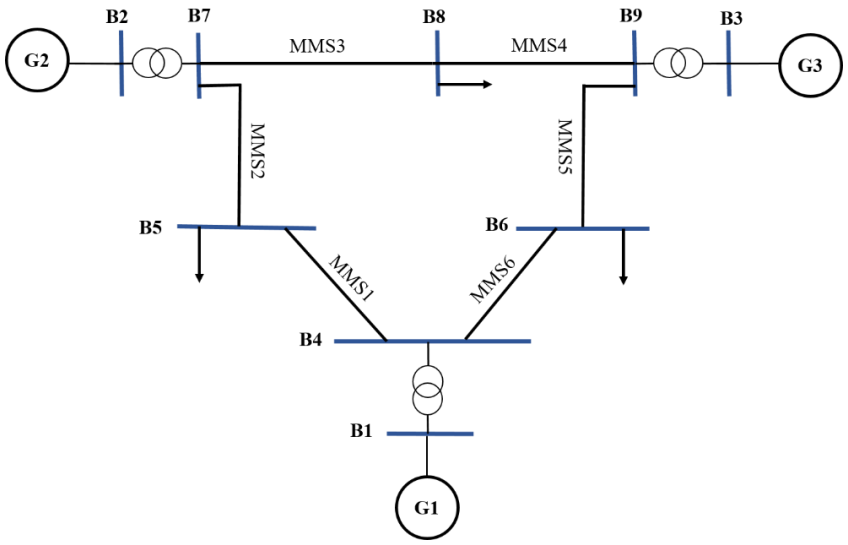

Figure 3-3. Single line diagram of IEEE 9-bus system

3.3.2 IEEE 39-bus system

This power system is known as the New England system and consists of 39 buses, 10 synchronous generators, 34 transmission lines, and 19 electrical loads. Similar to the 9-bus system, the IEEE 39-bus system does not have any parallel transmission line. Therefore, the 34 MMSs are considered for this network. Since this power system has more equipment to cover a plausible number of scenarios, more cases are generated for each micro model in this test system. For each MMS, 5000 cases are generated to cover credible scenarios. A six-order model is adopted for the generators. All generators are equipped with an automatic voltage regulator (AVR) of the IEEET1 type, a power system stabilizer (PSS) of the IEEEST type, and an IEEEG1 governor. The π model is used for modeling the AC transmission lines. The single line diagram of the IEEE 39-bus system is depicted in the following figure.

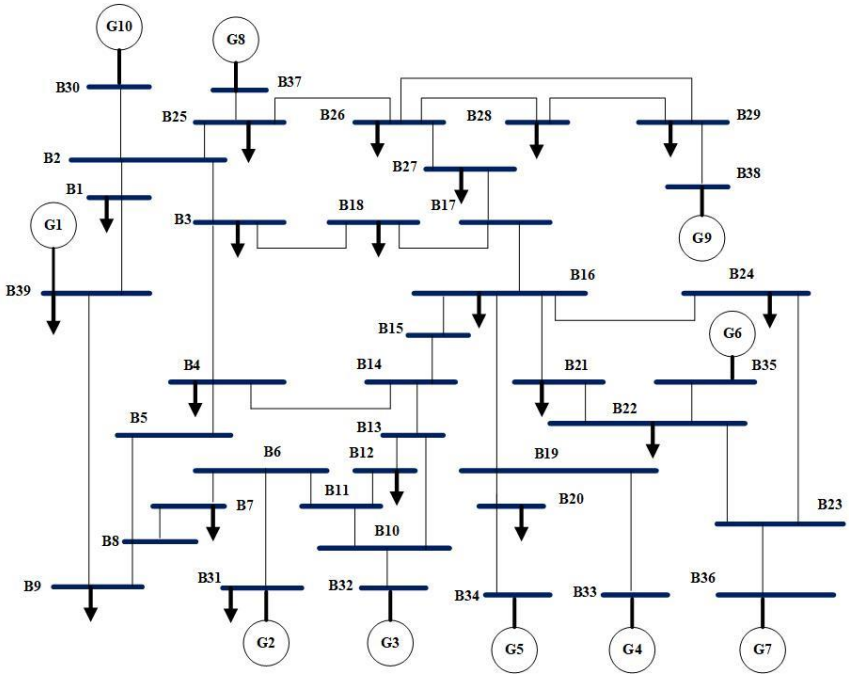

Figure 3-4. Schematic to show the single line diagram of IEEE 39-bus system

3.3.3 74-bus Nordic power network

As a real and large power network, a 74-bus Nordic power system is used in this study. This test system is comprises 20 synchronous generators, 74 buses, 52 transmission lines, and 24 electrical loads. There are 15 pairs of parallel lines (i.e., 30 transmission lines). Due to the presence

of parallel lines, there are accordingly 37 MMSs. To cover the credible number of scenarios for each MMS, 6000 cases are generated in this test system. It is worth mentioning that the 6000 cases are generated for parallel lines together. A six-order model is adopted for the generators. All of the generators are equipped with an automatic voltage regulator (AVR) of the Benutzerdefiniete model and the Benutzerdefiniete governor. The π model is used for modeling the AC transmission lines. The following figure shows the single line diagram of the 74-bus Nordic power network.

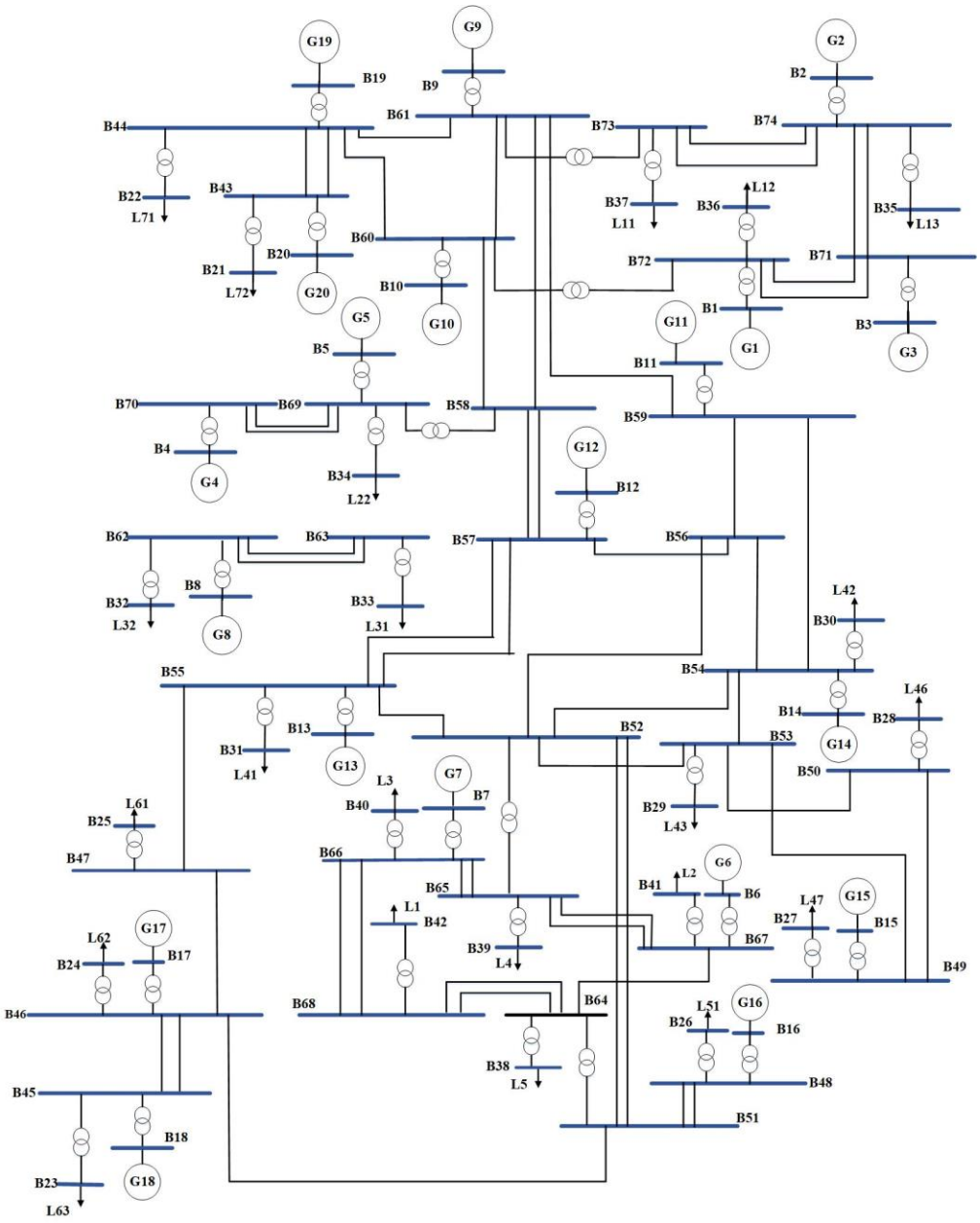

Figure 3-5. Single line diagram of 74-bus Nordic test system

The bulk scenarios are generated for the aforementioned power networks based on the micro model strategy. The scenarios are generated through DIgSILENT Programming Language (DPL) commands. It is worth mentioning that the full dynamic of power systems is considered in the scenario generation process using DIgSILENT PowerFactory software. The following table describes the scenario generation for three studied networks.

It is worth noting that different number of scenarios are generated for individual MMS in each power system depending on the size of the network. The exact number are determined based on trial and error. According to this method the generated scenarios can cover all possible patterns for each micro model in each power system.

Table 3-2. Summary of scenario generation process for studied network

Test System	**Number of MMSs**	**Number of scenarios for each MMS**	**Total number of generated scenarios**	**Simulation time for data generation**
IEEE 9-bus	6	2000	12000	~ 2 days
IEEE 39-bus	34	5000	170000	~ 20 days
74-bus Nordic	37	6000	222000	~ 32 days

3.4 Conclusion

In this chapter, the principle of the proposed micro model strategy is explained in detail. Moreover, the scenario generation process is discussed, which is the first stage for implementing data-driven methods. The strategy to change system parameters and cover credible scenarios are explained. Three power systems, including IEEE 9-bus, IEEE 39-bus, and 74-bus Nordic Network, are employed as test systems. Finally, the utilized software to generate datasets and the simulation time for bulk scenario generation is illustrated. In the following chapters, two novel frameworks for RCA prediction are proposed based on the micro model strategy.

4 MACHINE LEARNING-BASED CONTROLLED ISLANDING AND LOAD SHEDDING PREDICTION TO PREVENT POWER SYSTEM TRANSINET INSTABILITY USING WIDE-AREA MEASUREMENTS

4.1 Introduction

A novel RCA prediction framework is proposed in this chapter to address the drawbacks of existing methods. The proposed framework consists of three main modules, including transient stability prediction, coherency prediction, and RCA prediction, designed for each set of micro model. A combination of controlled islanding and load shedding is considered as RCA to stabilize unstable scenarios. An efficient classifier is employed in all three modules to enhance the prediction accuracy. The proposed framework is able to predict load shedding and islanding pattern following an instability prediction in a reasonable amount of time, which is necessarily shorter than the available time to prevent instability and perpetuate system integrity. Moreover, an efficient classifier is designed in all three modules to enhance the prediction accuracy. Finally, the effectiveness of the proposed framework is tested via the IEEE 39-bus system and the 74-bus Nordic power network.

4.2 Methodology

The proposed framework have two stages: 1) offline calculation and optimization to train machine learning modules, and 2) online prediction. The offline stage involves determining the stability status, identifying coherency patterns, and extracting optimal islanding patterns and load shedding patterns in an offline manner. Using the generated dataset for each MMS, three different modules are trained by machine learning engines. In the online stage, the coherency pattern is predicted following an instability prediction. Next, based on the generator groups the proper RCA (i.e. islanding boundaries and load shedding) is predicted. The schematic of the proposed framework is depicted in figure 4-1. The details of the classification method and three prediction modules are presented in the following subsections.

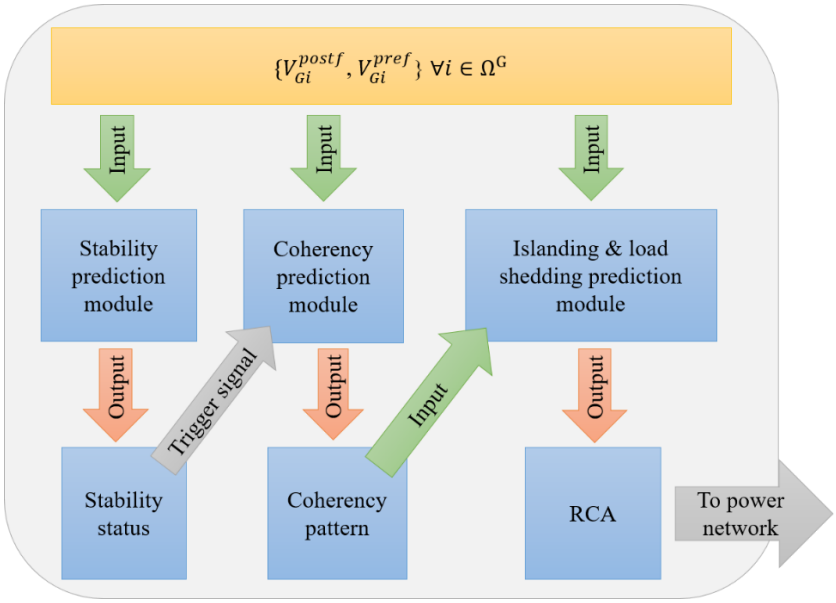

Figure 4-1, Schematic of the proposed framework

4.2.1 Offline training stage

In this part, the offline training process of the machine learning models used in all prediction modules of the framework is explained. An ANN-based collaborative binary-real differential evolution (CBRDE) [104] is employed, and the Levenberg-Marquardt (LM) algorithm [105] is utilized for fine-tuning of ANN weights for the machine learning models related to all prediction modules in the proposed framework.

The binary deferential evolution (binary-DE) is developed to evolve the network structure, and a real-DE is presented to optimize the weights and bias of the neural network, which is called collaborative binary-real differential evolution (CBRDE). ANN has two main parts, network structure, which includes the number of hidden nodes, and connections including bias and weights. Network connections are encoded by binary string, and weights are encoded by real values because this encoding method improves both network evolution and weight adaption. Despite the number of input and output neurons that are problem dependent, the hidden neurons are user-specified and denoted as MJ. In ANN, the network structure depends on the number of hidden neurons in the hidden layer and connections between input and output neurons with hidden neurons. The activity status of hidden neurons is shown with a binary string S, which is 0 or 1 and the string length is the number of hidden neurons MJ.

Assume a three layer ANN with I input neurons, J hidden neurons, and K output neurons.

$$W_1 = (w_{ij}^1)_{I*MJ} \tag{1.4}$$

$$B_1 = (b_{1j})_{MJ*1} \tag{2.4}$$

$$W_2 = (w_{jk}^2)_{MJ*K} \tag{3.4}$$

$$B_2 = (b_{2j})_{K*1} \tag{4.4}$$

$$W = \{W_1, B_1, W_2, B_2\} \tag{5.4}$$

Where $W_1, B_1, W_2, and\ B_2$ are weight matrix between input layer and hidden layer, bias vector in hidden layer, weight matrix between hidden layer and output layer, and bias vector in output layer. Also, W is connection weight set with dimension of $MD = I * MJ + MJ + MJ * K + K$. Thus each ANN can be represented with equation (6.4) which NP is population size. In the following figure, the structure of the implemented ANN is illustrated.

$$ANN^l(t) = \{S^l, W^l\} \quad l = 1, 2, \dots, NP \tag{6.4}$$

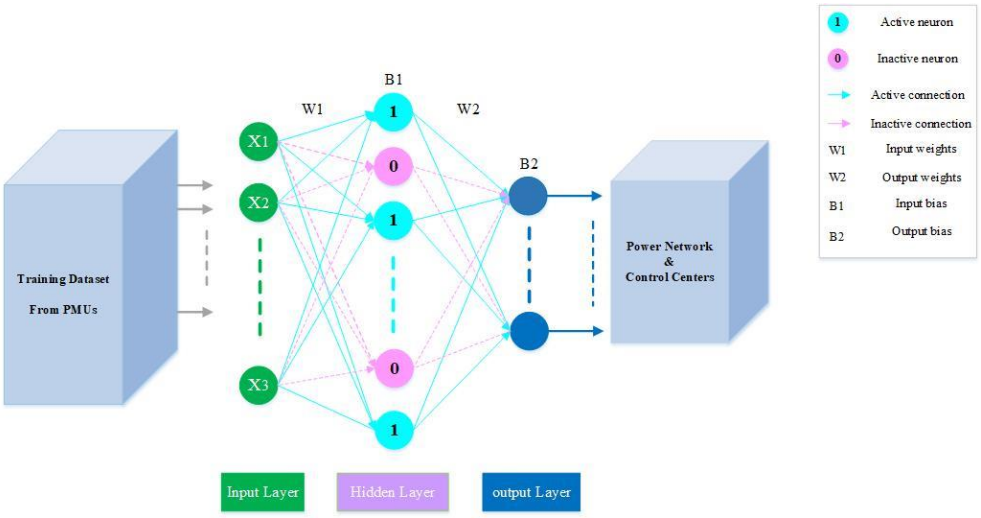

Figure 4-2. Schematic to show the structure of employed ANN

So far, mixed-coding scheme is introduced. In the following, the other parts of CBRDE is discussed in detail. First one is fitness value. The Normalized Mean Squared Error on training data set is used as fitness function. For the l^{th} network the fitness value is computed as follows.

Consider$X_P = \left[x_{p1}, x_{p2}, \dots, x_{pl}\right]^T$,$H_p^l = \left[h_{p1}^l, h_{p2}^l, \dots, h_{pJ}^l\right]^T$, $O_p^l = \left[o_{p1}^l, o_{p2}^l, \dots, o_{pK}^l\right]^T$ as training set, output vector from hidden layer, and output vector from output layer respectively which are computed by the following equations.

$$H_p^l = f_1(D^l * (W_1^l)^T * X_p + D^l * B_1^l) \tag{7.4}$$

$$O_p^l = f_2((W_2^l)^T * D^l * H_p^l + B_2^l) \tag{8.4}$$

$$f_1(x) = \frac{1}{1 + \exp(-x)} \tag{9.4}$$

$$f_2(x) = x \tag{10.4}$$

Where $D^l = diag(S^l)$ i.e. diagonal $MJ * MJ$ matrix. The fitness value for l^{th} ANN network is computed by equation (11.4).

$$fitness(ANN^l) = \frac{1}{PK}\sum_{p=1}^{P}\sum_{k=1}^{K}(y_{pk} - O_{pk}^l)^2 \tag{11.4}$$

Where $Y_p = \left[y_{p1}, y_{p2}, \dots, y_{pk}\right]^T$ the expected output of input pattern p and P is the number of training set examples. The second step is initialization of population. In this regard, *NP* individual networks generate such as $ANN^1(0), ANN^2(0), \dots, ANN^{NP}(0)$ so that

$$ANN^l(0) = \{S^l(0), W^l(0)\}\ for\ l = 1,2, \dots, NP \tag{12.4}$$

$$S^l(0) = round(rand(1, MJ)) \tag{13.4}$$

$$W^l(0) = -ones(1, MD) + 2 * rand(1, MD) \tag{14.4}$$

The third stage of CBRDE is mutation. Assume l^{th}individual network at generation *t* be $ANN^l(t) = \{S^l(t), W^l(t)\}$. A mutant network is represented as $ANN_m^l(t) = \{MS^l(t), MW^l(t)\}$ and $MS^l(t), MW^l(t)$ are calculated by following equations if$rand(0,1) > 0.5$.

$$MS^l(t) = S^l(t) \oplus \left(\left\lceil F * \left(S^{r1}(t) - S^l(t)\right)\right\rceil \oplus \left\lceil F * \left(S^{r2}(t) - S^{r3}(t)\right)\right\rceil\right) \tag{15.4}$$

$$MW^l(t) = W^l(t) + F * \left(W^{r1}(t) - W^l(t)\right) + F * \left(W^{r2}(t) - W^{r3}(t)\right)) \tag{16.4}$$

Otherwise

$$MS^l(t) = S^{r1}(t) \oplus \lceil F * (S^{r2}(t) - S^{r3}(t)) \rceil \quad (17.4)$$

$$MW^l(t) = W^{r1}(t) + F * (W^{r2}(t) - W^{r3}(t)) \quad (18.4)$$

Where $\lceil \quad \rceil$is ceil function and it rounds toward infinity. Also, $\oplus$ is XOR operator. Also, $F \in (0,1)$ is the scaling factor and r_1, r_2, r_3 are the mutually different integers randomly chosen from$[1, NP] \backslash l$. The next part of CBRDE method is crossover. The individual network is combined the mutated network using the following hybrid scheme to generate the trial network $ANN_c^l(t) = \{CS^l(t), CW^l(t)\}$ where$CS^l(t) = [cs_1^l, cs_2^l, \dots, cs_{MJ}^l]$, $CW^l(t)\left[cw_1^l(t), cw_2^l(t), \dots, cw_{MD}^l(t)\right]$ DE crossover plays a vital role for generating offspring individuals in the $\mathrm{NP} - 1$ individuals in hybrid crossover. This offspring will be generated by the subsequent equations.

$$cs_j^l(t) = \begin{cases} ms_j^l(t), if\ r_j \le CR\ or\ j = rn(j) \\ s_j^l(t), \qquad otherwise \end{cases} \quad for\ j = 1,2, \dots, MJ \quad 19.2$$

$$cw_k^l(t) = \begin{cases} mw_k^l(t), if\ r_k \le CR\ or\ k = rn(j) \\ w_k^l(t), \qquad otherwise \end{cases} \quad for\ k = 1,2, \dots, MD \quad 20.2$$

Where $r_j, r_k \in (0,1)$ are random numbers; $rn(j) \in [1, MJ]$ and $rn(k) \in [1, MD]$ are integer random numbers. The *CR* is a crossover probability constant which is belong to (0,1)interval. $ms_j^l(t)$and $s_j^l(t)$ are the j^{th} component of the vectors $MS^l(t)$ and $S^l(t)$ respectively. Also, $mw_k^l(t)$and $w_k^l(t)$ are the k^{th}elements of the vectors $MW^l(t)$ and $W^l(t)$ respectively. The last part of the CBRDE algorithm is best network selection. According to fitness value, the subsequent generation $ANN^l(t+1) = \{S^l(t+1), W^l(t+1)\}$ is selected from the target network $ANN^l(t) = \{S^l(t), W^l(t)\}$ and the trial network$ANN_c^l(t) = \{CS^l(t), CW^l(t)\}$. If the$fitness(ANN_c^l(t)) < fitness(ANN^l(t))$then$S^l(t+1) = CS^l(t)andW^l(t+1) = CW^l(t)$. Otherwise, $S^l(t+1) = S^l(t)$and$W^l(t+1) = W^l(t)$.

Until now, The CBRDE is introduced in detail, in the following paragraphs two stage training algorithm based on CBRDE and LM method is discussed comprehensively and the flowchart of this algorithm is represented. Since the CBRDE method is working based on local search, to improve local search capability this method is combined with LM backpropagation algorithm. According to the introduced CBRDE, the architecture and weights of AFNN are

optimized simultaneously. In the second stage LM backpropagation algorithm is adopted for fine-tuning the ANN weights. Two stop criteria has considered for this algorithm: 1) when a given MSE accuracy value ε is achieved; 2) the number of iteration specified by users is reached. In the following flowchart the algorithm has represented. When the generation t reaches a constant $maxG$, CBRDE stops and LM start with the best weights output by CBRDE as initial weights. LM method optimize and refine connection weights until stopping criteria reaches.

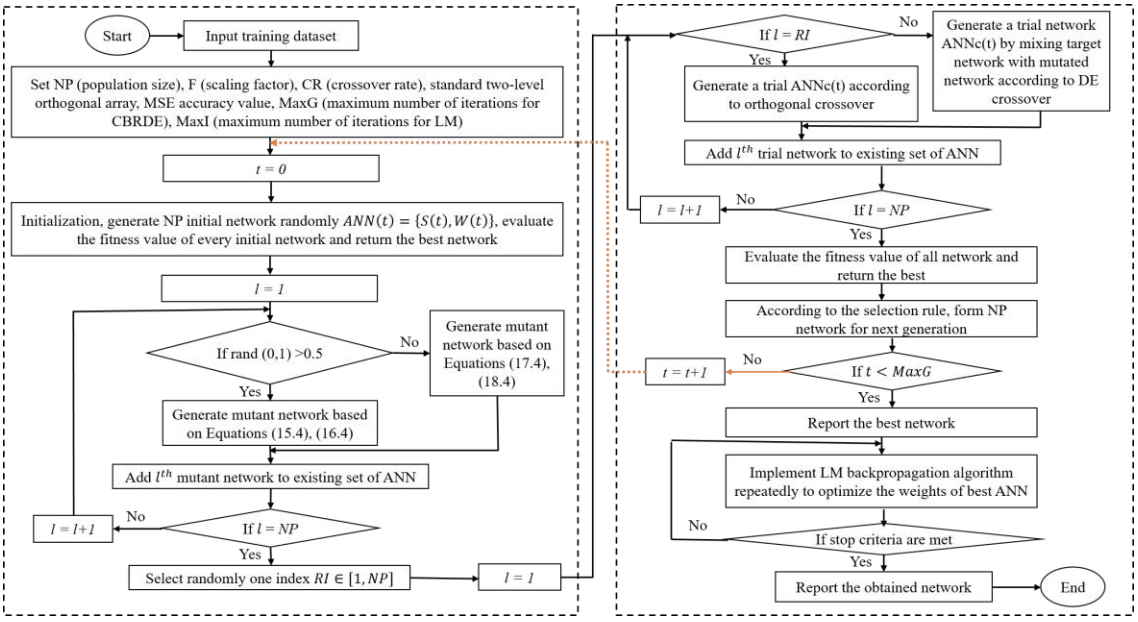

Figure 4-3. Flowchart to illustrate the employed CBRDE-LM ANN

The dataset and machine learning models can be updated periodically to cover new system upgrades (e.g., generation retirement, new generation interconnection, and building new transmission lines) to improve the performance and accuracy of the framework. Details of the modules and their classification algorithms are discussed in the next sections.

4.2.2 Transient stability prediction module

In normal operation conditions, the system is operated at a stable point, and there is a balance between electrical power (P_e) and the mechanical power (P_m) of generators. According to swing equations (21.4)-(22.4), the rotor angles of generators (δ) remain constant in the normal state of the power system.

$$M_i * \frac{d^2\delta_i}{dt^2} = P_{m_i} - P_{e_i} \quad i = 1,2,\dots,N_G \tag{21.4}$$

$$\frac{d\delta_i}{dt} = w_i - w_s \tag{22.4}$$

When a disturbance occurs in a power system, the balance between the electrical and mechanical power of generators is disrupted. Following the sudden imbalance between P_e and P_m, generators start to release/absorb kinetic energy and decelerate/accelerate. If all generators are able to damp and absorb this energy, the power system remains stable. The transient stability criterion in [106] is adopted to identify the power system's stability status in this study. The transient stability index (γ_k) is defined as follows.

$$\gamma_k = \frac{2\pi - \Delta\delta_k^{max}}{2\pi + \Delta\delta_k^{max}} \tag{23.4}$$

If γ_k is positive (i.e., $\gamma_k > 0$), the system is considered stable; if γ_k is negative (i.e., $\gamma_k < 0$), the system is considered unstable. A sample of stable and unstable scenarios is depicted in the following figure.

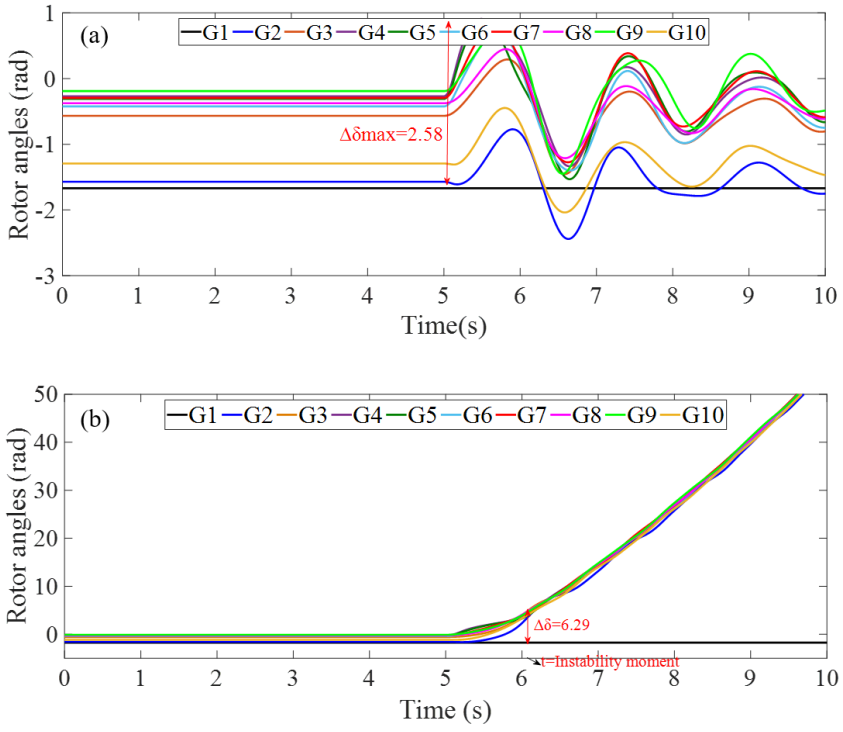

Figure 4-4. A sample scenario to show the differences between stable and unstable scenarios in IEEE 39-bus system (a) rotor angles of generators for a stable scenario, (b) rotor angles of generators for unstable scenario

Note that the instability moment can be determined using (23.4). In the offline simulations, γ_k is calculated for each time step after fault clearance. The instability moment t_{ins} is the first moment when $\gamma_k < 0$. All scenarios related to line ij are labeled 0 and 1 for stable and unstable cases, respectively.

According to the scenario generation process, the bulk scenario is generated for each micro model. Also, the stability status of each scenario is determined based on the defined criteria in (23.4). Based on the trained machine learning model for the offline dataset, the stability status of any new fault scenario can be predicted. Therefore, the stability prediction problem is converted into a supervised learning binary classification problem that can be solved by the utilized classifier. If a fault scenario is predicted as "unstable," the trigger signal will be sent to the next modules to predict the coherency pattern and appropriate RCAs.

4.2.3 Coherency prediction module

The generators of a stable power system operate synchronously as one coherent group in normal operating conditions. Following a large disturbance and in unstable conditions, the generators tend to oscillate against each other in the form of several coherent groups. Identifying coherent generators to perform an accurate RCA is necessary. Contrary to the previous methods that use slow coherency or rotor angles at the end of the simulation time to identify generator groups, in this module, the coherency patterns are identified based on the rotor angles of generators at the instability moment. The instability moment is the first instant that the $\gamma_k < 0$. Depending on the moment used for coherency pattern identification, a different number of coherency patterns can be extracted. It is obvious generator groups vary with time. For example, a random unstable scenario in the IEEE-39 bus system is depicted in the following figure.

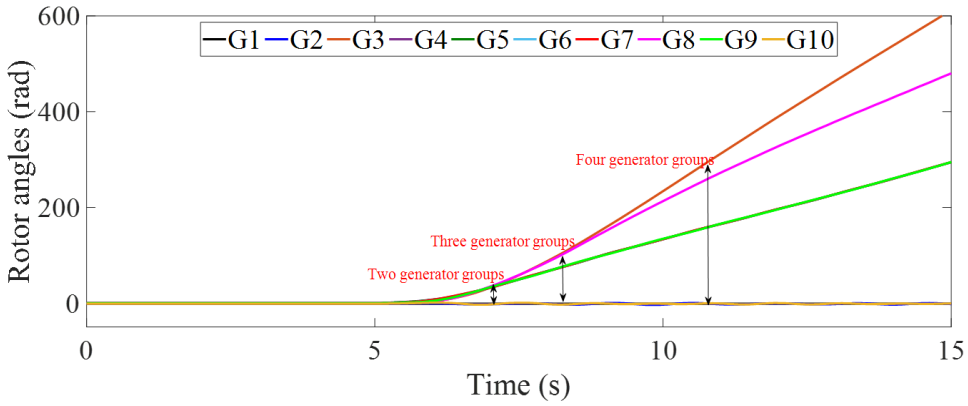

Figure 4-5. An unstable scenario to show the variation of number of coherency patterns over time

The moment employed to identify coherent generators is really important, and it totally affects the RCA module. The more number of generator groups leads to more costly RCA (i.e., an extra amount of load shedding) and also costly restoration process. The goal of the proposed framework is to minimize the number of coherent groups and thereby the number of resulting islands to optimize RCA. The RCA scheme design depends on the number of coherent groups and the moments employed to identify coherent generators. Optimal RCA is determined by identifying coherency patterns close to the time when a power network loses synchronism. According to the instability moment definition, the maximum difference between rotor angles is slightly greater than 2π radians at the instability moment [13], [106]. In a network with N generators, the maximum and minimum angles and the maximum difference between rotor angles at the instability moment are defined as follows:

$$\delta_{max}(t_{ins}) = \max(\delta_1, \delta_2, \dots, \delta_N)_{t=t_{ins}} \tag{24.4}$$

$$\delta_{min}(t_{ins}) = \min(\delta_1, \delta_2, \dots, \delta_N)_{t=t_{ins}} \tag{25.4}$$

$$\delta_{max}(t_{ins}) - \delta_{min}(t_{ins}) = 2\pi + \varepsilon \tag{26.4}$$

where ε is a small positive number. According to the coherency concept, the rotor angle difference of generators in the same coherency groups is less than 180 degrees (π radians) at the instability moment. Assuming there exists a case with four coherency groups at the instability moment, the maximum angle difference should be at least 540 degrees (3π radians), which is in contradiction to the instability moment definition. Therefore, the initial assumption of having four or more coherency groups at the instability moment must be false, and hence there exist only two or, in rare cases three coherency groups (i.e., one group around 180°, one group around 0° degrees, and the third group around -180°) at the instability moment which proves the claim. Assuming there are three generators in a specific case and at the instability moment, there is a generator (i.e., G3) with a rotor angle of the following value.

$$\delta_3(t_{ins}) = \frac{\delta_1(t_{ins}) + \delta_2(t_{ins})}{2} \tag{27.4}$$

In this case, the angle difference between any two generators may be exactly 180 degrees. In other words, having three groups at the instability moment is possible. With this respect, the

number of coherent generator groups is two or three at the instability moment, as shown in the following figure.

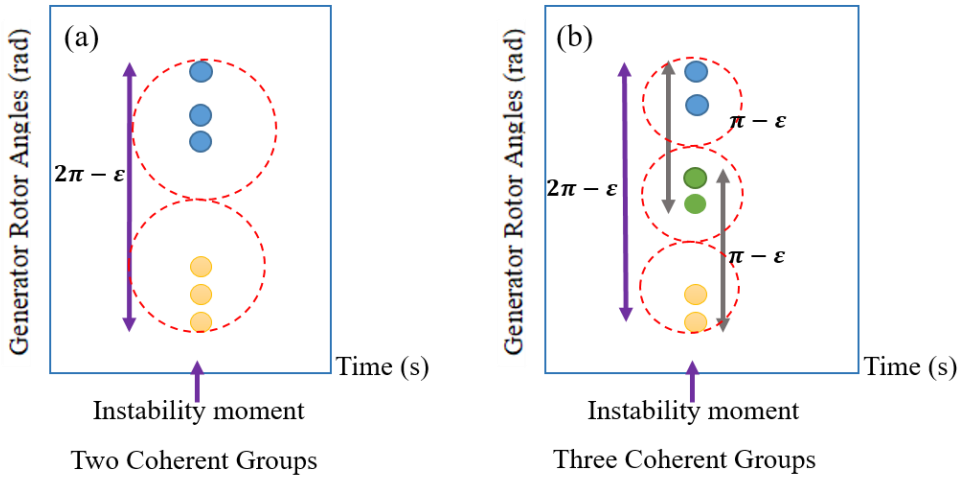

Figure 4-6. Coherent groups of generators at the instability moment: (a) two groups and (b) three groups

To extract the coherency patterns, an algorithm based on K-means is employed. According to the proposed algorithm, K-means for three groups of generators is applied first. Then, cluster centers are iteratively updated to the means of the rotor angle data points assigned to them. If the electrical distance between the centers of the three groups meets the criteria, the number of coherent generator groups remains at three; otherwise, K-means for two groups is simulated, and the generators are classified into two coherent groups. The flowchart of the proposed algorithm to identify coherent generators for each unstable scenario in an offline manner is illustrated in the figure below.

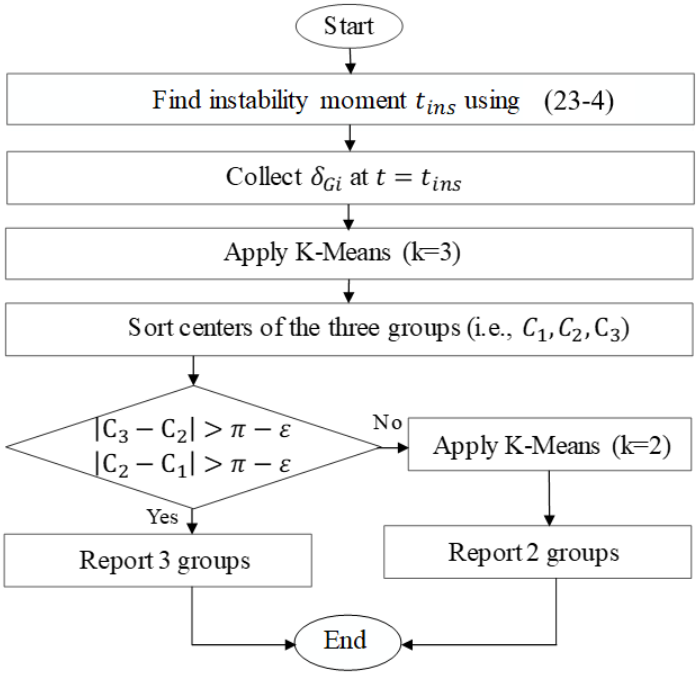

Figure 4-7. The flowchart of proposed coherency identification method

Using the proposed algorithm, the minimum number of coherency pattern for each unstable scenario related to each micro model is determined in an offline fashion. The introduced classifier is employed for each micro model to predict the coherency patterns. It is worth mentioning that the micro model strategy simplifies coherency prediction and increases the overall accuracy by classifying the transmission lines. Since some transmission lines only have one coherency pattern and according to the micro model strategy definition, transmission lines are classified into two groups: critical and non-critical. The following equations determine the criticality of each transmission line.

$$M_{ij} = \frac{N_{ij}^{U}}{N_{ij}^{S}} \times \left\lceil \frac{N_{ij}^{CP} - 1}{N_{ij}^{CP} + 1} \right\rceil \times 100 \tag{28.4}$$

$$LC_{ij} = \begin{cases} 1 & M_{ij} \neq 0 \\ 0 & otherwise \end{cases} \tag{29.4}$$

where $\lceil \bullet \rceil$ represents the ceil function and zero and one represent non-critical and critical lines, respectively. M_{ij} is a criterion that determines the criticality of lines and also specifies the percentage of unstable cases for critical lines. N_{ij}^{U}, N_{ij}^{S}, and N_{ij}^{CP} , are number of unstable cases, number of generated cases, and number of coherency patterns for line ij, respectively. Those lines

without unstable cases or with only one coherency pattern are considered non-critical lines. Based on the defined criteria, non-critical lines clearly have only one coherency pattern, and once an unstable scenario is predicted for them, the proper RCA can be directly predicted according to their coherency patterns. Therefore, the micro model strategy and line categorization solve a big challenge in predicting coherency for non-critical lines and improve the accuracy of coherency prediction for critical lines. The pre-fault and post-fault voltage values of generator terminals are fed into the designed classifier as input to predict the coherency patterns for critical lines. In addition, the determined coherency patterns are considered as output. Therefore, the coherency prediction module for each micro model is converted to a multi-class classification problem.

To sum it up, when a fault occurs on a transmission line, and the stability prediction module predicts the status of the scenario as "unstable," the coherency prediction module predicts the coherency pattern for all critical lines in real-time. As it is mentioned, non-critical lines have only one coherency pattern; thus, no coherency prediction is needed for these lines, and the only existing coherency pattern is sent to the RCA prediction module.

4.2.4 Remedial control action prediction module

In this module, the proper RCA is predicted for any new unstable fault scenario identified by the first module and based on the coherency pattern predicted by the second module. In this study, a combination of controlled islanding and load shedding is considered as the RCA. To predict RCA, proper RCA should be calculated for each unstable scenario in the offline process. RCA calculation inherently is an optimization problem that optimally determines the appropriate RCAs based on the input fault scenario with computational time on the order of hundreds of milliseconds to a few seconds depending on the optimization methods and the size of the power network [93], [98]. In this study, a mixed-integer linear programming (MILP) model is utilized to determine the optimal RCA. The splitting points, generation changes, and amounts of load shedding can be obtained by solving an optimization problem. The goal of the objective function is to minimize the total amount of load shedding and the total number of line switches. The objective function is given by the following equation.

$$\min\Big(\sum_{i \in \Omega^L} \alpha_i \Delta P_i^{shed} + \sum_{i \in \Omega^G} RC_i(\Delta P g_i^+ + \Delta P g_i^-) + \sum_{i \in \Omega^B} \sum_{j \in \Omega^B} \beta_{ij} U_{ij}\Big) \tag{30.4}$$

Where Ω^{L}, Ω^{G}, and Ω^{B}represent the set of loads, set of generators, and set of buses, respectively. Also, α_i and β_{ij} are penalty factors for load shedding at bus *i*, and switching line *ij*, respectively. The $\Delta P_i^{shed}$and $\Delta P_{Gi}^{+/-}$ indicate load shedding at bus *i*, and generation increment/decrement of generator *i* after islanding. The RC_i parameter is a specific amount for each generator, which is the primary response of a generator to a contingency. When a line is switched off, the corresponding binary variable is 1 (i.e., $U_{ij} = 1$), and otherwise 0 (i.e., $U_{ij} = 0$).

To consider the dynamic model of generators, the swing equations related to the response of generators to the contingency are considered in the optimization problem. The power swing equations are integrated into optimization problem by the following equations.

$$M_i\ddot{\delta}_i + D_i\dot{\delta}_i = P_{m_i} - P_{e_i} \quad i \in \Omega^G \tag{31.4}$$

$$P_{e_i} = E_i \cdot \sum_{j\in\Omega^G} Y_{ij} \cdot E_j \cos(\theta_i - \theta_j) \tag{32.4}$$

$$\dot{\delta}_i = \omega_i - \omega_0 \tag{33.4}$$

These equations are discretized using the trapezoidal rule as follows. The n and h indicate the discretization step counter and discretization time step, respectively.

$$M_i\left(\omega_i^{n+1} - \omega_i^n\right) + D_i\left(\delta_i^{n+1} - \delta_i^n\right) = \frac{h}{2}\cdot\left(P_{m_i} - \sum_{i\in\Omega^B} P_{e_i}^{n+1} + P_{m_i} - \sum_{i\in\Omega^B} P_{e_i}^{n}\right) \ \forall i \in \Omega^G \tag{34.4}$$

$$\delta_i^{n+1} - \delta_i^n = \frac{h}{2}(\omega_i^{n+1} - \omega_0 + \omega_i^n - \omega_0) \tag{35.4}$$

To check the transient stability condition after islanding the below criteria should be satisfied for each island.

$$\left|\delta_i^k - \delta_j^k\right| \le 2\pi \quad \forall i,j \in \Omega^G \tag{36.4}$$

Since the DC power flow is ignoring the reactive power and voltage, the AC power flow equations are included in the optimization problem. Also, the AC power flow equations are linearized using Taylor series and the obtained results are included in the optimization problem.

$$P_{ij} = V_i * V_j * \left(G_{ij} * Cos\delta_{ij} + B_{ij} * Sin\delta_{ij}\right) - V_i^2 * G_{ij} \tag{37.4}$$

$$Q_{ij} = V_i * V_j * \left(G_{ij} * Sin\delta_{ij} - B_{ij} * Cos\delta_{ij}\right) + V_i^2 * (B_{ij} - \frac{B_{ij}^{sh}}{2}) \quad (38.4)$$

$$P_{ij} = G_{ij} * \left(V_i + V_j - 1\right) + B_{ij} * \delta_{ij} + G_{ij} * (1 - 2 * V_i) \quad (39.4)$$

$$Q_{ij} = G_{ij} * \delta_{ij} - B_{ij} * \left(V_i + V_j - 1\right) + (2 * V_i - 1) * (B_{ij} - \frac{B_{ij}^{sh}}{2}) \quad (40.4)$$

Note that, after islanding the voltage and angle differences should be close to normal operating conditions which means ($V_i = V_j \approx 1, \delta_{ij} \approx 0$). Active and reactive power balance equations for each bus are given Equations (41.4)-(43.4).

$$\sum_{j=1}^{N_{Bus}} P_{ij} = (\, Pg_i^0 + \Delta Pg_i^+ - \Delta Pg_i^-) - (Pd_i - \Delta Pd_i^{shed}) \quad (41.4)$$

$$\sum_{j=1}^{N_{Bus}} Q_{ij} = (\, Qg_i^0 + \Delta Qg_i^+ - \Delta Qg_i^-) - (Qd_i - \Delta Qd_i^{shed}) \quad (42.4)$$

$$\Delta Qd_i^{shed} = \Delta Pd_i^{shed} * tan\varphi_i \quad (43.4)$$

Considering line switching status, the new power flow equation is as follow

$$P_{ij} = G_{ij} * \left(V_i + V_j - 1\right) + B_{ij} * \delta_{ij} + G_{ij} * (1 - 2 * V_i) * U_{ij} \quad (44.4)$$

The new equation need to be linearized. To achieve this goal, an auxiliary variable P_{ij}^f is defined. According to this, the power balance equations are such as:

$$P_{ij}^f = (G_{ij} * \left(V_i + V_j - 1\right) + B_{ij} * \delta_{ij} + G_{ij} * (1 - 2 * V_i)) \quad (45.4)$$

$$-M * \left(1 - U_{ij}\right) \leq P_{ij} - P_{ij}^f \leq M * (1 - U_{ij}) \quad (46.4)$$

$$-P_{ij}^{max} * U_{ij} \leq P_{ij} \leq P_{ij}^{max} * U_{ij} \quad (47.4)$$

Where $M$is a large number, the similar equations can be written for reactive balance. The operational constraints are given by:

$$0 \leq \Delta Pg_i^+ \leq \Delta Pg_i^{max+} \qquad i \in \Omega^g \quad (48.4)$$

$$0 \leq \Delta Pg_i^- \leq \Delta Pg_i^{max-} \qquad i \in \Omega^g \quad (49.4)$$

$$0 \le \Delta Qg_i^+ \le \Delta Qg_i^{max+} \qquad i \in \Omega^g \tag{50.4}$$

$$0 \le \Delta Qg_i^- \le \Delta Qg_i^{max-} \qquad i \in \Omega^g \tag{51.4}$$

$$V_i^{min} \le V_i \le V_i^{max} \qquad i \in \Omega^b \tag{52.4}$$

To check the connectivity of each island and dis-connectivity of different islands, four constraints are added to the optimization problem. In this regard, the $N_{bus} \times N_{bus}$ adjacency matrix is formed for the islanded network. A new matrix $A^{con-dis}$ is defined. For example, for two islands with N and M coherent generators in each island, respectively, $A^{con-dis}$ can be represented in the following form:

$$A_{N_G \times N_G}^{con-dis} = \begin{bmatrix} a_{11} & \dots & a_{1N} & b_{11} & \dots & b_{1M} \\ \vdots & \ddots & \vdots & \vdots & \ddots & \vdots \\ a_{N1} & \dots & a_{NN} & b_{N1} & \dots & a_{NM} \\ c_{11} & \dots & c_{1N} & d_{11} & \dots & d_{1N} \\ \vdots & \ddots & \vdots & \vdots & \ddots & \vdots \\ c_{M1} & \dots & c_{MN} & d_{N1} & \dots & d_{NN} \end{bmatrix} \tag{53.4}$$

The elements of $A_{N_G \times N_G}^{con-dis}$ matrix are obtained by the Dijkstras algorithm [107].

$$A_{ij}^{con-dis} = \begin{cases} 1 & if \text{ Dijkstras} \ge 1 \\ 0 & otherwise \end{cases} \tag{54.4}$$

Then, four linear constraints are integrated to check the connectivity of coherent generators in each island and dis-connectivity of non-coherent generators in separate islands, as follows

$$A_{N \times N} = I_{N \times N} \tag{55.4}$$

$$B_{N \times M} = Z_{N \times M} \tag{56.4}$$

$$C_{M \times N} = Z_{M \times N} \tag{57.4}$$

$$D_{M \times M} = I_{M \times M} \tag{58.4}$$

where I and Z are identity and zero matrices, respectively. By solving the MILP optimization problem, the islanding and load shedding patterns of unstable cases are extracted in offline simulations.

So far, the islanding boundaries and amount of load shedding for each load are calculated for each unstable scenario in an offline fashion. However, islanding boundaries and load shedding results are predicted using two modules, which can be run at the same time.

Since the micro model strategy is used, there are few islanding patterns for each MMS.

Therefore, for each MMS, a classifier is trained using the generated dataset. Regarding the interdependency of islanding problem and coherent generators, the coherency patterns are considered as input along with pre-fault and post-fault voltage values of generators' terminals. In addition, the islanding patterns for each line are considered as output. As it is mentioned, the number of islanding patterns for each MMS is a finite number. Therefore, the prediction of islanding patterns can be viewed as a supervised learning multi-class classification problem.

The optimized amount of load shedding and location of loads to be shed are obtained by running the above-mentioned optimization problem considering operational constraints. The load shedding prediction module predicts the amount of load shedding at each load bus. Although the corresponding output variable ΔP_i^{Shed} from the optimization problem is a continuous variable, each load bus has specific feeders, and it is not possible to shed any amount of load. Therefore, the amount of load shedding is normalized for each load using the following equation. Also, the load shedding results are rounded up to the predefined classes to make the prediction more straightforward.

$$\Delta P_i^{Shed} = \frac{\Delta P_i^{Shed}\ (calculated)}{P_{Li}} \tag{59.4}$$

For each load 11 feeders are considered as below.

Table 4-1. Discretizing the amount of load shedding

$\Delta \boldsymbol{P_i^{Shed}}$ (%)	Class number 1-11	Final amount of load shedding (%)
$\boldsymbol{L = 0}$	1	0
$\boldsymbol{0 < L \leq 10}$	2	10
$\boldsymbol{10 < L \leq 20}$	3	20
$\boldsymbol{20 < L \leq 30}$	4	30
$\boldsymbol{30 < L \leq 40}$	5	40
$\boldsymbol{40 < L \leq 50}$	6	50
$\boldsymbol{50 < L \leq 60}$	7	60
$\boldsymbol{60 < L \leq 70}$	8	70
$\boldsymbol{70 < L \leq 80}$	9	80
$\boldsymbol{80 < L \leq 90}$	10	90
$\boldsymbol{90 < L}$	11	100

Therefore, the linear regression problem is converted to a multi-class classification problem by discretizing the load shedding variables. The load shedding prediction module provides two pieces of information: 1) load to be shed (location), and 2) amount of load shedding for each load. From the simulation results, it turned out that for each micro model set, there is a specific set of loads (SSLs) that require load shedding. Therefore, the micro model strategy simplifies the load shedding prediction significantly by reducing the number of targets for the designed classifier. Similar to the islanding prediction module, the pre-fault and post-fault voltage values of generators and coherency patterns are considered as inputs. Also, the SSLs that need load shedding with the obtained results from the optimization problem are fed into the designed classifier as output. Note that the predicted amount of load shedding might be overestimated; however, considering the severity of a power system blackout and its economic consequences, a slightly higher amount of load shedding can be neglected.

So far, three modules, including transient stability, coherency, and RCA prediction modules, are explained in detail. To sum it up, a comprehensive diagram of the proposed framework is depicted in the following figure. As mentioned, only one coherency pattern exists for each non-critical line. Thus, for that pattern, the proper RCA is predicted using the last module of the proposed framework.

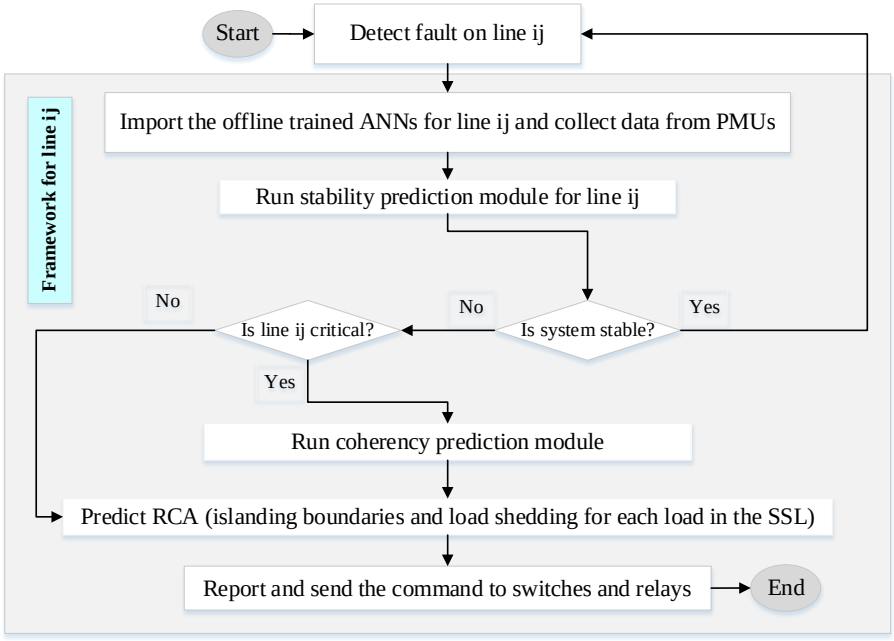

Figure 4-8. A comprehensive flowchart of the proposed framework

4.3 Simulation results and discussion

Two test systems, including the IEEE 39-bus system and 74-bus Nordic power network, are used to verify the performance of the proposed framework. Bulk scenarios are generated through DIgSILENT Programming Language (DPL) commands for both systems, as discussed in chapter 3. Full dynamic simulations are performed using DIgSILENT PowerFactory to monitor the rotor angle dynamics before and after applying the proposed RCA scheme. The optimization model for RCA calculation (i.e., determining the islanding boundaries and amount of load shedding) is coded in the GAMS environment and solved using the CPLEX solver. The ANN training and coherency identification are performed using MATLAB. All simulations are performed on an Intel 3.4 GHz CPU with 16 GB of RAM. For both test systems, 80% of the generated dataset is randomly selected for training the machine learning models, and the remaining 20% is used to test the framework's performance. In the next subsections, different modules' performances are shown in detail for two case studies.

4.3.1 Case1: IEEE 39-Bus system

As discussed in chapter 3, there is no parallel line in the IEEE 39-bus system. Therefore, the number of MMSs and the number of transmission lines are the same and equal to 34. According to the criticality criteria, the MMSs are categorized into two groups, including critical and non-critical. For critical MMSs, all three modules are implemented. However, only stability and RCA prediction modules are run for non-critical lines.

4.3.1.1 Transient stability prediction module

In this module, the stability status of each fault event is investigated. Because there are 10 generators in the IEEE 39-bus system, data are collected from all generators using 10 post-fault cycles (PFCs). 34 modules are run to predict the stability status of each MMS. For each MMS, 20% and 80% of the dataset are selected for test and training. Using K-fold (K=5), the classifier for each MMS is trained and tested using a different set of data. The following table shows the percentage of stable and unstable cases and the average accuracy of this module for different MMSs.

Table 4-2. Accuracies of stability prediction module for MMSs in IEEE 39-bus system

MMS	Number of stable cases	Number of unstable cases	M_{ij}	Accuracy of stable cases	Accuracy of unstable cases
{1-2}	4825	175	3.5%	99.28%	98.32%
{1-39}	4849	151	3.02%	99.31%	98.89%
{2-3}	4722	278	5.56%	99.55%	98.37%
{2-25}	4326	674	13.48%	98.89%	98.75%
{3-4}	4697	303	6.06%	99.1%	98.66%
{3-18}	4685	315	6.3%	99.66%	98.36%
{4-5}	4893	107	2.14%	99.38%	98.72%
{4-14}	4871	129	2.58%	99.17%	98.91%
{5-6}	4818	182	3.64%	99.09%	98.63%
{5-8}	4724	276	5.52	98.87%	98.82%
{6-7}	4803	197	3.94%	99.73%	98.31%
{6-11}	4896	104	2.08%	99.29%	98.65%
{7-8}	4911	89	1.78%	99.58%	98.39%
{8-9}	4915	85	1.7%	99.13%	98.7%
{9-39}	4787	213	4.26%	99.81%	98.27%
{10-11}	4652	348	6.96%	99.08%	98.79%
{10-13}	4679	321	6.5%	98.94%	98.87%
{13-14}	4795	205	4.1%	99.17%	98.69%
{14-15}	4757	243	4.86%	99.11%	98.9%
{15-16}	4192	808	16.17%	99.88%	98.27%
{16-17}	3879	1121	22.42%	99.29%	98.72%
{16-19}	3908	1092	21.85%	99.17%	98.38%
{16-21}	3919	1081	21.63%	98.88%	98.75%
{16-24}	3905	1095	21.9%	99.47%	98.83%
{17-18}	4324	676	13.52%	99.26%	98.68%
{17-27}	4491	509	10.18%	99.75%	98.39%
{21-22}	4208	792	15.84%	99.01%	98.62%
{22-23}	4051	949	18.98%	99.38%	98.75%
{23-24}	4588	412	8.97%	98.95%	98.84%
{25-26}	4283	717	14.34%	99.19%	98.58%

{26-27}	3673	1327	26.54%	99.38%	98.71%
{26-28}	3672	1328	26.55%	99.14%	98.86%
{26-29}	3683	1317	26.35%	98.92%	98.79%
{28-29}	3063	1937	38.74%	99.27%	98.64%

According to the results obtained from stability prediction module, the average accuracy of this module for each MMS is more than 98.6%. The overall accuracy of this module for IEEE 39-bus system is 98.95%.

4.3.1.2 Coherency prediction module

According to the algorithm shown in the methodology section (figure), the coherency patterns for unstable cases are identified at the instability moment. As it is mentioned, the MMS can be classified into two groups, including critical and non-critical MMSs, based on the number of coherency patterns. The following figure shows the critical lines for the IEEE 39-bus system.

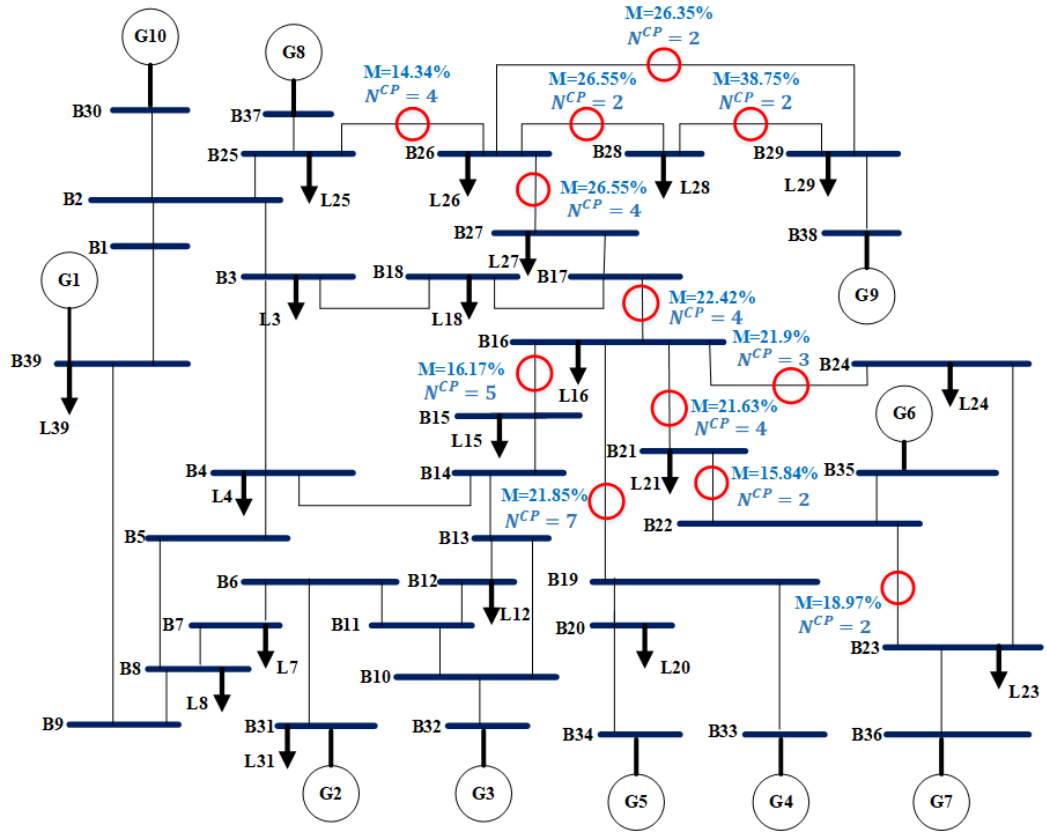

Figure 4-9. Schematic to show the number of coherency patterns along with percentage of unstable cases in IEEE 39-bus system

In addition, an unstable scenario is chosen to show the importance of minimizing the number of coherency patterns for optimizing RCA. To do so, a three-phase fault is applied on MMS {16-19} at t=5s for 186 ms. For this scenario, the deviations of generator rotor angles in different time windows are shown in figure 10-4. The rotor angles from t=6~7 s are shown in figure 10-4 (a). Transient stability analysis based on this time interval results in only two coherent groups of generators and, thereby, partitions the power system into two islands without any load shedding. Additionally, as shown in figure 10-4 (b), there are three coherent groups of generators according to the rotor angle dynamics for a longer time window from t=6~9 s. In this case, maintaining transient stability is achieved by partitioning the power system into three smaller islands with a total of 19.9 MW load shedding. Also, as shown in figures 10-4 (c) and (d), longer time windows result in a greater number of coherency groups and additional amounts of load shedding. According to the obtained results, RCA schemes with a smaller number of islands can reduce the amount of load shedding. Therefore, in the RCA scheme design, it is desirable to minimize the number of islands as much as possible. In this regard, two or three coherent groups of generators are considered for each unstable scenario.

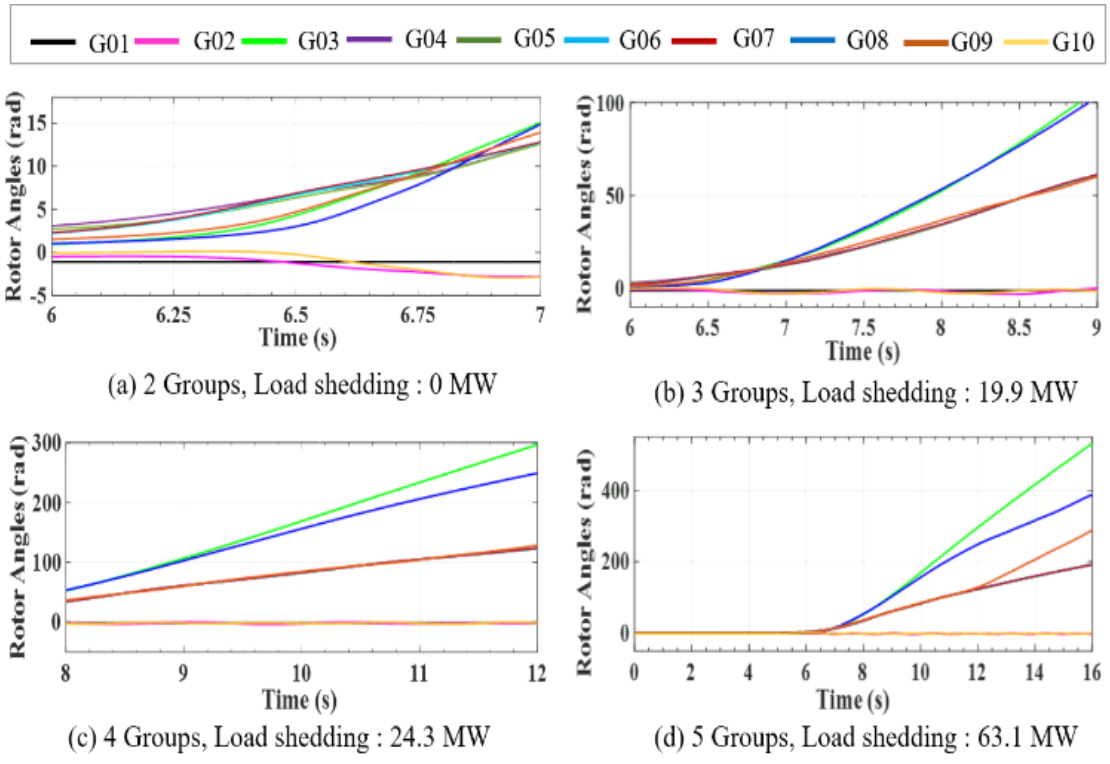

Figure 4-10. Schematic to show the variation of coherent generators over time and the required RCA to stabilize the network for different number of generator groups

The coherency patterns for each MMS are shown in the following table. Also, the accuracy of the coherency prediction module for each MMS in the IEEE 39-bus system is represented.

Table 4-3. Coherency patterns for different MMSs in IEEE 39-bus system and accuracy of coherency of prediction module

MMS	N^{CP}	**Group 1**	**Group 2**	**Accuracy of coherency prediction module**
{1-2}	1	G1	G2-G10	100 %
{1-39}	1	G1, G10	G2-G9	100 %
{2-3}	1	G1-G3, G10	G4-G9	100 %
{2-25}	1	G1-G2, G10	G3- G9	100 %
{3-4}	1	G1-G3, G8-G10	G4-G7	100 %
{3-18}	1	G1-G3, G10	G4-G9	100 %
{4-5}	1	G1	G2-G10	100 %
{4-14}	1	G1	G2-G10	100 %
{5-6}	1	G1-G3	G4-G10	100 %
{5-8}	1	G1-G3	G4-G10	100 %
{6-7}	1	G1-G3	G4-G10	100 %
{6-11}	1	G2-G3	G1, G4-G9	100 %
{7-8}	1	G1	G2-G10	100 %
{8-9}	1	G1	G2-G10	100 %
{9-39}	1	G1	G2-G10	100 %
{10-11}	1	G2-G3	G1, G4-G9	100 %
{10-13}	1	G3	G1-G2, G4-G10	100 %
{13-14}	1	G2, G3	G1, G4-G10	100 %
{14-15}	1	G1-G2, G10	G3-G9	100 %
{15-16}	5	G1-G3, G8-G10	G4-G7	95.19 %
		G1-G3, G8, G10	G4-G7, G9	
		G9	G1-G8, G10	
		G1, G2, G10	G3-G9	
		G1, G2, G8-G10	G3-G7	
{16-17}	4	G9	G1-G8, G10	95.61 %
		G1-G2, G8-G10	G3-G7	

		G8-G9	G1-G7, G10	
		G1-G3, G8-G10	G4-G7	
{16-19}	7	G1-G3, G8-G10	G4-G7	94.8 %
		G1-G3, G8, G10	G4-G7, G9	
		G1, G2	G3-G10	
		G1, G2, G10	G3-G9	
		G1	G2-G10	
		G9	G1-G8, G10	
		G1, G2, G8-G10	G3-G7	
{16-21}	3	G6-G7	G1-G5, G8-G10	94.23 %
		G9	G1-G8, G10	
		G4-G7	G1-G3, G8-G10	
{16-24}	2	G6-G7	G1-G5, G8-G10	95.63 %
		G9	G1-G8, G10	
{17-18}	1	G8-G9	G1-G7, G10	100 %
{17-27}	1	G9	G1-G8, G10	100 %
{21-22}	2	G6-G7	G1-G5, G8-G10	94.42 %
		G6	G1-G5, G7-G10	
{22-23}	2	G6-G7	G1-G5, G8-G10	93.96 %
		G4-G7	G1-G3, G8-G10	
{23-24}	1	G6-G7	G1-G5, G8-G10	100 %
{25-26}	4	G9	G1-G8, G10	95.66 %
		G8-G9	G1-G7, G10	
		G1, G2 G8-G10	G3-G7	
		G1-G3, G8-G10	G4-G7	
{26-27}	4	G9	G1-G8, G10	94.88 %
		G8-G10	G1-G7	
		G8-G9	G1-G7, G10	
		G1, G2, G8-G10	G3-G7	
{26-28}	2	G9	G1-G8, G10	94.14 %
		G8-G9	G1-G7, G10	
{26-29}	2	G9	G1-G8, G10	94.59 %

		G8-G9	G1-G7, G10	
{28-29}	2	G9	G1-G8, G10	93.74 %
		G8-G9	G1-G7, G10	

It is worth mentioning that $N^{CP}$is the number of dominant coherency patterns, which are patterns repeated more than two times. For example, MMS {1-2} has 175 unstable cases. Among those cases, the coherency pattern for 172 cases is {G1}, {G2-G10}. Three cases have different patterns. Because those cases are not repeated at least three times, they are not considered in the coherency prediction module. To show the effectiveness of the micro model strategy, a comparison is made on the coherency prediction module with previous methods. The results of the comparison are shown in the following table. The proposed framework exhibits high accuracy (more than 93%) in predicting coherent generator groups following a disturbance for all critical lines. The mean accuracy of the proposed coherency prediction module for all lines is about 98.14%. The table below shows that the previous methods achieved less than 90% accuracy. Considering the required number of PFCs, the proposed method remarkably improves the coherency prediction.

Table 4-4. Comparison between existing method and proposed framework for coherency prediction

MMS	**Proposed Framework**	**DT [92]**	**ANN [93]**	**QR [24]**
	10 PFCs	20 PFCs		
{16-17}	95.61%	86.16%	77.63%	86.31%
{16-19}	94.8%			
{16-21}	94.23%			
{15-16}	95.19%			
{16-24}	95.63%			
{21-22}	94.42%			
{22-23}	93.96%			
{25-26}	95.66%			
{26-27}	94.88%			
{26-28}	94.14%			
{26-29}	94.59%			
{28-29}	93.74%			

4.3.1.3 RCA prediction module

As discussed, this module has two parts including islanding boundaries prediction and load shedding prediction. First, using introduced optimization method in methodology section, the islanding pattern are determined for each unstable scenario. The islanding patterns are obtained for each MMS are represented in the following table. In addition, the prediction accuracy for islanding prediction is indicated for each MMS.

Table 4-5. Islanding patterns and islanding prediction module's accuracies for all MMSs in 39-bus system

MMS	Number of islanding patterns	Switched lines	Accuracy of islanding prediction module
{1-2}	1	1-2, 9-39	100 %
{1-39}	2	2-25, 2-3, 9-39 2-25, 2-3, 5-8, 7-8	96.31 %
{2-3}	2	2-25, 18-17, 14-15 2-25, 18-17, 4-14, 13-14	97.69 %
{2-25}	1	2-3, 2-25, 4-5, 6-11	100 %
{3-4}	4	3-4, 4-5, 13-14, 17-18, 25-26 3-18, 4-14, 13-14, 25-26 2-3, 3-4, 14-15, 25-26 2-3, 4-5, 4-14, 15-16, 25-26	95.83 %
{3-18}	2	2-25, 18-17, 14-15 2-25, 18-17, 4-14, 13-14	97.85 %
{4-5}	1	1-2, 9-39	100 %
{4-14}	1	1-2, 9-39	100 %
{5-6}	2	1-2, 3-4, 15-14 1-2, 4-5, 13-14	96.11 %
{5-8}	2	1-2, 3-4, 15-14 1-2, 4-5, 13-14	97.36 %
{6-7}	2	1-2, 3-4, 15-14 1-2, 4-5, 13-14	96.4 %

{6-11}	2	5-6, 6-7, 13-14 5-6, 7-8, 13-14	96.05 %
{7-8}	1	1-2, 9-39	100 %
{8-9}	1	1-2, 9-39	100 %
{9-39}	1	1-2, 9-39	100 %
{10-11}	2	5-6, 6-7, 13-14 5-6, 7-8, 13-14	97.62 %
{10-13}	1	6-11, 13-14	100 %
{13-14}	2	5-6, 6-7, 13-14 5-6, 7-8, 13-14	97.12 %
{14-15}	1	2-3, 2-25, 4-5, 6-11	100 %
{15-16}	12	4-14, 13-14, 17-18, 17-27 3-4, 4-5, 13-14, 16-17 3-18, 14-15, 17-27 2-3, 3-4, 15-16, 17-27 3-4, 4-5, 13-14, 17-18, 25-26 3-18, 4-14, 13-14, 25-26 2-3, 3-4, 14-15, 25-26 2-3, 4-5, 4-14, 15-16, 25-26 17-27, 25-26 3-18, 16-17, 25-26 2-3, 2-25, 4-5, 6-11 2-3, 4-5, 6-11, 17-27	96.28 %
{16-19}	13	4-14, 13-14, 17-18, 17-27 3-4, 4-5, 13-14, 16-17 3-18, 14-15, 17-27 2-3, 3-4, 15-16, 17-27 3-4, 4-5, 13-14, 17-18, 25-26 3-18, 4-14, 13-14, 25-26 2-3, 3-4, 14-15, 25-26	96.21 %

		2-3, 4-5, 4-14, 15-16, 25-26	
		1-2, 4-5, 6-11	
		2-3, 2-25, 4-5, 6-11	
		1-2, 9-39	
		17-27, 25-26	
		2-3, 4-5, 6-11, 17-27	
{16-21}	7	16-21, 16-24	96.24 %
		17-27, 25-26	
		3-18, 16-17, 25-26	
		4-14, 13-14, 17-18, 17-27	
		3-4, 4-5, 13-14, 16-17	
		3-18, 14-15, 17-27	
		2-3, 3-4, 15-16, 17-27	
{16-24}	3	16-21, 16-24	97.33 %
		17-27, 25-26	
		3-18, 16-17, 25-26	
{17-18}	2	2-3, 2-25, 3-4, 16-17	97.26 %
		2-25, 3-18, 16-17	
{17-27}	2	17-27, 25-26	98.12 %
		3-18, 16-17, 25-26	
{21-22}	2	16-21, 16-24	96.87 %
		16-21, 22-23	
{22-23}	5	16-21, 16-24	97.23 %
		4-14, 13-14, 17-18, 17-27	
		3-4, 4-5, 13-14, 16-17	
		3-18, 14-15, 17-27	
		2-3, 3-4, 15-16, 17-27	
{23-24}	1	16-21, 16-24	100 %
{25-26}	9	17-27, 25-26	97.58 %
		3-18, 16-17, 25-26	

		2-3, 2-25, 3-4, 16-17	
		2-25, 3-18, 16-17	
		2-3, 4-5, 6-11, 17-27	
		4-14, 13-14, 17-18, 17-27	
		3-4, 4-5, 13-14, 16-17	
		3-18, 14-15, 17-27	
		2-3, 3-4, 15-16, 17-27	
{26-27}	7	17-27, 25-26	96.82 %
		3-18, 16-17, 25-26	
		1-2, 3-4, 16-17	
		1-2, 2-3, 17-27	
		2-3, 2-25, 3-4, 16-17	
		2-25, 3-18, 16-17	
		2-3, 4-5, 6-11, 17-27	
{26-28}	4	17-27, 25-26	97.11 %
		3-18, 16-17, 25-26	
		2-3, 2-25, 3-4, 16-17	
		2-25, 3-18, 16-17	
{26-29}	4	17-27, 25-26	97.4 %
		3-18, 16-17, 25-26	
		2-3, 2-25, 3-4, 16-17	
		2-25, 3-18, 16-17	
{28-29}	4	17-27, 25-26	95.81 %
		3-18, 16-17, 25-26	
		2-25, 3-18, 16-17	
		2-3, 2-25, 3-4, 16-17	

As can be seen in the above table, the islanding patterns are predicted with high accuracy for all MMSs in the IEEE 39-bus system. To show the impact of considering coherency output as an input for this module, a comparison is performed for critical MMSs, and the results are

represented in the following table. This comparison proves the enhancement of islanding prediction accuracy by using coherency patterns as an input for the prediction module.

Table 4-6. Comparison between accuracies of islanding prediction for critical MMSs without/with coherency results as input

MMS	Accuracy without coherency results as an input (%)	Accuracy with coherency patterns as an input (%)
{16-17}	93.61	97.06
{16-19}	92.89	96.21
{16-21}	91.85	96.24
{15-16}	92.97	96.28
{16-24}	94.23	97.33
{21-22}	93.56	97.19
{22-23}	92.81	96.59
{25-26}	93.12	97.58
{26-27}	93.18	96.82
{26-28}	93.22	97.11
{26-29}	93.79	97.4
{28-29}	91.53	95.81

For each MMS, a small set of candidate loads for load shedding, referred to as the specific set of loads (SSL), are identified. Also, it reduces the solution space for the load shedding prediction and helps to decide how much and where to shed load with high accuracy. In this regard, the specific set of loads for each MMS are extracted using optimization and are shown in the following table for the IEEE 39-bus system. In addition, the average accuracy of the load shedding prediction module for each MMS is expressed.

Table 4-7. Specific set of loads for MMSs along with accuracy of load shedding prediction module for each MMS in IEEE 39-bus system

MMS	SSL	Accuracy of load shedding prediction module
{1-2}	$\{L_8\}$	97.53%

{1-39}	$\{L_7, L_8\}$	95.48%
{2-3}	-	100%
{2-25}	$\{L_8\}$	98.05%
{3-4}	$\{L_{31}, L_{39}\}$	95.65%
{3-18}	-	100%
{4-5}	$\{L_8\}$	96.81%
{4-14}	$\{L_8\}$	98.2%
{5-6}	-	100%
{5-8}	-	100%
{6-7}	-	100%
{6-11}	$\{L_{31}, L_{12}\}$	97.81%
{7-8}	$\{L_8\}$	96.32%
{8-9}	$\{L_8\}$	98.11%
{9-39}	$\{L_7, L_8\}$	96.7%
{10-11}	$\{L_{31}\}$	98.15%
{10-13}	$\{L_{31}, L_{12}\}$	95.84%
{13-14}	$\{L_{31}, L_{12}\}$	96.44%
{14-15}	$\{L_8\}$	97.53%
{15-16}	$\{L_{39}\}$	96.32%
{16-17}	$\{L_{39}\}$	96.88%
{16-19}	$\{L_7, L_8, L_{31}, L_{39}\}$	96.76%
{16-21}	$\{L_{31}, L_{39}\}$	94.36%
{16-24}	$\{L_7, L_8, L_{31}, L_{39}\}$	95.72%
{17-18}	$\{L_{26}, L_{28}\}$	95.55%
{17-27}	$\{L_{26}, L_{28}\}$	95.12%
{21-22}	$\{L_{39}, L_{21}\}$	96.18%
{22-23}	$\{L_{39}, L_{21}\}$	95.46%
{23-24}	-	100%
{25-26}	$\{L_{26}, L_{28}\}$	94.83%
{26-27}	$\{L_{26}, L_{28}\}$	96.31%
{26-28}	$\{L_{26}, L_{27}, L_{28}\}$	97.13%
{26-29}	$\{L_{26}, L_{27}, L_{28}\}$	96.58%
{28-29}	$\{L_{26}, L_{27}, L_{28}, L_{29}\}$	94.29%

The accuracies that are shown in the table are the average accuracy for all loads in each SSL related to the evaluated MMS. In fact, each load is predicted separately. For example, for two MMSs, the detail of the load shedding prediction module is illustrated in the following figure.

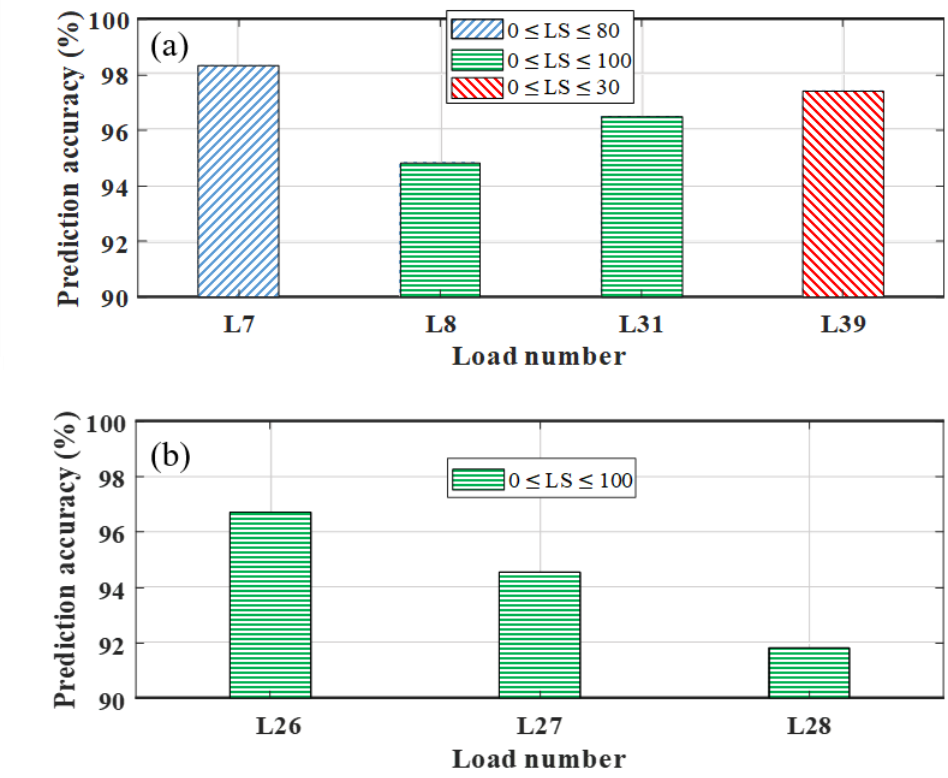

Figure 4-11. The detail of load shedding prediction module accuracies for MMSs (a) {16-19} and (b) {26-29} in IEEE 39-bus system

4.3.1.4 Evaluation of PMU noise impact on the performance of the proposed framework

In this part, white Gaussian noise with a signal-to-noise ratio of 34 dB is applied to the whole dataset. The training process is repeated for critical lines in the IEEE 39-bus system. The accuracies of the stability, coherency, and islanding prediction modules are given in table 8. Although the prediction accuracies are slightly decreased for all lines and in all modules, the three modules still have high and acceptable accuracies. Moreover, the total error of the PMU measurements should be less than 1% according to IEEE C37.118-2011, which is less than the amount considered. Therefore, the proposed framework can perform well in the presence of PMU noise.

Table 4-8. The accuracies of stability, coherency, and islanding prediction modules in the presence of PMU noise for critical MMSs in IEEE 39-bus system

MMS	Stability prediction accuracy without/with PMU noise (%)	Coherency prediction accuracy without/with PMU noise (%)	Islanding prediction accuracy without/with PMU noise (%)
{16-17}	99.05/ 97.24	95.61/ 94.08	97.06/ 94.93
{16-19}	98.78/ 96.81	94.8/ 92.73	96.21/ 94.36
{16-21}	98.81/ 96.49	94.23/ 92.88	96.24/ 94.28
{15-16}	99.07/ 96.87	95.19/ 93.13	96.28/ 94.51
{16-24}	99.15/ 97.38	95.63/ 93.71	97.33/ 95.58
{21-22}	98.82/ 96.67	94.42/ 92.65	97.19/ 94.92
{22-23}	99.06/ 96.9	93.96/ 92.53	96.59/ 94.61
{25-26}	98.89/ 96.51	95.66/ 94.03	97.58/ 95.85
{26-27}	99.04/ 96.88	94.88/ 93.11	96.82/ 94.33
{26-28}	99.01/ 96.58	94.14/ 92.7	97.11/ 95.58
{26-29}	98.85/ 96.42	94.59/ 93.22	97.4/ 95.73
{28-29}	98.95/ 96.75	93.74/ 92.19	95.81/ 94.28

4.3.1.5 A comparison between RCA calculation and RCA prediction

To better indicate the effectiveness of the proposed framework, two unforeseen scenarios for MMS {16-19} and MMS {23-24} are used as a test scenario on critical and non-critical MMS, respectively.

4.3.1.5.1 Unstable scenario on critical line

A three-phase fault is applied on a critical line (i.e., 16-19) at t =5 s and is cleared after 193 ms. Following fault detection and using the pre-fault and 10-cycle post-fault PMU data, the trained stability prediction module is run, and the status of the power system is predicted as unstable. Accordingly, the coherency prediction module identifies the coherency pattern. In this case, G1, G2, and G10 are in one coherent group, and the rest of the generators are in a second coherent group. Finally, the RCA prediction module determines the islanding boundaries and the amount of load shedding needed at each bus. As shown in table 5-4, there is only one islanding pattern for the predicted coherency pattern. Therefore, the system will be islanded immediately,

and the candidate loads (i.e., $\{L_7, L_8, L_{31}, L_{39}\}$) related to this MMS are predicted. The predicted amounts of load shedding are 10% of load 7 and 30% of load 8 without any load shedding for loads 31 and 39.

While the calculation time of RCAs is on the order of hundreds of ms, the prediction time is less than 10 ms for each module. Therefore, the predicted RCA can be applied in the system at t =5.679 s (i.e., 486 ms after clearing the fault, which is the time considering communication latencies and performing prediction modules). The rotor angle dynamics for the evaluated scenario are depicted in the following figure. If the operator takes action based on RCA calculation instead of RCA prediction, the islands identified will be the same as the islands predicted by the proposed module. In this case, the amount of load shedding is 26.32% of load 8. If the calculated RCA is initiated within less than 500 ms after clearing the fault, the system remains stable; otherwise, one of the islands will become unstable. Because the RCA calculation takes around 0.2-1 s based on the network size and considering communication latencies, the fastest calculated RCA can be applied at t =5.869 s. As shown in figure 12 (a), the first island becomes unstable. On the other hand, the proposed framework stabilizes both islands, as shown in figure 12 (b).

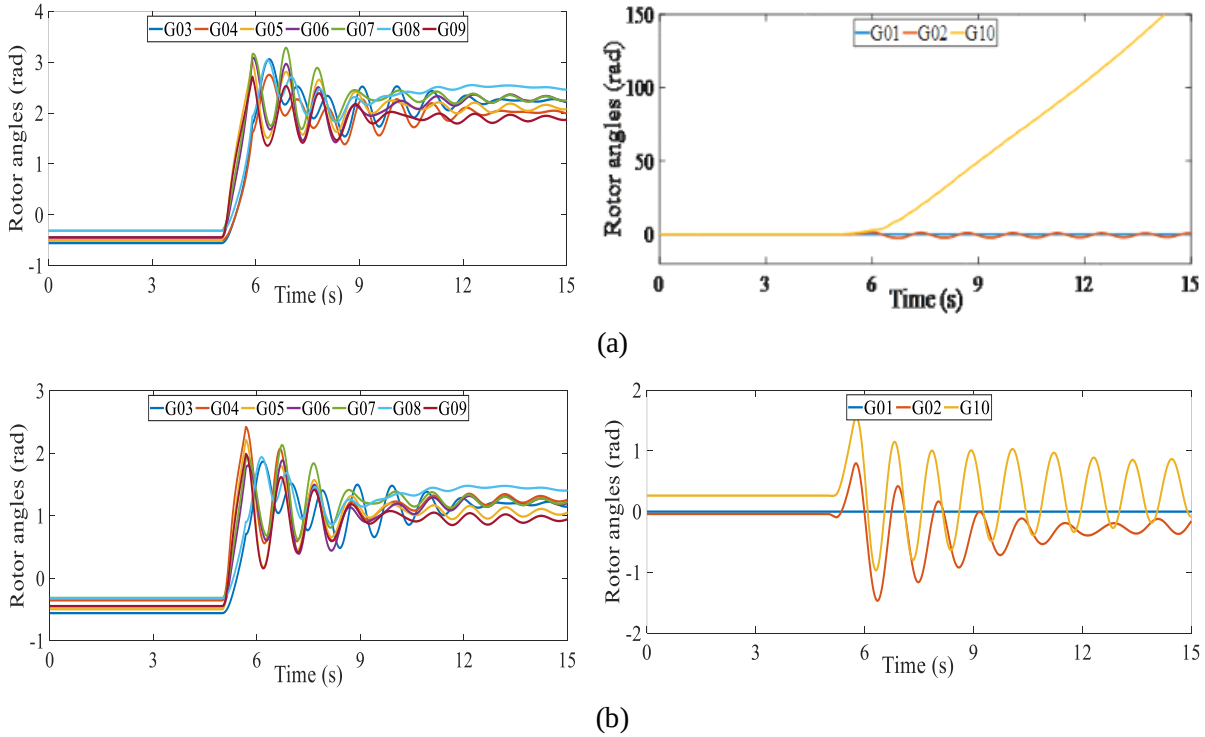

Figure 4-12. Generator rotor angles of island 1 and island 2 for critical line 16-19 after applying the (a) calculated RCA and (b) predicted RCA.

4.3.1.5.2 Unstable scenario on non-critical line

In this part, a three-phase fault is applied on a non-critical line (i.e., 23-24) at t=5 s for 200 ms. Since this non-critical line has only one coherency pattern, the predicted islanding and load shedding decisions are applied immediately after clearing the fault, similar to an event-based approach. Considering the communication delays, the predicted RCA trips lines 16-21 and 16-24 without any load shedding, which is applied 440 ms after clearing the fault. The same RCA is also calculated using the optimization problem, which takes 193 ms, and considering communication delays, the calculated RCA could be applied at t=5.793 s. According to figure 13, the time-consuming calculation-based RCA is not sufficiently fast and effective to prevent transient instability in one of the resulting islands, while the proposed prediction-based RCA maintains transient stability.

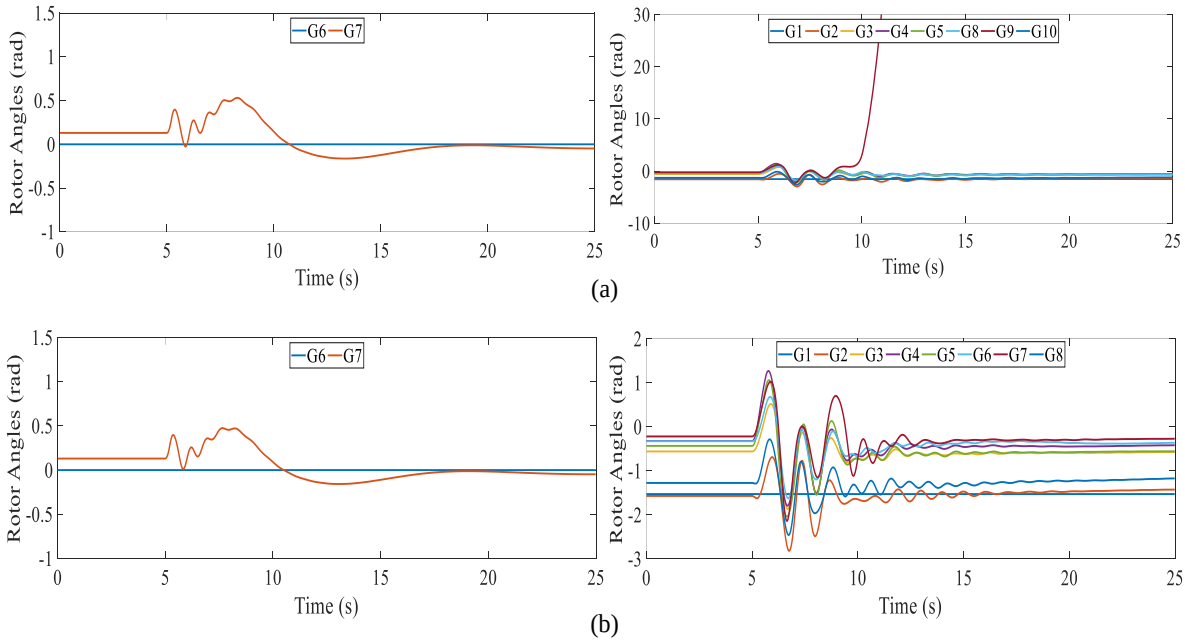

Figure 4-13. Generator rotor angles of island 1 and island 2 for non-critical line 23-24 after applying the (a) calculated RCA and (b) predicted RCA.

4.3.2 Case2: 74-bus Nordic power system

To assess the performance of the proposed technique on a large system, the developed modules have been applied to the 74-bus Nordic power system. As mentioned in chapter 3, the Nordic system has 37 MMS due to the presence of parallel lines. For each MMS, 6000 scenarios are generated, then critical and non-critical MMSs are selected based on defined criteria in (28.4)-

(29.4). As shown in figure 4-14, there are 10 critical MMSs in this test system. All three modules are run for the Nordic test system, and the results are shown in the following tables.

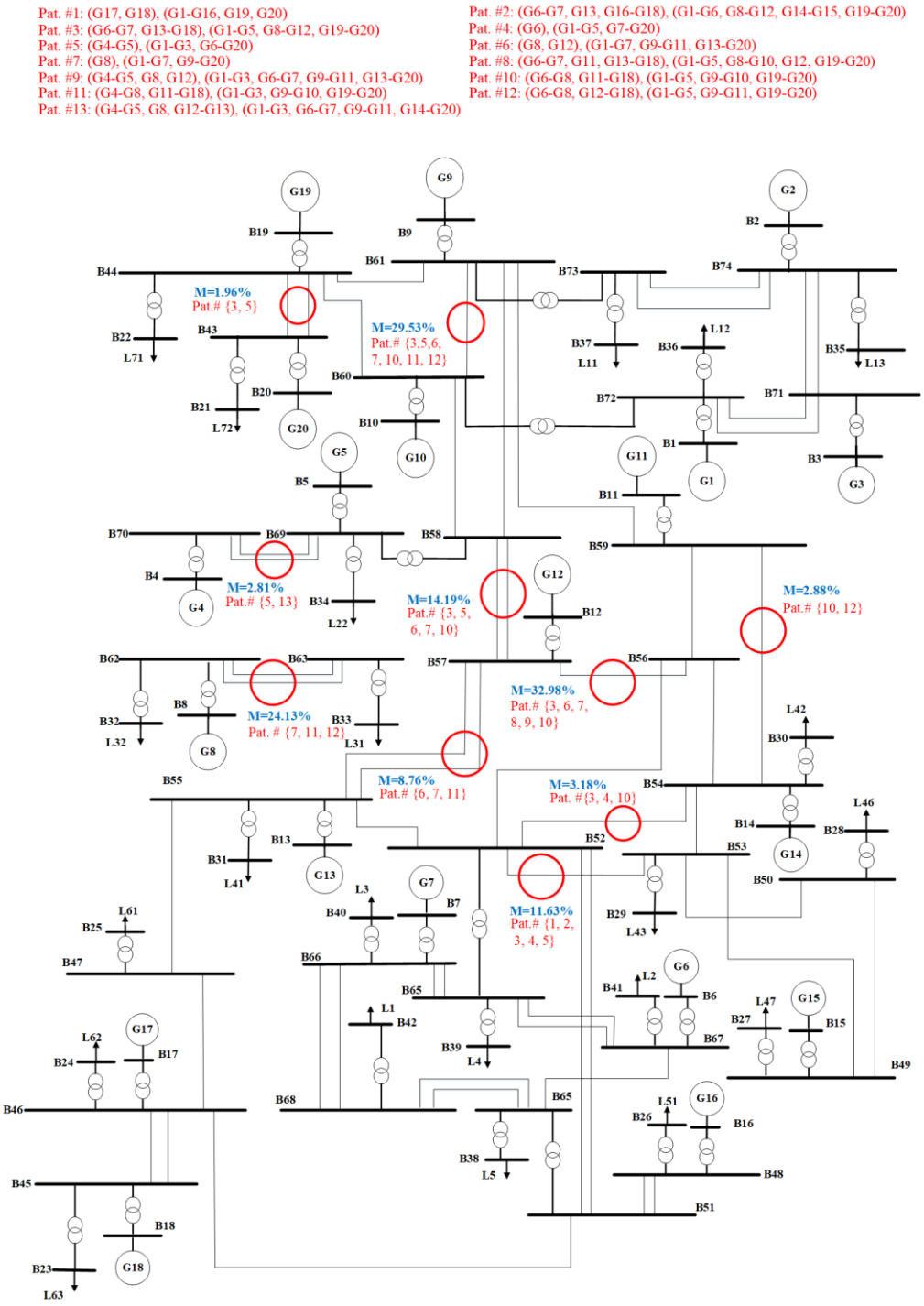

Figure 4-14. Diagram of Nordic power network representing the critical MMSs with their coherency patterns and percentage of their unstable cases

First, the stability prediction module is designed for each MMS. The percentage of unstable cases, criticality criteria, and the number of coherency patterns for all MMSs are represented in table 4-9.

Table 4-9. Data related to the stability prediction module for all MMSs in Nordic test system

MMS	Percentage of unstable cases	M_{ij} (%)	Prediction accuracy of stable cases	Prediction accuracy of stable cases
{43-44, 43-44*}	1.96%	1.96%	99.81 (%)	98.11 (%)
{46-45, 46-45*}	16.24%	0	99.83 (%)	99.15 (%)
{46-47}	5.45%	0	99.72 (%)	98.29 (%)
{50-49}	0.98%	0	99.89 (%)	97.81 (%)
{51-46}	1.54%	0	99.68 (%)	98.08 (%)
{48-51, 48-51*}	0	0	100 (%)	100 (%)
{51-52, 51-52*}	0	0	100 (%)	100 (%)
{49-53}	0	0	100 (%)	100 (%)
{50-53}	2.74%	0	99.75 (%)	98.26 (%)
{53-52}	11.63%	11.63%	99.92 (%)	98.38 (%)
{54-52}	3.18%	3.18%	99.8 (%)	98.24 (%)
{53-54}	1.48%	0	99.87 (%)	97.93 (%)
{47-55}	0	0	100 (%)	100 (%)
{52-55}	0	0	100 (%)	100 (%)
{56-52}	0	0	100 (%)	100 (%)
{54-56}	2.39%	0	99.85 (%)	98.39 (%)
{55-57, 55-57*}	8.76%	8.76%	99.8 (%)	98.71 (%)
{56-57}	32.98%	32.98%	99.74 (%)	99.25 (%)
{58-57, 58-57}	14.19%	14.19%	99.84 (%)	98.66 (%)
{54-59}	2.88%	2.88%	99.75 (%)	98.37 (%)
{56-59}	2.25%	0	99.88 (%)	98.54 (%)
{44-60}	0.6%	0	99.78 (%)	97.61 (%)
{58-60}	3.11%	0	99.72 (%)	98.33 (%)
{44-61}	1.32%	0	99.87 (%)	98.09 (%)
{61-58}	3.41%	0	99.81 (%)	98.65 (%)
{59-61}	1.93%	0	99.79 (%)	98.47 (%)

{60-61}	29.53%	29.53%	99.7(%)	98.39 (%)
{63-62, 63-62*}	24.13%	24.13	99.63 (%)	98.92 (%)
{66-65, 66-65*}	0	0	100 (%)	100 (%)
{64-67}	0	0	100 (%)	100 (%)
{65-67, 65-67*}	0	0	100 (%)	100 (%)
{64-68, 64-68*}	0	0	100 (%)	100 (%)
{66-68, 66-68*}	1.47%	0	99.75 (%)	98.38 (%)
{69-70, 69-70*}	2.81%	2.81%	99.88 (%)	98.57 (%)
{74-71, 74-71*}	0.78%	0	99.93 (%)	97.78 (%)
{72-71, 72-71*}	0	0	100 (%)	100 (%)
{74-73, 74-73*}	0	0	100 (%)	100 (%)

Using the proposed algorithm, the MMSs' coherency patterns are extracted at the instability moment for each unstable scenario. The patterns for each MMS are shown in table 4-10.

Table 4-10. Number of coherency patterns, coherency patterns, and the accuracy of the coherency prediction module for all MMS in Nordic power system

MMS	N_{ij}^{CP}	**Group1**	**Group2**	**Prediction accuracy of coherency patterns**
{43-44, 43-44*}	2	G4-G5 G6-G7, G13-G18	G1-G3, G6 -G20 G1-G5, G8-G12, G19-G20	99.42 %
{46-45, 46-45*}	1	G17, G18	G1-G16, G19-G20	100 %
{46-47}	1	G17, G18	G1-G16, G19-G20	100 %
{50-49}	1	G6, G7, G8, G12-G18	G1-G5, G9-G11, G19-G20	100 %
{51-46}	1	G17, G18	G1-G16, G19-G20	100 %
{48-51, 48-51*}	0	-	-	-
{51-52, 51-52*}	0	-	-	-
{49-53}	0	-	-	-
{50-53}	1	G6	G1-G5, G7-G20	100 %

{53-52}	5	G6-G7 G13, G16-G18	G1-G5, G8-G12, G14-G15, G19-G20	93.79 %
		G6-G7, G13-G18	G1-G5, G8-G12, G19-G20	
		G17, G18	G1-G16, G19-G20	
		G6	G1-G5, G7-G20	
		G4, G5	G1-G3, G6-G20	
{54-52}	3	G6-G8, G11-G18	G1-G5, G9-G10, G19-G20	98.75 %
		G6-G7, G13-G18	G1-G5, G8-G12, G19-G20	
		G6	G1-G5, G7-G20	
{53-54}	1	G6-G7, G13-G18	G1-G5, G8-G12, G19-G20	100 %
{47-55}	0	-	-	-
{52-55}	0	-	-	-
{56-52}	0	-	-	-
{54-56}	1	G6,G7, G11, G13-G18	G1-G5, G8-G10,G12,G19,G20	100 %
{55-57, 55-57*}	3	G8, G12	G1-G7, G9-G11, G13-G20	95.48 %
		G8	G1-G7, G9-G20	
		G4- G8, G11-G18	G1-G3, G9-G10, G19-G20	
{56-57}	6	G8, G12	G1-G7, G9-G11, G13-G20	94.07 %
		G6-G7, G13-G18	G1-G5, G8-G12, G19-G20	
		G8	G1-G7, G9-G20	
		G6-G7, G11, G13-G18	G1-G5, G8-G10, G12, G19-G20	
		G4-G5, G8, G12	G1-G3, G6-G7, G9-G11, G13-G20	
		G6-G8, G11-G18	G1-G5, G9-G10, G19-G20	
{58-57, 58-57*}	5	G6-G7, G13-G18	G1-G5, G8-G12, G19-G20	95.66 %
		G8	G1-G7, G9-G20	
		G4-G5	G1-G3, G6-G20	
		G8, G12	G1-G7, G9-G11, G13-G20	
		G6-G8, G11-G18	G1-G5, G9-G10, G19-G20	
{54-59}	2	G6-G8, G12-G18	G1-G5, G9-G11, G19-G20	98.81 %

		G6-G8, G11-G18	G1-G5, G9-G10, G19-G20	
{56-59}	1	G6-G8, G12-G18	G1-G5, G9-G11, G19-G20	100 %
{44-60}	1	G4-G8, G11-G18	G1-G3, G9-G10, G19-G20	100 %
{58-60}	1	G6-G7, G13-G18	G1-G5, G8-G12, G19-G20	100 %
{44-61}	1	G4-G8, G11-G18	G1-G3, G9-G10, G19-G20	100 %
{61-58}	1	G6-G7, G13-G18	G1-G5, G8-G12, G19-G20	100 %
{59-61}	1	G6-G7, G13-G18	G1-G5, G8-G12, G19-G20	100 %
{60-61}	7	G6-G7, G13-G18	G1-G5, G8-G12, G19-G20	93.82 %
		G6-G8, G11-G20	G1-G5, G9-G10, G19-G20	
		G4-G8, G11-G18	G1-G3, G9-G10, G19-G20	
		G6-G8, G12-G18	G1-G5, G9-G11, G19-G20	
		G8, G12	G1-G7, G9-G11, G13-G20	
		G4-G5	G1-G3, G6-G20	
		G8	G1-G7, G9-G20	
{63-62, 63-62*}	3	G8	G1-G7, G9-G20	95.82 %
		G4-G8, G11-G18	G1-G3, G9-G10, G19-G20	
		G6-G8, G11-G18	G1-G5, G9-G10, G19-G20	
{66-65, 66-65*}	0	-	-	-
{64-67}	0	-	-	-
{65-67, 65-67*}	0	-	-	-
{64-68, 64-68*}	0	-	-	-
{66-68, 66-68*}	1	G6-G7, G13-G18	G1-G5, G8-G12, G19-G20	100 %
{69-70, 69-70*}	2	G4-G5	G1-G3, G6-G20	96.58 %
		G4-G5, G8, G12-G13	G1-G3, G6-G7, G9-G11, G14-G20	
{74-71, 74-71*}	1	G4-G8, G11-G18	G1-G3, G9-G10, G19-G20	100 %
{72-71, 72-71*}	0	-	-	-
{74-73, 74-73*}	0	-	-	-

Since the output of the coherency prediction module is used as an input for the islanding and load shedding prediction modules, it is of paramount importance to increase the accuracy of

the coherency prediction module. Using generated dataset comprised of 222000 cases for the whole system and identified coherency patterns for all unstable scenarios (15081 cases). For the sake of comparison, four strategies are defined to highlight the advantages of the micro model strategy and the importance of identifying coherency patterns at the instability moment as two contributions of the proposed framework.

a) Time of identifying the coherency patterns: End of simulation time
Considered dataset: The whole dataset in one module ignoring the micro model strategy

This case is what the existing methods are using for coherency prediction. The coherency patterns are identified at the end of simulation time and the dataset is built for the whole system. All lines are evaluated by a single dataset and framework. In this case, based on the obtained data at the end of the simulations there are 1615 patterns for the whole network. The coherency prediction accuracy is 81.3% in this case which shows ignoring the proposed strategies significantly deteriorates the prediction accuracy for a large-scale power system.

b) Time of identifying the coherency patterns: End of simulation time
Considered dataset: The dataset built for each line separately based on the micro model strategy

In this part, the coherency patterns have extracted for all MMSs at the end of simulation time. Then, machine learning methods are employed to predict the coherency groups related to the MMS on which the fault has occurred. Since coherency patterns are extracted at the end of simulation time the number of coherency groups is not limited anymore and can be two, three, or more (2-19 groups in this case). For example, for MMS {43-44, 43-44*}, there are 63 different patterns comprised of 2-10 coherent groups. Moreover, some patterns are repeated only once or twice that affects the accuracy of the coherency prediction module remarkably. The coherency prediction for each micro model is performed separately and the average accuracy is 89.52% in this case, which is significantly lower than the accuracy of the proposed framework (i.e., 98.97%).

C) Time of identifying the coherency patterns: Instability moment
Considered dataset: The whole dataset in one module ignoring the micro model strategy

In this case, the number of coherency patterns for all unstable scenarios at the instability moment is 16 patterns for the whole system. The coherency prediction accuracy, in this case, is 94.19%, which is less than the average accuracy of 98.97% when the micro model strategy is employed for the same dataset.

D) **Time of identifying the coherency patterns: Instability moment**

Considered dataset: The dataset built for each line separately based on the micro model strategy

This case which utilizes the proposed strategies has the highest accuracy. The coherency prediction accuracy, in this case, is 98.97%. The obtained results show that the proposed framework keeps the accuracies at acceptable values for large-scale power systems while the existing methods fail to retain good accuracies for these systems.

So far, the stability and coherency prediction modules are evaluated using the Nordic test system. The subsequent paragraphs present the results related to RCA prediction modules. First, using the optimization methods the islanding patterns, SSLs, amounts of load shedding are determined for each MMS in the offline calculation. Then, two classifiers are trained for each MMS for online prediction of islanding boundaries and load shedding patterns. The islanding patterns and accuracy of islanding prediction are shown in table 4-11.

Table 4-11. Islanding patterns, and the accuracy of islanding prediction module for all MMSs in Nordic power network

MMS	Number of islanding patterns	Islanding patterns	Accuracy of islanding prediction module
{43-44, 43-44*}	2	60-58, 61-58, 57-58 55-57, 56-52, 56-54, 54-59	99.13 %
{46-45, 46-45*}	2	51-46, 47-47 51-46, 55-47	98.16 %
{46-47}	2	51-46, 47-47 51-46, 55-47	98.4 %
{50-49}	2	57-58, 56-59, 54-59 57-58, 56-57, 56-52, 54-59	98.09 %
{51-46}	2	51-46, 47-47	98.22 %

		51-46, 55-47	
{48-51, 48-51*}	-	-	-
{51-52, 51-52*}	-	-	-
{49-53}	-	--	-
{50-53}	1	64-67, 65-67	100 %
{53-52}	7	52-51, 55-52, 57-55, 65-67,66-65 53-52, 54-52, 56-52,57-55 56-52, 56-54, 57-55,54-59 51-46, 47-47 51-46, 55-47 64-67, 65-67 60-58, 61-58, 57-58	96.33 %
{54-52}	3	57-58, 59-61 57-55, 56-52, 56-54 64-67, 65-67	97.92 %
{53-54}	1	57-55, 56-52, 56-54	100 %
{47-55}	-	-	-
{52-55}	-	-	-
{56-52}	-	-	-
{54-56}	1	56-57, 55-57, 59-61	100 %
{55-57, 55-57*}	3	56-57, 57-55, 57-58 62-63 58-60, 58-61, 59-61	97.8 %
{56-57}	7	56-57, 55-57,57-58 57-55, 56-52, 56-54, 54-59 57-55, 56-57, 56-59, 54-59 63-62 57-55,56-57, 59-61 60-58, 61-58, 56-57, 55-57 57-58, 59-61	97.15 %
{58-57, 58-57*}	6	57-55, 56-52, 56-54, 54-59 57-55, 56-57, 56-59, 54-59	97.62 %

		63-62	
		60-58, 58-61, 57-58	
		55-57, 57-58, 56-57	
		57-58, 59-61	
{54-59}	2	57-58, 56-59, 54-59	98.34 %
		57-58, 56-57, 56-52, 54-59	
{56-59}	2	57-58, 56-59, 54-59	98.7 %
		57-58, 56-57, 56-52, 54-59	
{44-60}	1	61-58, 60-58, 59-61	100 %
{58-60}	2	57-55, 56-52, 56-54, 54-59	98.37 %
		57-55, 56-57, 56-59, 54-59	
{44-61}	1	61-58, 60-58, 59-61	100 %
{61-58}	2	57-55, 56-52, 56-54, 54-59	98.86 %
		57-55, 56-57, 56-59, 54-59	
{59-61}	2	57-55, 56-52, 56-54, 54-59	98.13 %
		57-55, 56-57, 56-59, 54-59	
{60-61}	9	55-57, 56-52, 56-54, 54-59	95.96 %
		55-57, 56-57, 56-59, 54-59	
		57-58, 59-61	
		58-61, 59-61, 60-58	
		54-59, 56-59, 57-58	
		56-57, 57-58, 56-52, 56-54, 54-59	
		57-58, 56-57,57-55	
		62-63	
		60-58, 61-58, 57-58	
{63-62, 63-62*}	3	63-62	97.84 %
		58-61, 59-61, 60-58	
		57-58, 59-61	
{66-65, 66-65*}	-	-	-
{64-67}	-	-	-
{65-67, 65-67*}	-	-	-
{64-68, 64-68*}	-	-	-

{66-68, 66-68*}	2	55-57, 56-52, 56-54, 54-59 55-57, 56-57, 56-54, 54-59	98.24 %
{69-70, 69-70*}	2	60-58, 61-58, 57-58 46-47, 52-55, 56-57, 58-61, 58-60	97.89 %
{74-71, 74-71*}	1	61-58, 61-59, 60-58	100 %
{72-71, 72-71*}	-	-	-
{74-73, 74-73*}	-	-	-

In addition, the specific set of loads (SSLs), and the average prediction accuracy for each MMS in Nordic power network are represented in table 4-12.

Table 4-12. The SSLs and average accuracy of load shedding prediction module for all MMSs in Nordic power network

MMS	**Specific set of loads (SSL)**	**Average accuracy of load shedding prediction module**
{43-44, 43-44*}	-	100 %
{46-45, 46-45*}	$\{L_{25}\}$	98.24 %
{46-47}	$\{L_{25}\}$	97.85%
{50-49}	$\{L_{25}, L_{26}, L_{39}, L_{41}\}$	96.73 %
{51-46}	$\{L_{25}\}$	98.04 %
{48-51, 48-51*}	-	-
{51-52, 51-52*}	-	-
{49-53}	-	-
{50-53}	-	100 %
{53-52}	$\{L_{23}, L_{24}, L_{25}, L_{26}, L_{31}, L_{39}, L_{41}\}$	95.33 %
{54-52}	$\{L_{23}, L_{24}, L_{39}, L_{41}\}$	96.77 %
{53-54}	$\{L_{23}, L_{24}, L_{39}, L_{41}\}$	96.6 %
{47-55}	-	-
{52-55}	-	-
{56-52}	-	-
{54-56}	$\{L_{23}, L_{24}, L_{25}, L_{26}, L_{31}, L_{39}, L_{41}\}$	95.82 %
{55-57, 55-57*}	$\{L_{26}, L_{27}, L_{32}, L_{33}, L_{38}, L_{39}, L_{41}\}$	94.87 %

{56-57}	$\{L_{23}, L_{24}, L_{25}, L_{26}, L_{31}, L_{39}, L_{41}\}$	95.26 %
{58-57, 58-57}	$\{L_{23}, L_{24}, L_{25}, L_{26}, L_{27}, L_{31}, L_{39}, L_{41}\}$	94.62 %
{54-59}	$\{L_{25}, L_{26}, L_{39}, L_{41}\}$	96.57%
{56-59}	$\{L_{25}, L_{26}, L_{39}, L_{41}\}$	97.22%
{44-60}	$\{L_{26}, L_{27}, L_{39}, L_{41}\}$	96.82 %
{58-60}	$\{L_{23}, L_{24}, L_{25}, L_{26}, L_{31}, L_{39}, L_{41}\}$	96.18 %
{44-61}	$\{L_{26}, L_{27}, L_{39}, L_{41}\}$	97.21 %
{61-58}	$\{L_{23}, L_{24}, L_{25}, L_{26}, L_{31}, L_{39}, L_{41}\}$	97.58 %
{59-61}	$\{L_{23}, L_{24}, L_{25}, L_{26}, L_{31}, L_{39}, L_{41}\}$	96.89 %
{60-61}	$\{L_{23}, L_{24}, L_{25}, L_{26}, L_{27}, L_{31}, L_{33}, L_{38}, L_{39}, L_{40}, L_{41}, L_{42}\}$	94.29 %
{63-62, 63-62*}	$\{L_{23}, L_{24}, L_{32}, L_{33}, L_{38}, L_{39}, L_{41}\}$	95.74 %
{66-65, 66-65*}	-	-
{64-67}	-	-
{65-67, 65-67*}	-	-
{64-68, 64-68*}	-	-
{66-68, 66-68*}	$\{L_{23}, L_{24}, L_{25}, L_{39}, L_{41}\}$	96.84 %
{69-70, 69-70*}	$\{L_{23}, L_{24}, L_{38}\}$	97.13 %
{74-71, 74-71*}	$\{L_{23}, L_{24}, L_{32}, L_{33}, L_{38}\}$	97.59 %
{72-71, 72-71*}	-	-
{74-73, 74-73*}	-	-

4.4 Conclusion

In this chapter, a new framework has been proposed to predict proper remedial control action (RCA) for preventing transient instability. To reduce the complexity of the problem and increase the prediction accuracy, the presented framework is implemented based on the micro model strategy, which means building a framework for individual lines separately and independently. This framework consists of three main modules, including transient stability, coherency, and RCA prediction. All three modules have been tested using the IEEE 39-bus system and 74-bus Nordic power network. The simulation results and comparisons show the effectiveness of the proposed framework.

5 A NOVEL FRAMEWORK FOR GENERATOR REJECTION PREDICTION TO PREVENT TRANSIENT INSTABILITY IN POWER SYSTEM USING WIDE-AREA MEASUREMENTS

5.1 Introduction

In this chapter, a novel generator rejection prediction is proposed to prevent transient instability in the power system. Since calculating the total amount of generator rejection and assigning the optimal amount of tripping to each generating facility is time-consuming, the optimal generator tripping calculation might be impractical for a real-life interconnected power system. In addition, communication delays deteriorate the efficiency of any wide-area remedial control action (RCA) in response to fault events which quickly evolve into transient instability. The proposed framework predicts the optimal generator rejection for critical generators based on pre-fault and post-fault generators' terminal voltage values. To simplify the problem, the proposed framework is designed for each set of micro models. The proposed framework consists of two main stages: offline optimization, which involves calculating proper RCAs using a full dynamic model of the power system for training the machine learning models, and online prediction. The effectiveness of the proposed framework is tested via the IEEE 9-bus system and the 74-bus Nordic test system.

5.2 Methodology

Generator rejection is one of the most commonly used RCAs to prevent transient instability [68-69]. Three important factors need to be considered while designing a generator rejection framework: 1) determining the accurate amount of generator rejection to stabilize the network, 2) identifying the critical generators, and 3) assigning the optimal amount of generator rejection to each critical generator. Therefore, generator shedding is an optimization problem, and it takes time to solve such a problem, especially for a large power network. In this regard, the generator rejection prediction is proposed, which moves the optimization problem to the offline training stage. After performing all calculations and optimization for each micro model set in an offline manner, three modules are trained to predict the proper RCA for each unstable scenario for individual MMSs. the first module predicts the stability status of the power network following a disturbance. If the system is predicted as unstable, the second module will be run and predict the critical generators. Finally, the amount of predicted generator shedding is assigned to each critical generator using the

third module. For prediction, the proposed classifier in chapter 4 (CBRDE-LM) is employed in all three modules. The following subsections discuss the principle of equal area criterion (EAC) and these three modules in detail.

5.2.1 Extended equal area criterion (EEAC)

The EEAC is an approach for assessing the transient stability of a multi-machine power system. It is a direct method that replaces the multi-machine power system with a two-machine equivalent network. Following a disturbance, the synchronous machines are categorized into two classes, including critical machines (CM) and non-critical machines (NM). Each generator that loses its synchronism will be considered as a critical machine. Then these two sets of machines are modeled as a two-machine equivalent system as follows.

$$M_{CM} = \sum_{i \in CM} M_i \,, \tag{1.5}$$

$$M_{NM} = \sum_{j \in NM} M_j \tag{2.5}$$

$$M_T = M_{CM} + M_{NM} \tag{3.5}$$

$$M = \frac{M_{CM} \cdot M_{NM}}{M_T} \tag{4.5}$$

$$\delta_{CM} = \frac{1}{M_{CM}} \cdot \sum_{i \in CM} M_i * \delta_i \tag{5.5}$$

$$\delta_{NM} = \frac{1}{M_{NM}} \cdot \sum_{j \in NM} M_j * \delta_j \tag{6.5}$$

Where M_{CM}, M_{NM}, and M denote the inertia coefficient for critical machines, non-critical machines, and system. δ_{CM} and δ_{NM} indicate the equivalent rotor angles for critical and non-critical machines. Using two machine system and following equations, the system converts into a single machine infinite bus system.

$$P_m = \frac{1}{M_T} \cdot \left(M_{NM} * \sum_{i \in CM} P_{mi} - M_{CM} \cdot \sum_{j \in NM} P_{mj} \right) \tag{7.5}$$

$$P_e = \frac{1}{M_T} \cdot \left(M_{NM} \cdot \sum_{i \in CM} P_{ei} - M_{CM} \cdot \sum_{j \in NM} P_{ej} \right) \tag{8.5}$$

$$\delta = \delta_{CM} - \delta_{NM}, \tag{9.5}$$

$$M \cdot \frac{d^2\delta}{dt^2} = P_m - P_e \tag{10.5}$$

where δ, M, P_m, and P_e represent rotor angle, inertia, mechanical power, and electrical power related to the equivalent SMIB system, respectively. Using the measurements data from the network and the above equations for SMIB, the $P - \delta$ curve is plotted, and the required assessment to find the stability status and amount of generator rejection to stabilize the network are calculated based on the energy concept. It is worth noting that the multi-machine equivalent keeps the characteristics of the system machines and topology. Therefore, the results and solutions of the established SMIB are in perfect agreement with the corresponding solution of the entire system.

5.2.2 Transient stability assessment

In normal operation conditions, the system is operated at a stable point, and there is a balance between electrical power and the mechanical power of generators. When a disturbance occurs in a power network, generators start fluctuating and gain kinetic energy. If the generators can absorb the released energy, the system goes to another stable point and remains stable. Otherwise, the system becomes unstable. To determine the stability status of the power system, the $P - \delta$ curve is plotted using pre-fault, during-fault, and post-fault data. For better understanding, a random $P - \delta$ is illustrated in figure 5-1.

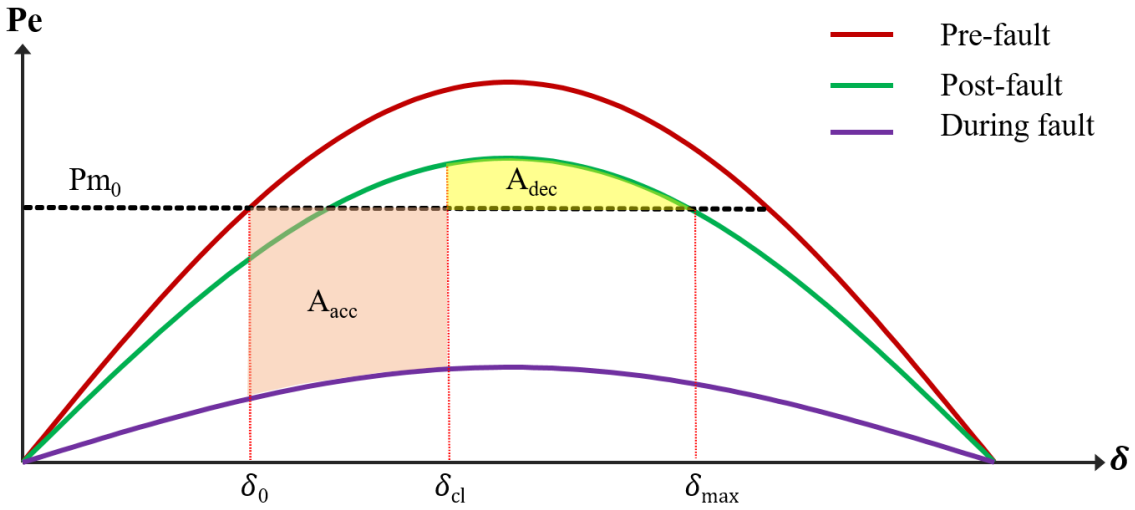

Figure 5-1. A representation of equal area criterion for a random scenario

As shown in figure 5-1, A_{acc} is the amount of energy of generators that increases during the fault and A_{dec} is the maximum energy that the power system can dissipate in the post-fault condition. The δ_0, δ_{cl}, and $\delta_{max} = \delta_u$ denote the rotor angle of SMIB at the fault moment, at the moment of clearing the fault, and the moment of instability, respectively. The stability status of the power system can be determined by calculating the difference between A_{acc} and A_{dcc} as follows:

$$A_{acc} = \int_{\delta_0}^{\delta_{cl}} (P_{m_0} - Pe_{Duringfault}(\delta))d\delta \tag{11.5}$$

$$A_{dcc} = \int_{\delta_{cl}}^{\delta_u} (Pe_{postfault}(\delta) - P_{m_0})d\delta \tag{12.5}$$

$$\eta = A_{dec} - A_{acc} \tag{13.5}$$

Where η represents the stability margin. According to this criterion, if $\eta < 0$, the system is unstable, otherwise the system remains stable.

5.2.3 Critical generator identification

As mentioned, critical generators are generators that lose their synchronism following a disturbance. When an out-of-step is detected for a generator, the generator is labeled as a critical machine. Since all the calculations are performed offline, the critical generators are identified at the end of the simulation time. In the following figure, the critical and non-critical generators are determined for a random unstable scenario.

$$CM_i = \begin{cases} 1 & out\ of\ step = 1 \\ 0 & otherwise \end{cases} \quad i = 1,2,..,N_G \tag{14.5}$$

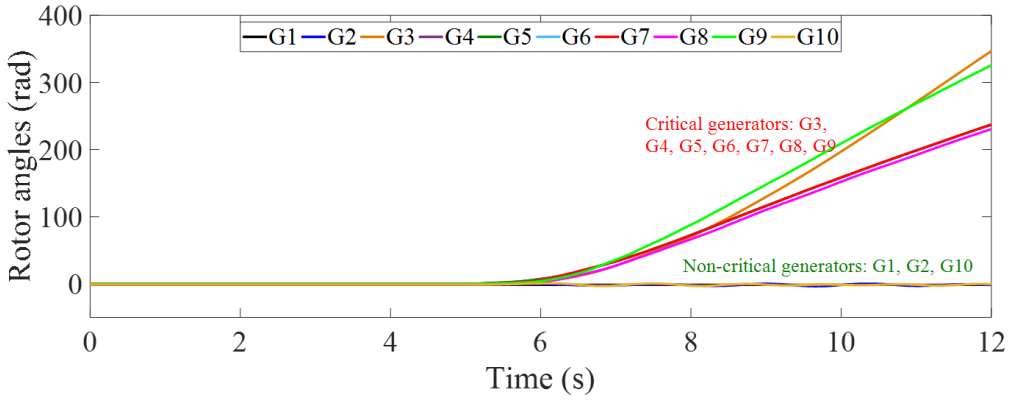

Figure 5-2. Identifying critical and non-critical generators for an unstable scenario

Since identifying critical generators is performed offline, data of the entire system for the whole simulation time is available. Therefore, the critical generators can simply be extracted for each unstable scenario.

5.2.4 Generator Rejection calculation

Two pieces of information need to be calculated to obtain optimal generator rejection: 1) amount of generator rejection to stabilize the system and 2) distributing the generator rejection optimally among critical generators. First, the amount of required generator rejection is calculated to stabilize the power network using the $P-\delta$ curve. In this regard, the mechanical power of the equivalent generator in the SMIB system should be reduced to increase the deceleration area and preserve system stability. The process is shown in figure 5-3.

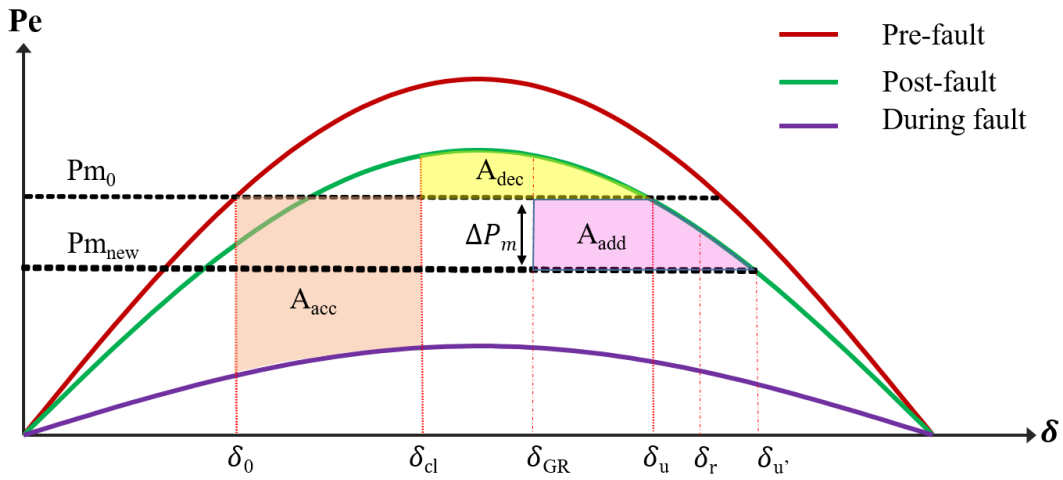

Figure 5-3. Schematic to show the process of increasing deceleration area by generator rejection

Where δ_{GR}, δ_r, and $\delta_{u'}$indicate the rotor angle at the moment generator rejection applied, the moment which rotor angle return, and the crossing point of post-fault electrical power and new mechanical power, respectively. According to above figure and equation (15.5), the amount of the required generator rejection and a new stability margin is calculated.

$$A_{acc} \leq A_{dec_{new}} = \int_{\delta_{cl}}^{\delta_{GR}} \left(Pe_{postfault}(\delta) - P_{m_0}\right)d\delta + \int_{\delta_{GR}}^{\delta_{u'}} \left(Pe_{postfault}(\delta) - P_{m_{new}}\right)d\delta \qquad (15.5)$$

As can be seen, there are two unknown variables in equation (15.5) (i.e. $P_{m_{new}}$, and $\delta_{u'}$). To calculate the amount of generator shedding ($\Delta P_m = Pm_0 - Pm_{new}$), a repetitive algorithm is

developed as shown in figure 4.5. First, an arbitrary value for $Pm_{new}^{(0)}$ necessarily lower than Pm_0 is chosen and using the SMIB, $P-\delta$ curve, $\delta_{u'}$ is determined. Then, $A_{dec_{new}}$ is calculated and compared with A_{acc}. If $A_{dec_{new}}^{(i)} = A_{acc} + \varepsilon$, where ε is a small positive constant. The process continues and the Pm_{new} will be updated until a stop criterion is satisfied.

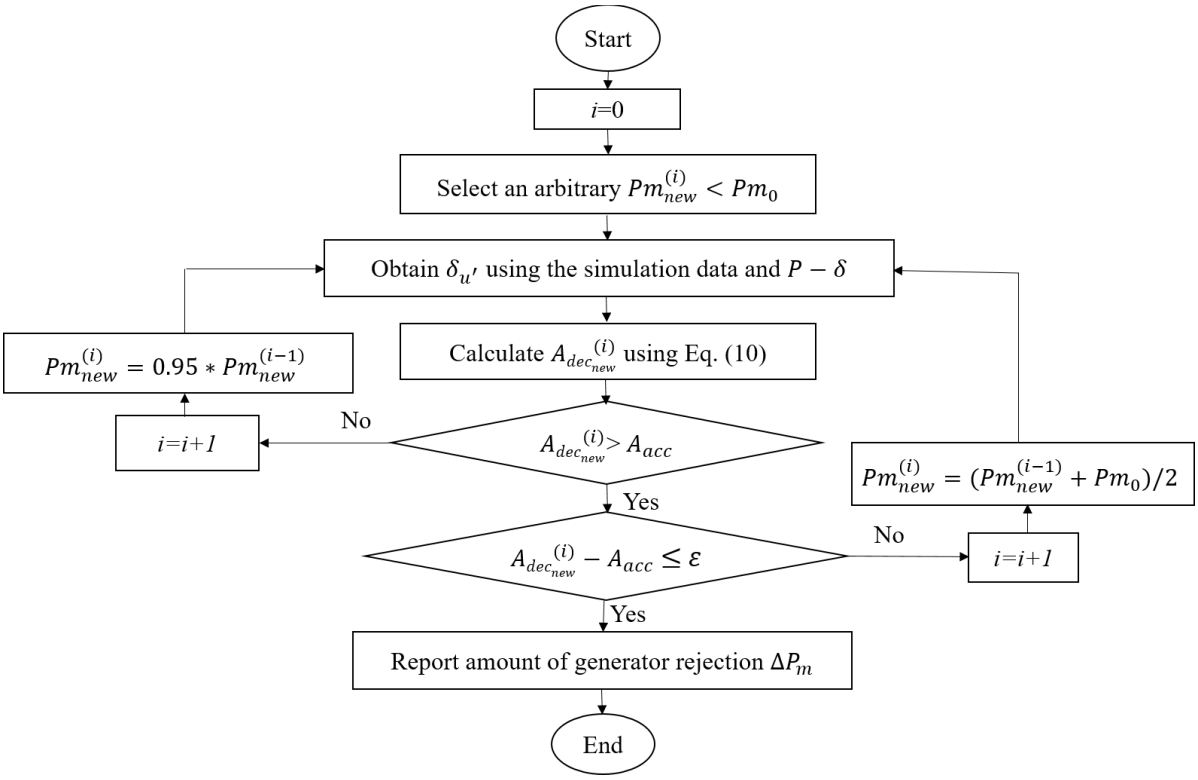

Figure 5-4. The flowchart of generator rejection calculation (ΔPm) algorithm

Since all these calculations are performed in an offline manner, the data are available, and computational time is not a concern. It is worth mentioning that only a specific amount of generator shedding is possible. In a real power network, a generating facility consists of multiple machines. In this study, 10 parallel machines with the same characteristics are considered to be in each power plant. Therefore only a specific amount of generator could be shed from each power plant. Take, for instance, a sample power network in figure 5-5; the calculated amount of generator shedding based on EEAC is 26.5 MW. However, the minimum amount of generator shedding, which is close to the calculated amount and is possible to trip immediately, is 30 MW. Therefore, the discretized essence of generator tripping should be considered in the offline calculation.

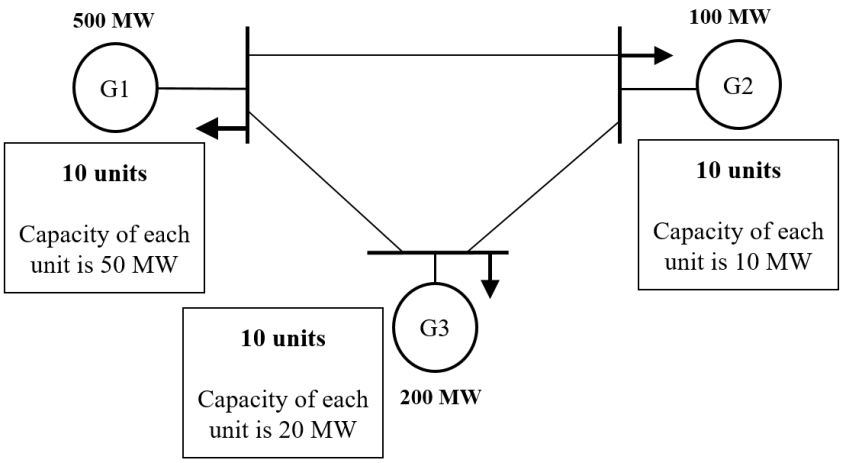

Figure 5-5. An example to show the discretize essence of generator shedding

So far, the required amount of generator shedding is calculated for the SMIB system. In the second part of the offline generator shedding calculation, the location of generator shedding should be determined optimally. To do so, an optimization problem is defined to assign the minimum amount of generator shedding to critical generators so that the summation of generator shedding is greater than or equal to the calculated amount of generator shedding, and maximizes the stability margin. The objective function, and the operational constraints, can be expressed as follows.

$$\min \sum_{i \in \Omega^G} \Delta P_{G_i} - \beta (A_{dec} - A_{Acc}) \tag{16.5}$$

$$\sum_{i \in \Omega^G} \Delta P_{G_i} \geq \Delta P_m \tag{17.5}$$

$$P_{G_i}^{min} \leq P_{G_i} \leq P_{G_i}^{max} \tag{18.5}$$

$$Q_{G_i}^{min} \leq Q_{G_i} \leq Q_{G_i}^{max} \tag{19.5}$$

A heuristic optimization algorithm is proposed to solve this problem. First, a random population is generated for critical generators. Among generated sets, those that satisfy $\sum_{i \in \Omega^G} \Delta P_{G_i} \geq \Delta P_m$ and operational constraints remain in the possible patterns, and others are removed. Next, the stability margin and objective function is calculated for all those cases. The optimal solution is selected among all possible patterns. As it is mentioned, the full dynamic of the system is considered in this optimization problem. To do so, Matlab and Power factory

(DIgSILENT) software are linked. Therefore, the possible patterns should preserve the system's stability as well. For *i* iterations, this process is repeated, and using the wolves algorithm, a set of possible patterns for generator shedding is obtained. The steps of the proposed algorithm are shown in the following figure.

Heuristic optimization Algorithm

Step1. Collect the data including ΔP_m, Critical generators, and amount of generation units steps for critical generators

Step2. Divide the ΔP_m between critical generators and form a set consist of all possible options $S^{(1)} = \left\{s_1^{(1)}, s_2^{(1)}, \dots, s_k^{(1)}\right\}$

Step3. $\forall\, S_j^{(1)} \in S^{(1)}$, if $\sum_{i=1}^{N_{CM}} \Delta P_{G_i}^{trip} \geq \Delta P_m$, form new $S^{(2)}$ icluding all cases satisfy this condition, $S^{(2)} = \left\{s_1^{(2)}, s_2^{(2)}, \dots, s_z^{(2)}\right\}$

Step4. Run the full dynamic simulation for those cases in $S^{(2)}$

Step5. Check stability status of all cases in *step4*, form $S^{(3)}$ including all cases stabilize the system, $S^{(3)} = \left\{s_1^{(3)}, s_2^{(3)}, \dots, s_x^{(3)}\right\}$

Step6. Calculate the stability margin for all cases in $S^{(3)}$

Step7. Report the best solution as optimize generator rejection scheme

Figure 5-6. Process of generator shedding optimization

5.3 Proposed framework

According to subsections (1.2.5)-(4.2.5), the methods for stability assessment, critical generator identification, and generator shedding optimization are explained in detail. As it is mentioned, the proposed framework consists of two main parts: the offline training stage and the online prediction stage. In this section, the above-mentioned methods are employed in the proposed framework to perform offline calculations. Furthermore, the introduced CBRDE-LM classifier in chapter 4 is employed as a machine learning engine to predict all three modules. In the following paragraphs, different parts of the proposed framework are explained point by point.

5.3.1 Bulk scenario generation

To train the machine learning models, bulk scenarios are generated for individual transmission lines (MMSs) to cover a credible number of scenarios. The dynamic behavior of the power network is closely related to fault location, fault duration, network configuration, and loading condition. Therefore, the random variation of these parameters is considered in the data generation process to generate a comprehensive dataset. Also, the data are generated for each MMS individually to reduce the problem's solution space, reduce the complexities of the prediction models and increase the prediction accuracy of the modules.

5.3.2 Transient stability prediction module

For all generated datasets, using the EEAC, the stability status of each scenario is determined. Scenarios with $\eta<0$ are labeled as unstable (i.e., 1), and scenarios with $\eta\geq0$ are labeled as stable (i.e., 0). Based on the generated dataset with two target classes, the stability prediction is converted to a binary classification problem. Using the pre-fault and post-fault voltage data of generator terminals, the machine learning engine is trained to predict the stability status of the power network. If a scenario is predicted as unstable, the trigger signal will be sent to the next modules to predict the critical generators and the amount of generator shedding for each critical generator.

5.3.3 Critical generator prediction module

According to the critical generator definition, the criticality of generators depends on the fault location. For a network with N_G number of generators, there are $2^{N_G}-1$ possible patterns for critical generators. Therefore, it is hard to identify critical generators online with high accuracy. Since there is a limited number of patterns for critical generators related to each MMS, using the micro model strategy reduces the complexity of the critical generator prediction significantly. In addition, according to the number of critical generator patterns for each micro model, MMSs can be classified into three groups as follows.

$$MMS_{i_C}=\begin{cases} Neutral & N_i^{CGP}=0 \\ Non-critical & N_i^{CGP}=1 \quad i=1,2,..,N_{MMS} \\ Critical & N_i^{CGP}\geq 2 \end{cases} \tag{20.5}$$

Where MMS_{i_C} and N_i^{CGP} represents the micro model set classes and the number of critical generator patterns forMMS_i, respectively. The neutral MMSs do not have any unstable cases in the scenario generation process. Therefore, if a fault occurs on these MMSs, no RCA action is required. In addition, sets of non-critical MMSs have only one pattern for critical generators. Therefore, the critical generator pattern prediction is not required for these MMSs, and the generator rejection prediction module is triggered following an instability detection immediately. Finally, the critical MMSs have a limited number of patterns for critical generators. Next, the patterns are extracted for each MMS. Since the number of patterns is limited, critical generator prediction is converted to a multi-class classification problem. Therefore, using pre-fault and post-fault voltage data and the generated dataset, the critical generator patterns for each critical MMS can be predicted by the CBRDE-LM classifier. It is worth noting that classifying the micro model sets and evaluating MMSs individually increase the average accuracy of this module significantly. To sum it up, if a fault scenario is predicted as unstable by the transient stability prediction module, the critical generator prediction module will predict the related critical generators and send the predicted critical generators pattern to the final module to predict the optimal amount of generator shedding as RCA.

5.3.4 Generator shedding Prediction module

As discussed, following an instability detection, the critical generators are predicted. Then, it is necessary to trip a specific number of units from each critical generator to stabilize the network. According to the heuristic optimization in the methodology section, the generation units' numbers that need to be shed from each critical generators are extracted for each unstable scenario. The number of generator tripping units can change from 0 (i.e., no generator shedding needed) and 10 (i.e., all the units of the power plants should be switched off).

$$\Delta P_{G_i}^{trip} \in \{k | \, 0 \leq k \leq 10, k \in z\}, \text{i} = 1,2,..,N_{CM} \tag{21.5}$$

If generator shedding is implemented for the entire network in one module, the generator shedding prediction should be implemented for all generators. However, only specific generators need generator shedding prediction when each MMS is evaluated separately. It significantly reduces the solution space and increases the overall accuracy of this module. Depending on the number of critical generators, the number of targets needing prediction is changed. Therefore, generator shedding prediction is an 11-classes classification problem with multi targets (i.e., the

number of critical generators related to each MMS). For individual MMSs, one classifier is trained for each critical generator related to that MMS. The pre-fault and post-fault voltage values of generator terminals, along with critical generator patterns, are fed into the classifier as input. Furthermore, the number of tripping units obtained from optimization is considered as output. To clarify the number of classifier in the generator shedding prediction module, a sample network is shown in the following figure as an example.

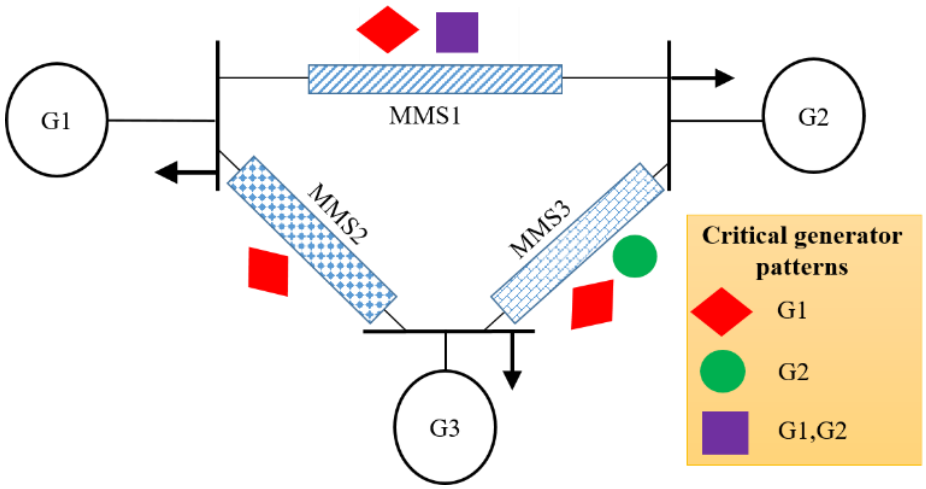

Figure 5-7. Sample power system to show the required number of classifier for generator shedding prediction

The MMS1 is a critical micro model. It has two patterns for critical generators, including G1 and G2. Therefore, two classifiers are trained in the generator shedding prediction module: 1) predict the number of units that need to be shed from G1 and 2) another classifier to predict generator shedding for G2. However, the MMS2 is a non-critical micro model. This MMS has only one critical generator for all unstable scenarios. Therefore, only one classifier is designed for G1 to predict the number of tripping units from this generator to preserve the system's stability. A comprehensive diagram of the proposed framework is illustrated in figure 5-8.

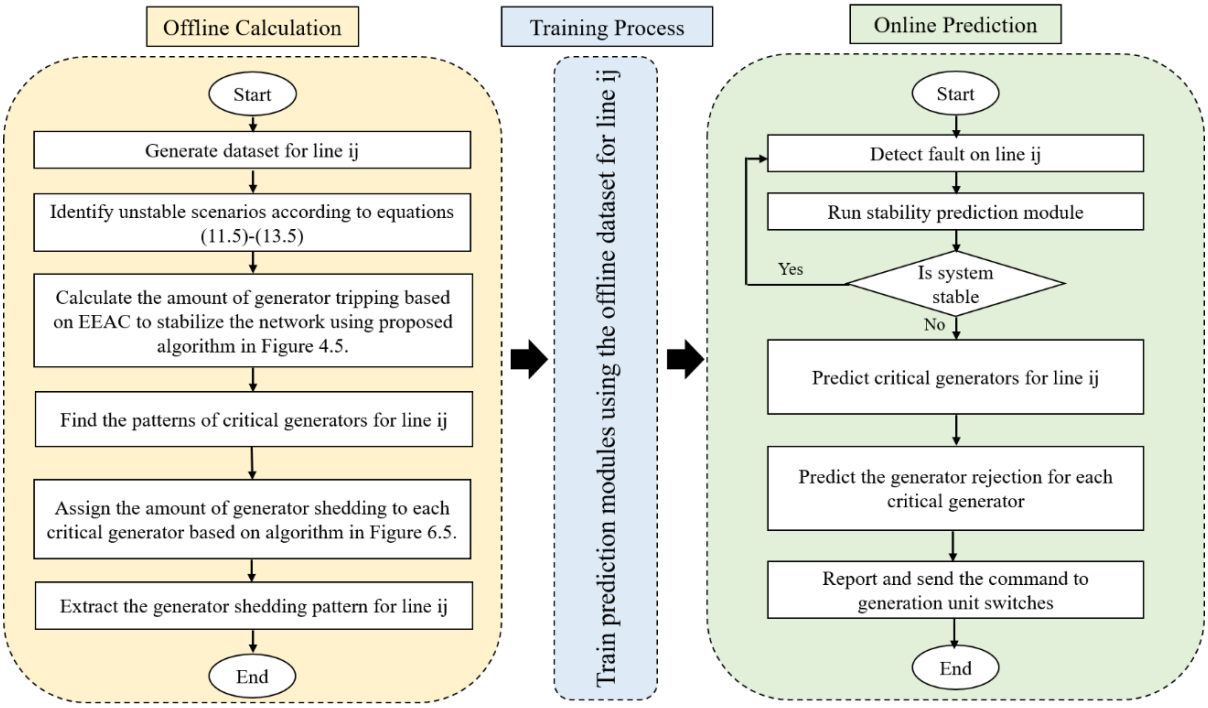

Figure 5-8. A comprehensive diagram of the proposed framework to predict optimal generator rejection for line ij

It is worth mentioning that the generator shedding could lead to an imbalance between generation and load in the network. However, the main focus of this framework is to prevent transient instability. In addition, the load shedding prediction is performed in chapter 4. Although it can be considered in the optimization problem, it increases the computational time significantly. Therefore, the load shedding is ignored in this framework. After stopping transient instability, the imbalance between generation and load could be simply calculated and applied to the network to improve the voltage and frequency of the system buses.

5.4 Simulation results and discussion

The performance of the proposed framework is validated using the IEEE 9-bus and 74-bus Nordic test systems. Bulk scenarios are generated using DIgSILENT programming language (DPL) commands. Full dynamic simulations are performed using DIgSILENT PowerFactory to derive the rotor angle curves of the power network before and after applying RCA. All the calculations, optimizations, and machine learning model training are coded and run using

MATLAB. In addition, DIgSILENT and MATLAB are linked to apply possible solutions in each step of optimization. All simulations are performed on an Intel 3.4 GHz CPU with 16 GB of RAM.

5.4.1 Case1: IEEE 9-bus system

As expressed in chapter 3, this network has 6 MMS. For Each MMS, 2000 scenarios are generated. To cover credible number of scenarios, important parameters including fault location, fault duration time, and system loading are varied randomly. Also, N-1 and N-2 contingencies are considered. The detail of the scenario generation process is expressed in chapter 3. All three modules are run for each MMS in this network to evaluate the effectiveness of the proposed framework.

5.4.1.1 Transient stability prediction

In this module, the stability status of each fault scenario is predicted. First, using (11.5)-(13.5), the stability status of each scenario is investigated in an offline fashion. The terminal voltage of generators, including one pre-fault data and 10 post-fault cycles (PFCs) as inputs and the stability status of the power network (0 or 1) as output are fed into the machine learning engine for training. For both test systems, 80% of the generated dataset is randomly selected for training the machine learning models, and the remaining 20% is used to test the performance of the framework. The accuracies of the transient stability prediction module for each line are presented in table 5-1.

Table 5-1. Number of unstable cases and accuracy of transient stability prediction module for all MMSs in IEEE 9-bus system

MMS	Number of unstable Cases	Prediction accuracy
{5-4}	361/2000 (18.05%)	99.16%
{5-7}	875/2000 (43.75%)	99.48%
{7-8}	302/2000 (15.1%)	98.84%
{8-9}	484/2000 (24.2%)	99.05%
{9-6}	467/2000 (23.35%)	98.76%
{4-6}	469/2000 (23.45%)	99.11%

5.4.1.2 Critical generator prediction

In this part, the critical generator patterns are extracted for each MMS in an offline process to train the machine learning model. The critical generator patterns for each MMS of the IEEE 9-bus test system are demonstrated in figure 5-9. Next, using the input data (i.e., the pre-fault and post-fault voltage values) and the output data (i.e., the critical generators patterns), the critical generators can be predicted using the CBRDE-LM classifier. The accuracy of critical generator prediction module for all lines are shown in table 5-2.

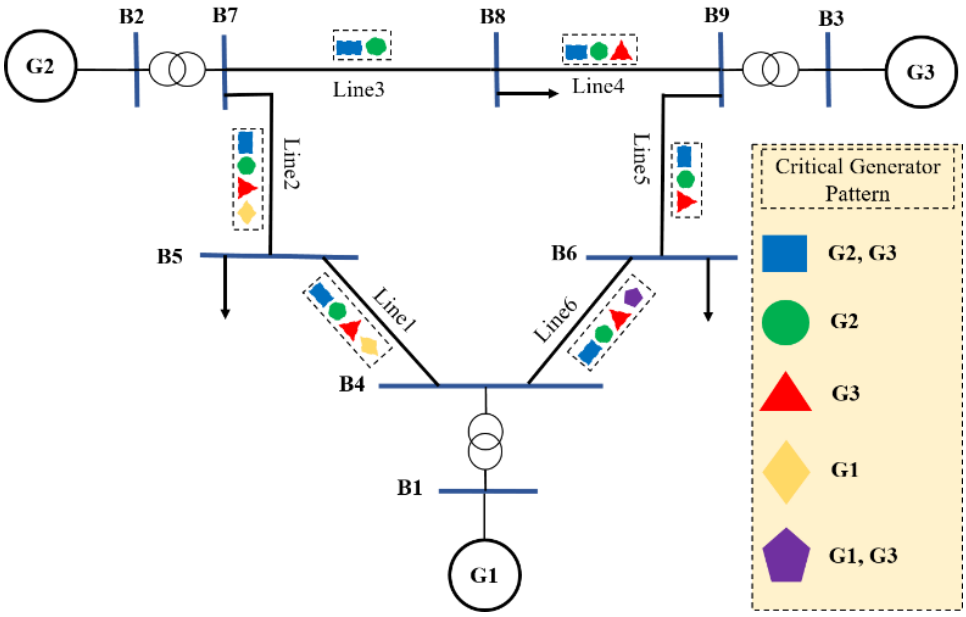

Figure 5-9. Schematic of single line diagram of IEEE 9-bus system along with critical generator patterns for each MMS

Table 5-2. Accuracy of critical generator prediction module for all MMSs in IEEE 9-bus system

MMS	Number of critical generator patterns	Prediction accuracy	Average accuracy using MMS strategy	Accuracy without using MMS strategy
{5-4}	4	96.39%	96.77%	94.89%
{5-7}	4	97.06%		
{7-8}	2	97.22%		
{8-9}	3	96.87%		
{9-6}	3	96.68%		
{4-6}	4	96.44%		

According to table 5-2, the average accuracy of critical generator prediction modules using the micro model strategy is approximately 2% higher than the prediction accuracy of previous methods (i.e., the methods predict critical generators using the whole dataset of the system in one prediction module). To make this comparison, the same dataset has been used (i.e., 12000 scenarios). The classifier is trained using pre-fault and post-fault voltage values of generator terminals as inputs and 5 patterns of critical generators as targets). This comparison shows the effectiveness of the micro model strategy.

5.4.1.3 Generator shedding prediction

As it is mentioned, the patterns of generator rejection for all critical generators are identified using the heuristic optimization in the offline stage. Using the generated dataset depends on the critical generator patterns for each MMS, two/three classifiers are trained for each MMS and predict the amount of generator shedding for each critical generator. The prediction accuracy of the generator rejection prediction module for the IEEE 9-bus system is shown in table 5-3.

Table 5-3. Accuracy of generator shedding prediction module for each MMS in IEEE 9-bus system

MMS	**Accuracy of generator rejection prediction**			**Average accuracy of generator shedding prediction**
	G1	**G2**	**G3**	
{5-4}	89.11%	93.27%	94.66%	92.34%
{5-7}	91.85%	94.38%	94.07%	93.44%
{7-8}	-	95.23%	94.62%	94.92%
{8-9}	-	93.79%	94.16%	93.97%
{9-6}	-	93.18%	95.06%	94.12%
{4-6}	90.57%	94.3%	94.68%	93.18%

5.4.1.4 Comparing the performance of the proposed framework with the existing methods

As discussed, the previous methods can be categorized into two groups. In this part, a comprehensive comparison is performed to show the effectiveness of the proposed framework. A 3-phase fault is applied on MMS3 (i.e. {7-8}) at t=5 s and is cleared after 297 ms. The stability prediction module predicts the stability status of this scenario as unstable. The rotor angle instability for this scenario can be seen in figure 5-10. (a). First, the proposed optimization is run,

and the amount of necessary generator shedding is calculated 15.87 MW in this case. Also, the amount of generation shedding is calculated based on approximation (i.e., $\delta_u = \delta_{u'}$), and the calculated amount is 26.81 MW using the existing energy function-based methods. First, generator shedding is applied based on the previous energy function-based method, which uses an approximation to calculate the generator rejection quickly. Since these methods (based on estimation), trip the generators based on the sequence of out of step or energy index, the calculated amount is tipped from generator 3, (i.e., 4 units of G3 which is equal to 32 MW). Therefore, four units of G3 are tripped at t=5.72 s. As shown in figure 5-10. (b), these methods are fast enough to effectively stabilize the network. However, the amount of generator shedding is more than the required amount. Based on another approach, generator shedding is performed by running an optimization model with a computational time of about 500 ms. The optimal RCA decision is to trip one unit of G2. If this amount is tripped immediately, the system become stable. The optimal generator shedding is applied at t=6.197 s. The rotor angles of the generator after applying the calculated generator shedding are shown in figure 5-10. (c). since the generator rejection is applied relatively late, the system loses the synchronism. Finally, the proposed framework predicts that one unit of G2 and one unit of G3 (equal to 24.8 MW) need to be tripped to stabilize the network. The predicted generator rejection is applied at t=5.72 s and the rotor angles of generators are shown in figure 5-10. (d). Although the predicted amount of generator shedding is a bit more than optimize amount, it can stabilize the network, and it is more cost effective compare to the estimation method. This case study shows the effectiveness of the proposed framework. Although the generator rejection based on estimation can stabilize the network, it tripped around 9 MW more than the proposed framework. Figure 5-10. (b) and figure 5-10. (d) show the importance of choosing the right candidate generators for generator shedding. The obtained bus voltages are also illustrated in figure 5-11, for different generator shedding strategies.

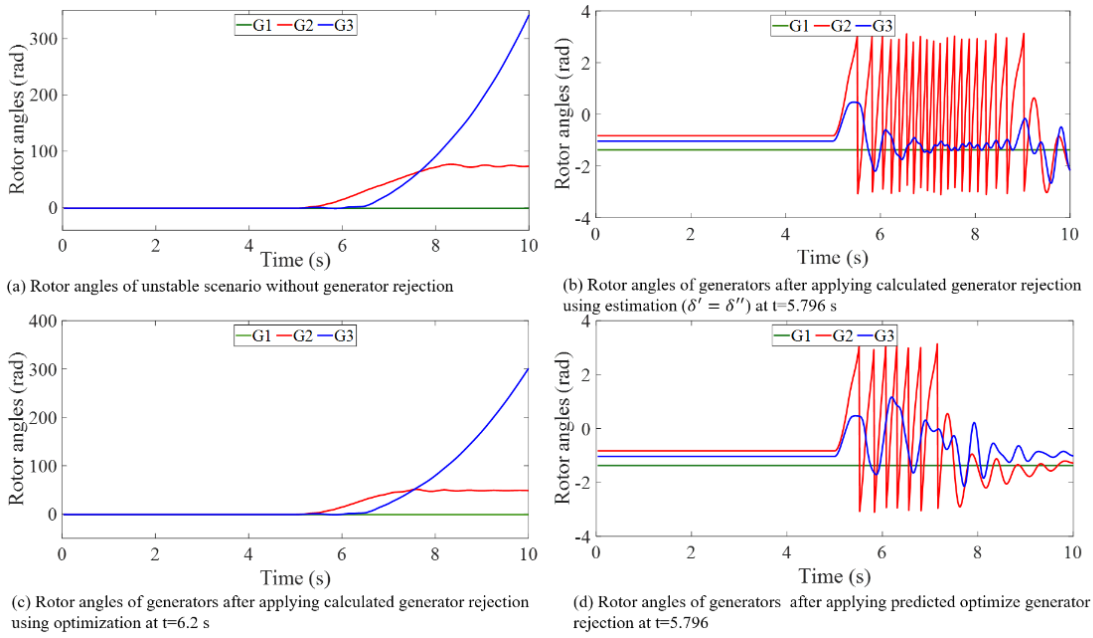

(a) Rotor angles of unstable scenario without generator rejection

(b) Rotor angles of generators after applying calculated generator rejection using estimation ($\delta' = \delta''$) at t=5.796 s

(c) Rotor angles of generators after applying calculated generator rejection using optimization at t=6.2 s

(d) Rotor angles of generators after applying predicted optimize generator rejection at t=5.796

Figure 5-10. The rotor angles of generators after applying different generator rejection strategies for a specific case study in the IEEE 9-bus system

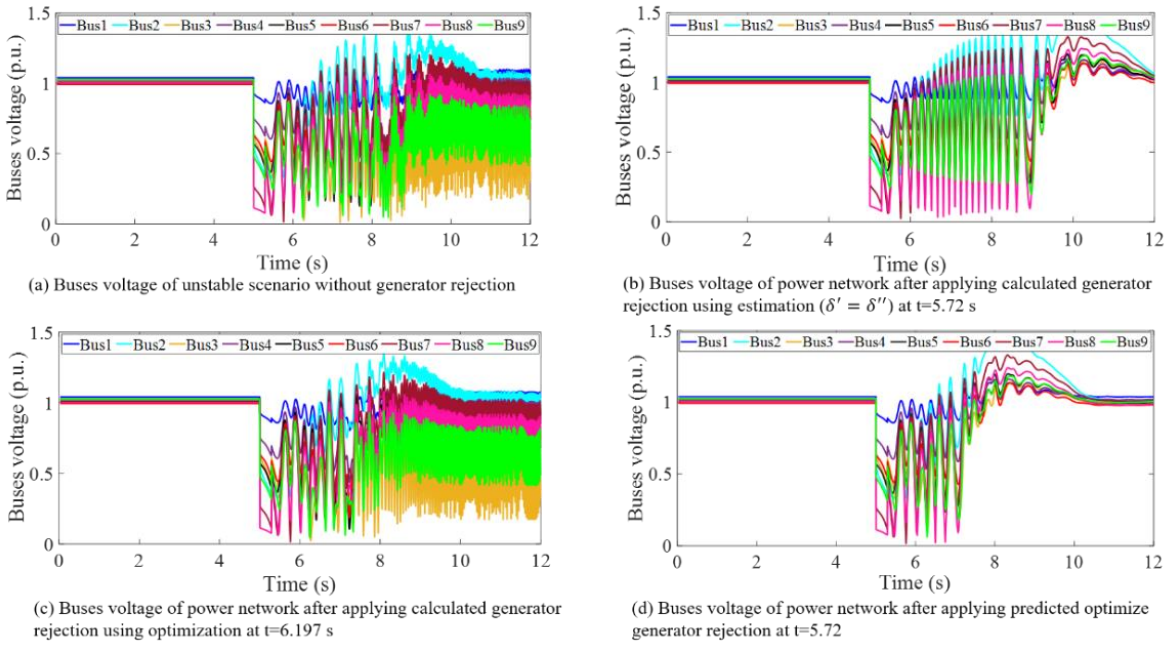

(a) Buses voltage of unstable scenario without generator rejection

(b) Buses voltage of power network after applying calculated generator rejection using estimation ($\delta' = \delta''$) at t=5.72 s

(c) Buses voltage of power network after applying calculated generator rejection using optimization at t=6.197 s

(d) Buses voltage of power network after applying predicted optimize generator rejection at t=5.72

Figure 5-11. Voltage magnitudes after applying different generator rejection strategies for a specific case study in the IEEE 9-bus system

In addition, the summary of comparing different generator rejection methods and their performance is illustrated in the following table.

Table 5-4. Comparison of the proposed framework and existing methods for a random unstable scenario in the IEEE 9-bus system

Generator rejection strategy	**Execution time**		**Amount of generator shedding**		**Location of generator shedding**	**Stability of the network**
	Considering communication delays	**practicality**	$\sum_{i=1}^{N_{CM}} \Delta P_{G_i}^{trip}$	**practicality**		
Estimation	~ 450 ms	✓	34 MW	X	G3	stable
Optimization	~ 1-2 s	X	16.3	✓	G2	unstable
Proposed framework	~ 450 ms	✓	24.8 MW	✓	G2, G3	stable

5.4.2 Case2: 74-bus Nordic power system

To generalize the proposed methodology, the proposed framework is tested using the Nordic test system. As it is mentioned previously, the Nordic test system has 37 MMSs. According to the defined criteria (N^{CGP}) MMSs are categorized into three classes: 1) neutral, 2) non-critical, and 3) critical. The Nordic has 12 neutral MMS (i.e., there is no need to design RCA for these MMSs, because they do not have any unstable cases), and these MMSs are colored green in the diagram. In addition, 7 non-critical MMSs are exist in this test system (i.e., MMSs that have only one pattern for critical generators), and these MMSs are indicated using red color in the single line diagram. The remaining MMSs are critical and have at least 2 patterns for critical generators. These MMS are shown using blue color in the diagram. To cover credible number of scenarios, 6000 scenarios are generated for each MMS in the Nordic power system. The single-line diagram of the Nordic power system is depicted in figure 5-12. Also, four MMSs including two critical (i.e., {69-70, 69-70*} and {55-57. 55-57*}) and two non-critical (i.e., {59-54} and {46-45, 46-45*}) MMSs are indicated in the figure with circle. All three modules are implemented for those MMSs completely.

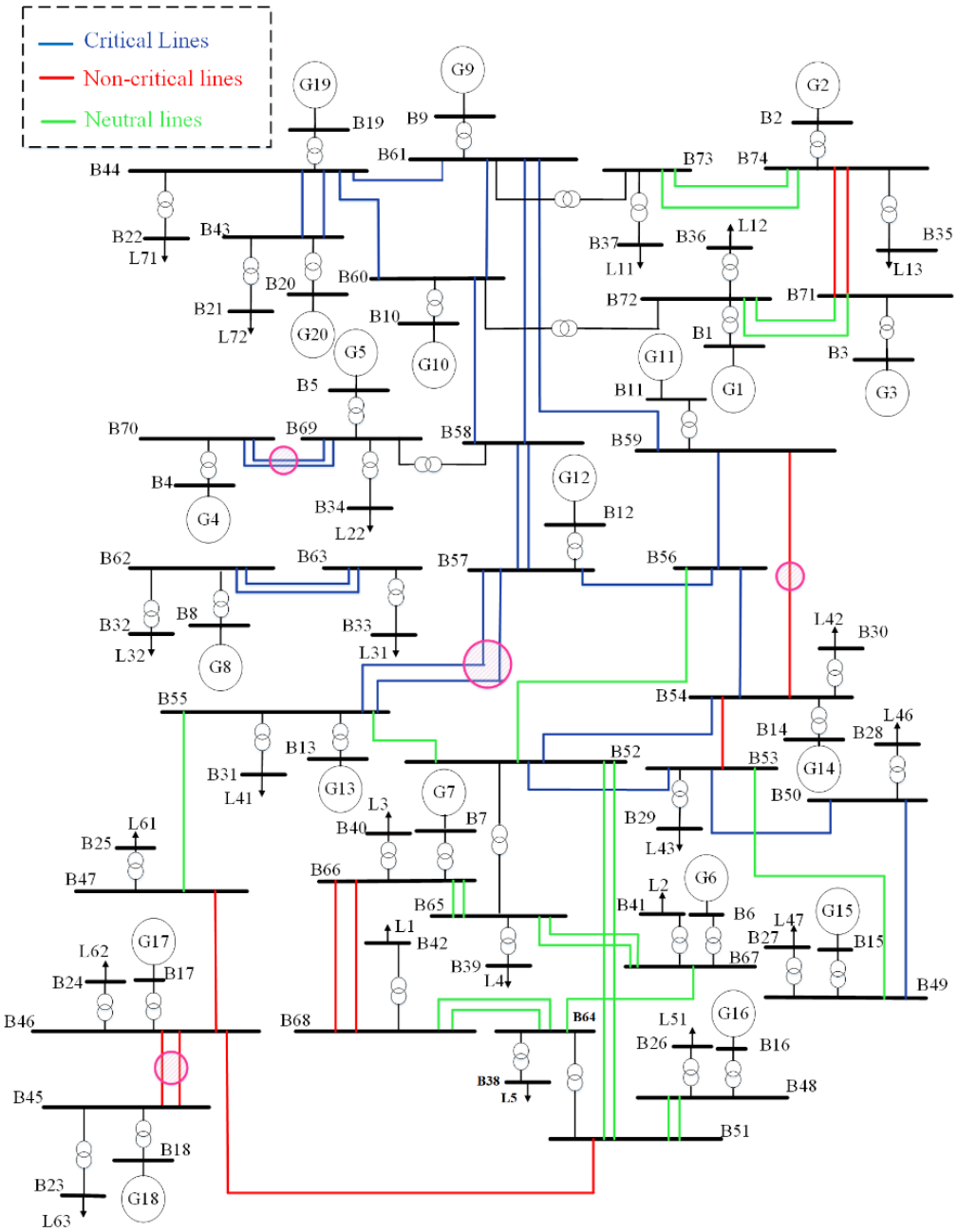

Figure 5-12. Single line diagram of the Nordic test system

According to the micro model strategy, the transient stability prediction module is run for all MMSs. The percentage of unstable cases for each MMS and the accuracy of the stability prediction module are shown in the following table.

Table 5-5. The percentage of unstable cases and average accuracy of transient stability prediction module for individual MMSs in Nordic test system

MMS	Percentage of unstable cases	Accuracy of transient stability prediction module
{43-44, 43-44*}	1.96%	98.96 %
{46-45, 46-45*}	16.24%	99.49 %
{46-47}	5.45%	99.01 %
{50-49}	0.98%	98.85 %
{51-46}	1.54%	98.88 %
{48-51, 48-51*}	0	100 %
{51-52, 51-52*}	0	100 %
{49-53}	0	100 %
{50-53}	2.74%	99.01 %
{53-52}	11.63%	99.15 %
{54-52}	3.18%	99.02 %
{53-54}	1.48%	98.9 %
{47-55}	0	100 %
{52-55}	0	100 %
{56-52}	0	100 %
{54-56}	2.39%	99.12 %
{55-57, 55-57*}	8.76%	99.25 %
{56-57}	32.98%	99.49 %
{58-57, 58-57}	14.19%	99.25 %
{54-59}	2.88%	99.06 %
{56-59}	2.25%	99.21 %
{44-60}	0.6%	98.69 %
{58-60}	3.11%	99.03 %
{44-61}	1.32%	98.98 %
{61-58}	3.41%	99.23 %
{59-61}	1.93%	99.13 %
{60-61}	29.53%	99.04 %
{63-62, 63-62*}	24.13%	99.27 %
{66-65, 66-65*}	0	100 %

{64-67}	0	100 %
{65-67, 65-67*}	0	100 %
{64-68, 64-68*}	0	100 %
{66-68, 66-68*}	1.47%	99.06 %
{69-70, 69-70*}	2.81%	99.22 %
{74-71, 74-71*}	0.78%	98.85 %
{72-71, 72-71*}	0	100 %
{74-73, 74-73*}	0	100 %

Next, the critical generator patterns are extracted for each micro model. In the following table, the critical generator patterns and the accuracy of the critical generator prediction module are illustrated for each MMS.

Table 5-6. Critical generator patterns and accuracy of critical generator prediction module for all MMSs in Nordic test system

MMS	N^{CGP}	**Set of critical generators**	**Critical generator Prediction**
{43-44, 43-44*}	11	G4, G6-G8, G11-G18	94.57 %
		G4	
		G4-G8, G11-G18	
		G4, G6-G8, G11, G13-G18	
		G4, G6-G8, G12-G18	
		G6-G8, G11-G18	
		G4, G8	
		G4, G8, G12	
		G6-G8, G11, G13-G18	
		G6-G8, G12-G18	
		G8	
{46-45, 46-45*}	1	G17, G18	100%
{46-47}	1	G17, G18	100%
{50-49}	4	G17, G18	95.84
		G6	

		G6-G8, G11-G18	
		G4, G6-G8, G11-G18	
{51-46}	1	G17, G18	100%
{48-51, 48-51*}	-	-	-
{51-52, 51-52*}	-	-	-
{49-53}	-	-	-
{50-53}	3	G6, G17-G18	95.31 %
		G6-G8, G12-G18	
		G6	
{53-52}	10	G6-G8, G11-G18	94.17 %
		G6	
		G6, G8, G12-G18	
		G6, G11-G18	
		G6-G8, G13-G18	
		G6-G8, G16-G18	
		G6-G8, G11, G13-G18	
		G6, G8	
		G4, G6-G8, G11-G18	
		G4	
{54-52}	8	G6-G8, G12-G18	94.31 %
		G4	
		G6, G17-G18	
		G6-G8, G11-G18	
		G8	
		G6	
		G17-G18	
		G4, G6	
{53-54}	1	G6-G8, G11-G18	100%
{47-55}	-	-	-
{52-55}	-	-	-
{56-52}	-	-	-
{54-56}	2	G8	96.54 %

		G6-G8, G11-G18	
{55-57, 55-57*}	8	G8	94.23 %
		G6-G8, G11-G18	
		G6-G8, G13-G18	
		G8, G12	
		G4, G8	
		G4-G8, G11-G18	
		G6-G8, G11, G13-G18	
		G4, G8, G12	
{56-57}	11	G6-G8, G11-G18	94.78 %
		G8	
		G6-G8, G12-G18	
		G8, G12	
		G4, G8, G12	
		G4, G6-G8, G11-G18	
		G4, G8	
		G4-G8, G11-G18	
		G4, G6-G8, G12-G18	
		G6-G8, G11, G13-G18	
		G4	
{58-57, 58-57*}	17	G6-G8, G11-G18	93.84 %
		G8	
		G4	
		G4, G5	
		G6, G7, G11-G18	
		G4, G6-G8, G13-G18	
		G4, G6-G7, G13-G18	
		G6-G8, G13-G18	
		G6-G8, G11, G13-G18	
		G6, G7, G11, G13-G18	
		G4, G6, G7, G11-G18	
		G4-G8, G11-G18	
		G4-G8, G12-G18	

		G6, G7, G12-G18	
		G6-G8, G12-G18	
		G8, G12	
		G4, G6-G8, G11-G18	
{54-59}	1	G11	100%
{56-59}	4	G11	94.96 %
		G6-G8, G11, G13-G18	
		G6-G8, G11-G18	
		G8	
{44-60}	6	G6-G8, G11-G18	94.72 %
		G6-G8, G12-G18	
		G6-G8, G11, G13-G18	
		G6-G8, G13-G18	
		G4, G6-G8, G11-G18	
		G6, G7, G11, G13-G18	
{58-60}	16	G6-G8, G11-G18	93.73 %
		G4, G6-G8, G11-G18	
		G6-G8, G13-G18	
		G4	
		G6-G8, G12-G18	
		G6-G8, G11, G13-G18	
		G4, G6-G8, G11, G13-G18	
		G6-G7, G11, G13-G18	
		G4, G6-G8, G13-G18	
		G6-G7, G13-G18	
		G4-G8, G11-G18	
		G6, G7, G11-G18	
		G4, G6, G7, G13-G18	
		G4-G8, G11, G13-G18	
		G6, G7, G12-G18	
		G6-G8, G14-G18	
{44-61}	9	G6-G8, G11-G18	95.41 %
		G4, G6-G8, G11-G18	

		G8	
		G6-G8, G13-G18	
		G6, G7, G13-G18	
		G6-G8, G13-G18	
		G6, G7, G12-G18	
		G6-G8, G11-G18	
		G4, G6-G8, G11-G18	
{61-58}	14	G6-G8, G11-G18	93.96 %
		G4, G6-G8, G13-G18	
		G6-G8, G11, G14-G18	
		G6, G7, G11-G18	
		G6-G8, G12-G18	
		G4, G6-G8, G12-G18	
		G6-G8, G11, G13-G18	
		G4	
		G6-G8, G13-G18	
		G6, G7, G11, G13-G18	
		G6, G7, G13-G18	
		G6, G7, G12-G18	
		G4, G6-G8, G11-G18	
		G4, G6, G7, G12-G18	
{59-61}	10	G6-G8, G11-G18	94.75 %
		G4-G8, G11-G18	
		G6, G7, G13-G18	
		G6, G7, G12-G18	
		G4, G6-G8, G12-G18	
		G6-G8, G11, G12-G18	
		G6-G8, G14-G18	
		G6-G8, G12-G18	
		G6-G8, G13-G18	
		G4, G6-G8, G11-G18	
{60-61}	16	G6-G8, G11-G18	93.82 %
		G1-G18	

		G4-G8, G11-G18	
		G4, G6-G8, G11-G18	
		G6-G8, G12-G18	
		G6-G8, G11, G13-G18	
		G4, G6-G8, G12-G18	
		G6-G8, G13-G18	
		G6, G7, G13-G18	
		G6, G7, G11, G13-G18	
		G8	
		G6, G7, G11-G18	
		G5-G8, G11-G18	
		G4, G6-G8, G13-G18	
		G4, G6-G8, G11, G13-G18	
		G6, G7, G12- G18	
{62-63, 62-63*}	2	G8 G6-G8, G11-G18	95.48 %
{66-65, 66-65*}	-	-	-
{64-67}	-	-	-
{65-67, 65-67*}	-	-	-
{64-68, 64-68*}	-	-	-
{66-68, 66-68*}	1	G6-G8, G11-G18	100%
{69-70, 69-70*}	2	G4 G6-G8, G11-G18	95.38 %
{74-71, 74-71*}	1	G6-G8, G11-G18	100%
{72-71, 72-71*}	-	-	-
{74-73, 74-73*}	-	-	-

Ac can be seen in the above table, there are 31 unique critical generator patterns for the Nordic power network. To show the effectiveness of the micro model strategy for the whole network using the entire dataset and these patterns, a CBRDE-LM is trained and tested. The obtained prediction accuracy is 93.22%. In addition, the average accuracy of the proposed framework for the Nordic system is 97.42%, considering the micro model strategy.

Since solving the optimization problem is time-consuming, two critical MMSs (69-70, 69-70*} and {55-57. 55-57*}), and two non-critical MMSs ({59-54} and {46-45, 46-45*}) are randomly selected to implement generator shedding prediction module and evaluate the effectiveness of the proposed framework. For all unstable scenarios related to the chosen MMSs, the heuristic optimization run and the number of generation units that need to be switched off are extracted for each critical generator. Then for each critical generator, a classifier is trained, and the number of generation units for generation tripping is predicted. The accuracy of the prediction module for each critical generator related to the evaluated MMSs are illustrated in the following table.

Table 5-7. Accuracies of different classifiers for each critical generator related to selected MMS in Nordic power system

MMS	**CGP**	**Accuracy of generator rejection prediction (%)**											
		G4	G6	G7	G8	G11	G12	G13	G14	G15	G16	G17	G18
{59-54}	G11	-	-	-	-	96.7	-	-	-	-	-	-	-
{46-45, 46-45*}	G17, G18	-	-	-	-	-	-	-	-	-	-	94.8	95.6
{69-70, 69-70*}	G4	97.3	-	-	-	-	-	-	-	-	-	-	-
	G6-G8, G11-G18	-	91.7	100	94.1	93.2	90.3	100	100	100	100	93.7	93.3
{55-57, 55-57*}	G8	-	-	-	96.2	-	-	-	-	-	-	-	-
	G6-G8, G11-G18	-	92.5	100	93.8	94.2	89.7	100	100	100	100	94.4	94.7
	G6-G8, G13-G18	-	91.9	100	93.5	-	-	100	100	100	100	96.1	95.3
	G8, G12	-	-	-	94.5	-	92.3	-	-	-	-	-	-
	G4, G8	96.8	-	-	93.3	-	-	-	-	-	-	-	-
	G4-G8, G11-G18	96.5	90.9	98.3	93.7	94.4	91.2	100	100	100	100	95.0	95.4
	G6-G8, G11, G13-G18	-	93.3	100	93.5	95.2	-	100	100	100	100	96.2	94.9
	G4, G8, G12	97.6	-	-	94.4	-	92.6	-	-	-	-	-	-

In the above table the accuracies of designed classifiers for each critical generator are illustrated. The average accuracy of generator shedding prediction module for each evaluated MMS are calculated and it is shown in table 5-8

Table 5-8. Average accuracy of generator shedding prediction module for four selected MMSs in Nordic test system

MMS	**Accuracy of generator shedding prediction module (%)**
{59-54}	96.7 %
{46-45, 46-45*}	95.2 %
{69-70, 69-70*}	96.67 %
{55-57, 55-57*}	95.85 %

5.5 Conclusion

In this chapter, a new framework has been proposed to predict generator shedding to prevent the transient instability. To reduce the complexity of the problem and increase the prediction accuracy, the presented framework is implemented for each set of the micro model (MMS) independently. This framework consists of three main modules including transient stability, critical generators, and generator shedding prediction. The last modules predict the number of units for each critical generator that needs to be switched off. All three modules have been tested using the IEEE 9-bus system and 74-bus Nordic power network. The simulation results and comparisons show the effectiveness of the proposed framework.

6 CONCLUSIONS AND FUTURE WORKS

6.1 Conclusions

This project intends to develop a comprehensive framework to predict appropriate remedial control actions for power systems to prevent cascading outages and blackouts following a large disturbance. The following paragraphs provide a chapter-wise summary of this project.

Chapter 1 introduces the importance of transient instability and blackout prevention. In addition, the application of WAMS and PMUs in power system control and monitoring is expressed. Also, communication delays related to the WAMS system and their impact on the effectiveness of the RCA are introduced. The drawbacks of previous remedial control actions are pointed out. Finally, the contributions of the proposed framework are highlighted.

A literature review is conducted on transient stability assessment in chapter 2. In addition, different power system states and the proper control action in each state are discussed. Also, a comprehensive literature review is performed on remedial control actions. The advantage and disadvantages of previous remedial control actions, including controlled islanding, generator shedding, load shedding, fast valving, and dynamic braking resistor, are assessed in detail.

In Chapter 3, the data generation process is explained. Also, the micro model strategy which is one of the main contributions of this thesis is discussed in this chapter. The proposed micro model strategy reduces the complexity of the remedial control action prediction problem and increases the prediction accuracies of the proposed framework modules. In addition, the dataset is built for every individual micro model for all three test systems.

Two novel RCA prediction schemes including controlled islanding plus load shedding and generator rejection are developed in chapters 4 and 5, respectively. Both the proposed schemes use a machine learning method called CBRDE-LM to perform predictions in different modules. The employed neural network optimizes the number of hidden layers and number of neurons for each problem. Also, the LM backpropagation is used for fine-tuning.

A combination of controlled islanding and load shedding is implemented as RCA in the first scheme. The proposed framework comprises three main modules including transient stability, coherency, and RCA prediction. A novel algorithm is proposed in the coherency prediction module to minimize the number of islands and reduce the restoration process cost. The proposed coherency identification method and micro model strategy significantly enhance the coherency prediction

module. In addition, the proposed framework is tested using the IEEE 39-bus test system and the 74-bus Nordic test system as a larger test case. The obtained results are shown the effectiveness of the proposed framework. As it is shown in the simulation results, the for quick instabilities, the previous methods are not able to stabilize the network. However, the proposed framework has the potential to prevent blackout with high accuracy. Moreover, the robustness of the framework is tested using noisy measurement data from PMU, and it shows promising results.

The second framework is composed of three modules including transient stability, critical generator, and generator shedding prediction. The framework is designed based on the micro model strategy. Compared with the existing methods, the obtained accuracies of the three modules are improved using the micro model strategy. To calculate the accurate amount of generator rejection, a heuristic optimization, considering the full dynamic model of the power network, is performed offline to minimize the generator shedding and maximize the stability margin. The patterns for generator shedding are extracted using offline calculations. Finally, the dataset is fed to the CBRDE-LM classifier to predict the optimal generator shedding quickly. The presented framework is tested on the IEEE 9-bus and Nordic test systems.

To sum it up, the previous RCA schemes are designed based on running optimization models and performing calculations online. However, due to the fast dynamics of rotor angle oscillations and considering communication latencies, there is limited time to compute RCA. This makes online RCA calculation impractical in events quickly evolving into transient instability. Therefore, RCA prediction is proposed to address this problem. Three main RCAs, including controlled islanding, load shedding, and generator tripping are modeled in this study.

6.2 Future works

According to the research carried out, the following research directions are recommended for future investigation:

1) Considering the rapid growth of renewable energy resources in modern power systems, the RCA prediction scheme needs to be studied in the presence of these resources.

2) Other RCAs, such as fast valving and dynamic braking resistors, or a combination of RCAs could be investigated.

3) Future work can also be planned to improve the accuracy of the stability prediction module (particularly for stable cases). Deep learning and reinforcement learning-based prediction methods can also be investigated to enhance prediction accuracy.

4) Different types of generators (e.g., hydro plants, thermal plants, DGs, etc.) and load clusters need to be accurately modeled in the RCA prediction scheme design.

REFERENCES

[1] R. Yousefian and S. Kamalasadan, “A review of neural network based machine learning approaches for rotor angle stability control,” ArXiv Prepr. ArXiv170101214, 2017.

[2] P. Crossley, F. Ilar, and D. Karlsson, “System protection schemes in power networks: existing installations and ideas for future development,” in 2001 Seventh International Conference on Developments in Power System Protection (IEE), 2001, pp. 450–453.

[3] P. Kundur et al., “Definition and classification of power system stability IEEE/CIGRE joint task force on stability terms and definitions,” IEEE Trans. Power Syst., vol. 19, no. 3, pp. 1387–1401, 2004.

[4] P. Kundur, “Power system stability,” Power Syst. Stab. Control, vol. 10, 2007.

[5] M. C. Passaro, A. P. A. da Silva, and A. C. Lima, “Preventive control stability via neural network sensitivity,” IEEE Trans. Power Syst., vol. 29, no. 6, pp. 2846–2853, 2014.

[6] H. Guo, C. Zheng, H. H.-C. Iu, and T. Fernando, “A critical review of cascading failure analysis and modeling of power system,” Renew. Sustain. Energy Rev., vol. 80, pp. 9–22, 2017.

[7] D. Wu et al., “An open-source model for simulation and corrective measure assessment of the 2021 Texas power outage,” ArXiv Prepr. ArXiv210404146, 2021.

[8] ENTSO-E, “Report on blackout in Turkey on 31st march 2015,” Proj. Group Turk., 2015.

[9] M. Bynum, A. Castillo, J.-P. Watson, and C. D. Laird, “Tightening McCormick relaxations toward global solution of the ACOPF problem,” IEEE Trans. Power Syst., vol. 34, no. 1, pp. 814–817, 2018.

[10] A. Atputharajah and T. K. Saha, “Power system blackouts-literature review,” in 2009 International Conference on Industrial and Information Systems (ICIIS), 2009, pp. 460–465.

[11] G. B. Anderson and M. L. Bell, “Lights out: impact of the August 2003 power outage on mortality in New York, NY,” Epidemiol. Camb. Mass, vol. 23, no. 2, p. 189, 2012.

[12] M. Vaiman et al., “Risk assessment of cascading outages: Methodologies and challenges,” IEEE Trans. Power Syst., vol. 27, no. 2, p. 631, 2012.

[13] F. R. Gomez, A. D. Rajapakse, U. D. Annakkage, and I. T. Fernando, “Support vector machine-based algorithm for post-fault transient stability status prediction using synchronized measurements,” IEEE Trans. Power Syst., vol. 26, no. 3, pp. 1474–1483, 2010.

[14] M. E. Aboul-Ela, A. A. Sallam, J. D. McCalley, and A. A. Fouad, “Damping controller design for power system oscillations using global signals,” IEEE Trans. Power Syst., vol. 11, no. 2, pp. 767–773, 1996.

[15] J. J. Sanchez-Gasca, N. W. Miller, A. Kurita, and S. Horiuchi, “Multivariable control for damping interarea oscillations in power systems,” IEEE Control Syst. Mag., vol. 9, no. 1, pp. 28–32, 1989.

[16] I. Kamwa, R. Grondin, and Y. Hébert, “Wide-area measurement based stabilizing control of large power systems-a decentralized/hierarchical approach,” IEEE Trans. Power Syst., vol. 16, no. 1, pp. 136–153, 2001.

[17] V. Centeno, J. De La Ree, A. G. Phadke, G. Michel, R. J. Murphy, and R. O. Burnett, “Adaptive out-of-step relaying using phasor measurement techniques,” IEEE Comput. Appl. Power, vol. 6, no. 4, pp. 12–17, 1993.

[18] D. M. Laverty, D. J. Morrow, A. McKinley, and M. Cregan, “OpenPMU: Open source platform for Synchrophasor applications and research,” in 2011 IEEE Power and Energy Society General Meeting, 2011, pp. 1–6.

[19] M. Shahraeini, M. H. Javidi, and Z. Haq, “Wide area measurement systems,” Adv. Top. Meas., pp. 303–322, 2012.

[20] F. Edition, “The Automation, Systems, and Instrumentation Dictionary,” 2003.

[21] M. Mokhtari, F. Aminifar, D. Nazarpour, and S. Golshannavaz, “Wide-area power oscillation damping with a fuzzy controller compensating the continuous communication delays,” IEEE Trans. Power Syst., vol. 28, no. 2, pp. 1997–2005, 2012.

[22] H. Hosseini, S. Naderi, and S. Afsharnia, “New approach to transient stability prediction of power systems in wide area measurement systems based on multiple-criteria decision making theory,” IET Gener. Transm. Distrib., vol. 13, no. 21, pp. 4960–4967, 2019.

[23] T. Minakawa, “The required technological breakthrough in developing universal emergency control systems in terms with transient and dynamic stability,” in 2000 IEEE Power Engineering Society Winter Meeting. Conference Proceedings (Cat. No. 00CH37077), 2000, vol. 1, pp. 66–71.

[24] S. M. Mazhari, N. Safari, C. Y. Chung, and I. Kamwa, “A quantile regression-based approach for online probabilistic prediction of unstable groups of coherent generators in power systems,” IEEE Trans. Power Syst., vol. 34, no. 3, pp. 2240–2250, 2018.

[25] V. Vittal, J. D. McCalley, P. M. Anderson, and A. A. Fouad, Power system control and stability. John Wiley & Sons, 2019.

[26] M. Pavella, D. Ernst, and D. Ruiz-Vega, Transient stability of power systems: a unified approach to assessment and control, vol. 581. Springer Science & Business Media, 2000.

[27] M. A. Pai, Energy function analysis for power system stability. Springer Science & Business Media, 2012.

[28] A. H. El-Abiad and K. Nagappan, "Transient stability regions of multimachine power systems," IEEE Trans. Power Appar. Syst., no. 2, pp. 169–179, 1966.

[29] H.-D. Chiang, F. F. Wu, and P. P. Varaiya, "Foundations of the potential energy boundary surface method for power system transient stability analysis," IEEE Trans. Circuits Syst., vol. 35, no. 6, pp. 712–728, 1988.

[30] T. Athay, R. Podmore, and S. Virmani, "A practical method for the direct analysis of transient stability," IEEE Trans. Power Appar. Syst., no. 2, pp. 573–584, 1979.

[31] H.-D. Chiang, F. F. Wu, and P. P. Varaiya, "A BCU method for direct analysis of power system transient stability," IEEE Trans. Power Syst., vol. 9, no. 3, pp. 1194–1208, 1994.

[32] H.-D. Chiang, Direct methods for stability analysis of electric power systems: theoretical foundation, BCU methodologies, and applications. John Wiley & Sons, 2011.

[33] G. A. Maria, C. Tang, and J. Kim, "Hybrid transient stability analysis (power systems)," IEEE Trans. Power Syst., vol. 5, no. 2, pp. 384–393, 1990.

[34] Y. Wu, M. Musavi, and P. Lerley, "Synchrophasor-based monitoring of critical generator buses for transient stability," IEEE Trans. Power Syst., vol. 31, no. 1, pp. 287–295, 2015.

[35] S. Zhang, Z. Zhu, and Y. Li, "A critical review of data-driven transient stability assessment of power systems: principles, prospects and challenges," Energies, vol. 14, no. 21, p. 7238, 2021.

[36] D. J. Sobajic and Y.-H. Pao, "Artificial neural-net based dynamic security assessment for electric power systems," IEEE Trans. Power Syst., vol. 4, no. 1, pp. 220–228, 1989.

[37] M. Vaughan, R. Schloss, S. Manson, S. Raghupathula, and T. Maier, "Idaho power RAS: A dynamic remedial action case study," 2010.

[38] V. Madani et al., "IEEE PSRC report on global industry experiences with system integrity protection schemes (SIPS)," IEEE Trans. Power Deliv., vol. 25, no. 4, pp. 2143–2155, 2010.

[39] J. Q. James, D. J. Hill, A. Y. Lam, J. Gu, and V. O. Li, “Intelligent time-adaptive transient stability assessment system,” IEEE Trans. Power Syst., vol. 33, no. 1, pp. 1049–1058, 2017.

[40] Z. Shi et al., “Convolutional neural network-based power system transient stability assessment and instability mode prediction,” Appl. Energy, vol. 263, p. 114586, 2020.

[41] J. Huang, L. Guan, Y. Su, H. Yao, M. Guo, and Z. Zhong, “Recurrent graph convolutional network-based multi-task transient stability assessment framework in power system,” IEEE Access, vol. 8, pp. 93283–93296, 2020.

[42] P. W. Sauer, M. A. Pai, and J. H. Chow, Power system dynamics and stability: with synchrophasor measurement and power system toolbox. John Wiley & Sons, 2017.

[43] C.-W. Hsu and C.-J. Lin, “A comparison of methods for multiclass support vector machines,” IEEE Trans. Neural Netw., vol. 13, no. 2, pp. 415–425, 2002.

[44] B. Wang, B. Fang, Y. Wang, H. Liu, and Y. Liu, “Power system transient stability assessment based on big data and the core vector machine,” IEEE Trans. Smart Grid, vol. 7, no. 5, pp. 2561–2570, 2016.

[45] Q. Wang, C. Pang, and H. Alnami, “Transient stability assessment of a power system using multi-layer SVM method,” in 2021 IEEE Texas Power and Energy Conference (TPEC), 2021, pp. 1–5.

[46] T. Amraee and S. Ranjbar, “Transient instability prediction using decision tree technique,” IEEE Trans. Power Syst., vol. 28, no. 3, pp. 3028–3037, 2013.

[47] N. Senroy, G. T. Heydt, and V. Vittal, “Decision tree assisted controlled islanding,” IEEE Trans. Power Syst., vol. 21, no. 4, pp. 1790–1797, 2006.

[48] Y. Chen, S. M. Mazhari, C. Y. Chung, S. O. Faried, B. Wang, and B. Hu, “Power system on-line transient stability prediction by margin indices and random forests,” in 2019 IEEE Electrical Power and Energy Conference (EPEC), 2019, pp. 1–6.

[49] P. Sarajcev, A. Kunac, G. Petrovic, and M. Despalatovic, “Power system transient stability assessment using stacked autoencoder and voting ensemble,” Energies, vol. 14, no. 11, p. 3148, 2021.

[50] M. He, J. Zhang, and V. Vittal, “Robust online dynamic security assessment using adaptive ensemble decision-tree learning,” IEEE Trans. Power Syst., vol. 28, no. 4, pp. 4089–4098, 2013.

[51] M. Sun, I. Konstantelos, and G. Strbac, “A deep learning-based feature extraction framework for system security assessment,” IEEE Trans. Smart Grid, vol. 10, no. 5, pp. 5007–5020, 2018.

[52] S. K. Azman, Y. J. Isbeih, M. S. El Moursi, and K. Elbassioni, “A unified online deep learning prediction model for small signal and transient stability,” IEEE Trans. Power Syst., vol. 35, no. 6, pp. 4585–4598, 2020.

[53] M. Zhang, J. Li, Y. Li, and R. Xu, “Deep learning for short-term voltage stability assessment of power systems,” IEEE Access, vol. 9, pp. 29711–29718, 2021.

[54] A. Gholami, T. Shekari, M. H. Amirioun, F. Aminifar, M. H. Amini, and A. Sargolzaei, “Toward a consensus on the definition and taxonomy of power system resilience,” IEEE Access, vol. 6, pp. 32035–32053, 2018.

[55] Z. Wang, X. Song, H. Xin, D. Gan, and K. P. Wong, “Risk-based coordination of generation rescheduling and load shedding for transient stability enhancement,” IEEE Trans. Power Syst., vol. 28, no. 4, pp. 4674–4682, 2013.

[56] S. Balaraman and N. Kamaraj, “Cascade BPN based transmission line overload prediction and preventive action by generation rescheduling,” Neurocomputing, vol. 94, pp. 1–12, 2012.

[57] P. Demetriou, M. Asprou, and E. Kyriakides, “A real-time controlled islanding and restoration scheme based on estimated states,” IEEE Trans. Power Syst., vol. 34, no. 1, pp. 606–615, 2018.

[58] B. Hoseinzadeh and C. L. Bak, “Centralized coordination of emergency control and protection system using online outage sensitivity index,” Electr. Power Syst. Res., vol. 163, pp. 413–422, 2018.

[59] S. Das and B. K. Panigrahi, “Prediction and control of transient stability using system integrity protection schemes,” IET Gener. Transm. Distrib., vol. 13, no. 8, pp. 1247–1254, 2019.

[60] N. K. Rajalwal and D. Ghosh, “Recent trends in integrity protection of power system: A literature review,” Int. Trans. Electr. Energy Syst., vol. 30, no. 10, p. e12523, 2020.

[61] Y. Zhang, M. E. Raoufat, and K. Tomsovic, “Remedial action schemes and defense systems,” Smart Grid Handb., pp. 1–10, 2016.

[62] F. R. G. Lezama, Prediction and Control of Transient Instability Using Wide Area Phasor Measurements. University of Manitoba (Canada), 2012.

[63] F. B. Prioste, P. P. C. Mendes, and C. Ferreira, “Power system transient stability enhancement by fast valving,” in 2004 IEEE/PES Transmision and Distribution Conference and Exposition: Latin America (IEEE Cat. No. 04EX956), 2004, pp. 639–644.

[64] R. Patel, T. S. Bhatti, and D. P. Kothari, “A modified approach to transient stability enhancement with fast valving and braking resistor applications,” Int. J. Electr. Power Energy Syst., vol. 28, no. 10, pp. 729–738, 2006.

[65] D.-H. Yoon, G. Jang, and Y.-H. Moon, “A study of the application of fast valving and braking resistor for an intelligent SPS,” Int. J. Electr. Power Energy Syst., vol. 53, pp. 818–823, 2013.

[66] R. Patel, T. S. Bhatti, and D. P. Kothari, “Improvement of power system transient stability by coordinated operation of fast valving and braking resistor,” IEE Proc.-Gener. Transm. Distrib., vol. 150, no. 3, pp. 311–316, 2003.

[67] D. Min et al., “Computing safety margins of a generation rejection scheme: A framework for online implementation,” IEEE Trans. Smart Grid, vol. 9, no. 3, pp. 2337–2346, 2016.

[68] I. R. Pordanjani, H. A. Abyaneh, S. H. Sadeghi, and K. Mazlumi, “Risk reduction in special protection systems by using an online method for transient instability prediction,” Int. J. Electr. Power Energy Syst., vol. 32, no. 2, pp. 156–162, 2010.

[69] A. A. Hajnorouzi, F. Aminifar, and H. A. Shayanfar, “Generation rejection scheme based on a combinational rotor angle trajectory prediction,” Sci. Iran., vol. 28, no. Special issue on collective behavior of nonlinear dynamical networks, pp. 1579–1591, 2021.

[70] Y.-J. Wang, C.-W. Liu, and Y.-H. Liu, “A PMU based special protection scheme: a case study of Taiwan power system,” Int. J. Electr. Power Energy Syst., vol. 27, no. 3, pp. 215–223, 2005.

[71] D.-H. Choi, S. H. Lee, Y. C. Kang, and J.-W. Park, “Analysis on special protection scheme of Korea electric power system by fully utilizing statcom in a generation side,” IEEE Trans. Power Syst., vol. 32, no. 3, pp. 1882–1890, 2016.

[72] J. Gou, Y. Liu, J. Liu, G. A. Taylor, and M. M. Alamuti, “Novel pair-wise relative energy function for transient stability analysis and real-time emergency control” IET Gener. Transm. Distrib., vol. 11, no. 18, pp. 4565–4575, 2017.

[73] S. Yang, Z. Hao, B. Zhang, and M. Hojo, “An accurate and fast start-up scheme for power system real-time emergency control,” IEEE Trans. Power Syst., vol. 34, no. 5, pp. 3562–3572, 2019.

[74] S. Robak, J. Machowski, M. M. Skwarski, and A. Smolarczyk, “Transient stability improvement by generator tripping and real-time instability prediction based on local measurements,” IEEE Access, vol. 9, pp. 130519–130528, 2021.

[75] T. Weckesser, H. Jóhannsson, and J. Østergaard, “Critical machine cluster identification using the equal area criterion,” in 2015 IEEE Power & Energy Society General Meeting, 2015, pp. 1–5.

[76] Y. Xue and M. Pavella, “Extended equal-area criterion: an analytical ultra-fast method for transient stability assessment and preventive control of power systems,” Int. J. Electr. Power Energy Syst., vol. 11, no. 2, pp. 131–149, 1989.

[77] G. Gan, Z. Zhu, G. Geng, and Q. Jiang, “An efficient parallel sequential approach for transient stability emergency control of large-scale power system,” IEEE Trans. Power Syst., vol. 33, no. 6, pp. 5854–5864, 2018.

[78] Q. Jiang, Y. Wang, and G. Geng, “A parallel reduced-space interior point method with orthogonal collocation for first-swing stability constrained emergency control,” IEEE Trans. Power Syst., vol. 29, no. 1, pp. 84–92, 2013.

[79] Z. Li, G. Yao, G. Geng, and Q. Jiang, “An efficient optimal control method for open-loop transient stability emergency control,” IEEE Trans. Power Syst., vol. 32, no. 4, pp. 2704–2713, 2016.

[80] J. A. Laghari, H. Mokhlis, A. H. A. Bakar, and H. Mohamad, “Application of computational intelligence techniques for load shedding in power systems: A review,” Energy Convers. Manag., vol. 75, pp. 130–140, 2013.

[81] J. López, Y.-C. Hsiao, T.-Y. Hsiao, and C.-N. Lu, “Adaptive system protection scheme using generalized pattern search,” in 2015 18th International Conference on Intelligent System Application to Power Systems (ISAP), 2015, pp. 1–6.

[82] H. Atighechi, P. Hu, S. Ebrahimi, J. Lu, G. Wang, and L. Wang, “An effective load shedding remedial action scheme considering wind farms generation,” Int. J. Electr. Power Energy Syst., vol. 95, pp. 353–363, 2018.

[83] M. G. Darebaghi and T. Amraee, “Dynamic multi-stage under frequency load shedding considering uncertainty of generation loss,” IET Gener. Transm. Distrib., vol. 11, no. 13, pp. 3202–3209, 2017.

[84] J. Liu, Y. Zhang, K. Meng, Z. Y. Dong, Y. Xu, and S. Han, “Real-time emergency load shedding for power system transient stability control: A risk-averse deep learning method,” Appl. Energy, vol. 307, p. 118221, 2022.

[85] T. Kyriakidis, R. Cherkaoui, and M. Kayal, “Generator coherency identification algorithm using modal and time-domain information,” in Eurocon 2013, 2013, pp. 1025–1032.

[86] J. H. Chow, R. Galarza, P. Accari, and W. W. Price, “Inertial and slow coherency aggregation algorithms for power system dynamic model reduction,” IEEE Trans. Power Syst., vol. 10, no. 2, pp. 680–685, 1995.

[87] J. H. Chow, J. Cullum, and R. A. Willoughby, “A sparsity-based technique for identifying slow-coherent areas in large power systems,” IEEE Trans. Power Appar. Syst., no. 3, pp. 463–473, 1984.

[88] K. K. Anaparthi, B. Chaudhuri, N. F. Thornhill, and B. C. Pal, “Coherency identification in power systems through principal component analysis,” IEEE Trans. Power Syst., vol. 20, no. 3, pp. 1658–1660, 2005.

[89] R. Agrawal and D. Thukaram, “Support vector clustering-based direct coherency identification of generators in a multi-machine power system,” IET Gener. Transm. Distrib., vol. 7, no. 12, pp. 1357–1366, 2013.

[90] P. N. Papadopoulos, T. Guo, and J. V. Milanović, “Probabilistic framework for online identification of dynamic behavior of power systems with renewable generation,” IEEE Trans. Power Syst., vol. 33, no. 1, pp. 45–54, 2017.

[91] T. Guo and J. V. Milanović, “Online identification of power system dynamic signature using PMU measurements and data mining,” IEEE Trans. Power Syst., vol. 31, no. 3, pp. 1760–1768, 2015.

[92] S. A. Siddiqui, K. Verma, K. R. Niazi, and M. Fozdar, “Real-time monitoring of post-fault scenario for determining generator coherency and transient stability through ANN,” IEEE Trans. Ind. Appl., vol. 54, no. 1, pp. 685–692, 2017.

[93] A. Kyriacou, P. Demetriou, C. Panayiotou, and E. Kyriakides, “Controlled islanding solution for large-scale power systems,” IEEE Trans. Power Syst., vol. 33, no. 2, pp. 1591–1602, 2017.

[94] Y. Liu and Y. Liu, “Aspects on power system islanding for preventing widespread blackout,” in 2006 IEEE International Conference on Networking, Sensing and Control, 2006, pp. 1090–1095.

[95] K. Sun, D.-Z. Zheng, and Q. Lu, “Splitting strategies for islanding operation of large-scale power systems using OBDD-based methods,” IEEE Trans. Power Syst., vol. 18, no. 2, pp. 912–923, 2003.

[96] L. Ding, F. M. Gonzalez-Longatt, P. Wall, and V. Terzija, “Two-step spectral clustering controlled islanding algorithm,” IEEE Trans. Power Syst., vol. 28, no. 1, pp. 75–84, 2012.

[97] K. Sun, D.-Z. Zheng, and Q. Lu, “A simulation study of OBDD-based proper splitting strategies for power systems under consideration of transient stability,” IEEE Trans. Power Syst., vol. 20, no. 1, pp. 389–399, 2005.

[98] P. A. Trodden, W. A. Bukhsh, A. Grothey, and K. I. M. McKinnon, “MILP formulation for controlled islanding of power networks,” Int. J. Electr. Power Energy Syst., vol. 45, no. 1, pp. 501–508, 2013.

[99] T. Ding, K. Sun, C. Huang, Z. Bie, and F. Li, “Mixed-integer linear programming-based splitting strategies for power system islanding operation considering network connectivity,” IEEE Syst. J., vol. 12, no. 1, pp. 350–359, 2015.

[100] P. A. Trodden, W. A. Bukhsh, A. Grothey, and K. I. McKinnon, “Optimization-based islanding of power networks using piecewise linear AC power flow,” IEEE Trans. Power Syst., vol. 29, no. 3, pp. 1212–1220, 2013.

[101] F. Teymouri, T. Amraee, H. Saberi, and F. Capitanescu, “Toward controlled islanding for enhancing power grid resilience considering frequency stability constraints,” IEEE Trans. Smart Grid, vol. 10, no. 2, pp. 1735–1746, 2017.

[102] T. Amraee and H. Saberi, “Controlled islanding using transmission switching and load shedding for enhancing power grid resilience,” Int. J. Electr. Power Energy Syst., vol. 91, pp. 135–143, 2017.

[103] S. Kamali, T. Amraee, and F. Capitanescu, “Controlled network splitting considering transient stability constraints,” IET Gener. Transm. Distrib., vol. 12, no. 21, pp. 5639–5648, 2018.

[104] L. Zhang, H. Li, and X.-G. Kong, “Evolving feedforward artificial neural networks using a two-stage approach,” Neurocomputing, vol. 360, pp. 25–36, 2019.

[105] J. J. Moré, “The Levenberg-Marquardt algorithm: implementation and theory,” in Numerical analysis, Springer, 1978, pp. 105–116.

[106] S. M. Mazhari, N. Safari, C. Y. Chung, and I. Kamwa, “A hybrid fault cluster and thévenin equivalent based framework for rotor angle stability prediction,” IEEE Trans. Power Syst., vol. 33, no. 5, pp. 5594–5603, 2018.

[107] D. B. Johnson, “A note on Dijkstra’s shortest path algorithm,” J. ACM JACM, vol. 20, no. 3, pp. 385–388, 1973.

APPENDIX I: TEST SYSTEMS DATA

The dynamic data of generators, excitation systems, line data for different test systems are represented in the following tables.

IEEE 9-bus system:

Table A.1. Dynamic model data of generators in IEEE 9-bus test system

Generator parameters	**G1**	**G2**	**G3**
MVA(base)	200	100	100
$\boldsymbol{Td_0'}$	3.73	0.8	0.806
$\boldsymbol{Td_0''}$	0.05	0.05	0.05
$\boldsymbol{Tq_0'}$	0	0.12	0.12
$\boldsymbol{Tq_0''}$	0.05	0.05	0.05
H	9.55	4.165	2.765
D	0	0	0
$\boldsymbol{X_d}$	0.36	1.72	1.68
$\boldsymbol{X_q}$	0.24	1.66	1.61
$\boldsymbol{X_d{}'}$	0.15	0.23	0.23
$\boldsymbol{X_q{}'}$	0	0.378	0.32
$\boldsymbol{X_d{}''}$	0.1	0.2	0.2
$\boldsymbol{X_q{}''}$	0.1	0.2	0.2
$\boldsymbol{X_l}$	0.083	0.141	0.94

Table A.2. Dynamic model data of excitation system in IEEE 9-bus test system

AVR Parameters	**G1**	**G2**	**G3**
type	IEEE DC1	IEEE DC1	IEEE DC1
Tr	0.06	0.001	0.06
Ka	0.001	400.	0.001
Ta	0.2	0.05	0.2
Tb	0.01	0.01	0.01
Tc	0	0.	0.

Te	0.5	0.95	0.5
Kf	0.085	0.04	0.085
Tf1	0.35	1.	0.35
E1	3.66	3.66	3.66
Se1	0.03	0.03	0.03
E2	4.89	4.89	4.89
Se2	0.1	0.1	0.1
Ke	-0.044	-0.17	-0.044
Vrmin	-1	-3.	-1.
Vrmax	1	0.001	1.

Table A.3. Transmission lines data of IEEE 9-bus system

Transmission lines parameter		**X (pu/m)**	**R (pu/m)**	**B (pu/m)**
From Bus	**To Bus**			
5	4	0.068	0.01	0.176
7	5	0.092	0.017	0.158
7	8	0.161	0.032	0.306
8	9	0.1738	0.039	0.358
9	6	0.0576	0.0085	0.149
6	4	0.1008	0.0119	0.209

IEEE 39-bus system

Table A.4. Dynamic model data of generators in IEEE 39-bus test system

Generator parameters	**G1**	**G2**	**G3**	**G4**	**G5**	**G6**	**G7**	**G8**	**G9**	**G10**
MVA base	200	100	200	200	100	200	200	200	200	2000
T'do	10.2	6.56	5.7	5.69	5.4	7.3	5.66	6.7	4.79	7
T''do	0.05	0.05	0.05	0.05	0.05	0.05	0.05	0.05	0.05	0.05
T'qo	1.5	1.5	1.5	1.5	0.44	0.4	1.5	0.41	1.96	0.7

T"q0	0.035	0.035	0.035	0.035	0.035	0.035	0.035	0.035	0.035	0.035
H	21	30.3	17.9	14.3	26	17.4	13.2	12.15	17.25	25
D	0	0	0	0	0	0	0	0	0	0
Xd	0.2	0.295	0.499	0.524	0.67	0.508	0.59	0.58	0.4212	0.4
Xq	0.138	0.282	0.474	0.516	0.62	0.482	0.584	0.56	0.41	0.38
X'd	0.062	0.069	0.106	0.0872	0.132	0.1	0.098	0.114	0.114	0.12
X'q	0.06	0.17	0.175	0.332	0.166	0.1628	0.372	0.1822	0.1174	0.16
X"d	0.05	0.05	0.09	0.07	0.089	0.08	0.088	0.09	0.09	0.08
X"q	0.05	0.05	0.09	0.07	0.089	0.08	0.088	0.09	0.09	0.08
X_l	0.025	0.035	0.060	0.059	0.054	0.0448	0.0644	0.056	0.0596	0.06

Table A.5. Dynamic model data of excitation system in IEEE 9-bus test system

AVR Parameters	**G1**	**G2**	**G3**	**G4**	**G5**	**G6**	**G7**	**G8**	**G9**	**G10**
Type	IEEE X1									
TR	0.01	0.01	0.01	0.01	0.01	0.01	0.01	0.01	0.01	0.01
KA	5	6.2	5	5	40	5	40	5	40	5
TA	0.06	0.05	0.06	0.06	0.02	0.02	0.02	0.02	0.02	0.02
TB	0	0	0	0	0	0	0	0	0	0
TC	0	0	0	0	0	0	0	0	0	0
VRMAX	5	5.2	5	5	10	5	6.5	5	10.5	10.5
VRMIN	-5	-5	-5	-5	-10	-5	-6.5	-5	-10.5	-10.5
KE	-0.05	-0.05	-0.02	-0.05	1	-0.04	1	-0.05	1	1
TE	0.25	0.41	0.5	0.5	0.785	0.471	0.73	0.528	1.4	1.4
KF	0.04	0.06	0.08	0.08	0.03	0.08	0.03	0.09	0.03	0.03
TF1	1	0.5	1	1	1	1.25	1	1.26	1	1
Switch	0	0	0	0	0	0	0	0	0	0
E1	1.7	3	3	3	3	3	3	3	3	3
SE(E1)	0.5	0.66	0.13	0.08	0.03	0.08	0.03	0.09	0.03	0.03
E2	3	4	4	4	4	4	4	4	4	4
SE(E2)	2	0.88	0.34	0.31	0.91	0.25	0.74	0.28	0.85	0.85

Table A.6. Transmission lines parameters in IEEE 39-bus test system

Transmission line parameters		**R**	**X**	**B**
From bus	To bus			
1	2	0.0035	0.0411	0.6987
1	39	0.0010	0.0250	0.7500
2	3	0.0013	0.0151	0.2572
2	25	0.0070	0.0086	0.1460
3	4	0.0013	0.0213	0.2214
3	18	0.0011	0.0133	0.2138
4	5	0.0008	0.0128	0.1342
4	14	0.0008	0.0129	0.1382
5	6	0.0002	0.0026	0.0434
5	8	0.0008	0.0112	0.1476
6	7	0.0006	0.0092	0.1130
6	11	0.0007	0.0082	0.1389
7	8	0.0004	0.0046	0.0780
8	9	0.0023	0.0363	0.3804
9	39	0.0010	0.0250	1.2000
10	11	0.0004	0.0043	0.0729
10	13	0.0004	0.0043	0.0729
13	14	0.0009	0.0101	0.1723
14	15	0.0018	0.0217	0.3660
15	16	0.0009	0.0094	0.1710
16	17	0.0007	0.0089	0.1342
16	19	0.0016	0.0195	0.3040
16	21	0.0008	0.0135	0.2548
16	24	0.0003	0.0059	0.0680
17	18	0.0007	0.0082	0.1319
17	27	0.0013	0.0173	0.3216
21	22	0.0008	0.0140	0.2565
22	23	0.0006	0.0096	0.1846
23	24	0.0022	0.0350	0.3610
25	26	0.0032	0.0323	0.5130

26	27	0.0014	0.0147	0.2396
26	28	0.0043	0.0474	0.7802
26	29	0.0057	0.0625	1.0290
28	29	0.0014	0.0151	0.2490

74-bus Nordic power system

Table A. 7. Dynamic model data of generators in 74-bus Nordic test system

Generator parameters	X_l	Td_0'	Td_0''	Tq_0'	Tq_0''	**H**	Xd	Xq	$X'd$	$X'q$	$X''d$	$X''q$
G1	0.15	5	0.05	0	0.1	3	1.1	0.7	0.25	0	0.2	0.2
G2	0.15	5	0.05	0	0.1	3	1.1	0.7	0.25	0	0.2	0.2
G3	0.15	5	0.05	0	0.1	3	1.1	0.7	0.25	0	0.2	0.2
G4	0.15	5	0.05	0	0.1	3	1.1	0.7	0.25	0	0.2	0.2
G5	0.15	5	0.05	0	0.1	3	1.1	0.7	0.25	0	0.2	0.2
G6	0.15	7	0.05	1.5	0.05	6	2.2	2	0.3	0.4	0.2	0.2
G7	0.15	7	0.05	1.5	0.05	6	2.2	2	0.3	0.4	0.2	0.2
G8	0.15	5	0.05	0	0.1	3	1.1	0.7	0.25	0	0.2	0.2
G9	0.15	5	0.05	0	0.1	3	1.1	0.7	0.25	0	0.2	0.2
G10	0.15	5	0.05	0	0.1	3	1.1	0.7	0.25	0	0.2	0.2
G11	0.15	5	0.05	0	0.1	3	1.1	0.7	0.25	0	0.2	0.2
G12	0.15	5	0.05	0	0.1	3	1.1	0.7	0.25	0	0.2	0.2
G13	0.15	7	0.05	0	0.1	2	1.55	1	0.3	0	0.2	0.2
G14	0.15	7	0.05	1.5	0.05	6	2.2	2	0.3	0.4	0.2	0.2
G15	0.15	7	0.05	1.5	0.05	6	2.2	2	0.3	0.4	0.2	0.2
G16	0.15	7	0.05	1.5	0.05	6	2.2	2	0.3	0.4	0.2	0.2
G17	0.15	7	0.05	1.5	0.05	6	2.2	2	0.3	0.4	0.2	0.2
G18	0.15	7	0.05	1.5	0.05	6	2.2	2	0.3	0.4	0.2	0.2
G19	0.15	5	0.05	0	0.1	3	1.1	0.7	0.25	0	0.2	0.2
G20	0.15	5	0.05	0	0.1	3	1.1	0.7	0.25	0	0.2	0.2

Table A.8. Dynamic model data of excitation system in Nordic test system

	ifdlim	**Ta**	**Tb**	**G**	**Kp**	**Tw**	**T1**	**T2**	**PSS_act**	**C**	**L1**	**L2**
G1	1.8991	10	20	70	75	15	0.2	0.01	1	0.1	-11	4
G2	1.8991	10	20	70	75	15	0.2	0.01	1	0.1	-11	4
G3	1.8991	10	20	70	75	15	0.2	0.01	1	0.1	-11	4
G4	1.8991	10	20	70	75	15	0.2	0.01	1	0.1	-11	4
G5	1.8991	10	20	70	75	15	0.2	0.01	1	0.1	-11	4
G6	3.062	5	12.5	120	75	15	0.22	0.012	1	0.1	-20	5
G7	3.062	5	12.5	120	75	15	0.22	0.012	1	0.1	-20	5
G8	1.8991	10	20	70	75	15	0.2	0.01	1	0.1	-11	4
G9	1.8991	10	20	70	75	15	0.2	0.01	1	0.1	-11	4
G10	1.8991	10	20	70	75	15	0.2	0.01	1	0.1	-11	4
G11	1.8991	10	20	70	75	15	0.2	0.01	1	0.1	-20	4
G12	1.8991	10	20	70	75	15	0.2	0.01	1	0.1	-20	4
G13	2.9579	4	20	50	-	-	-	-	-	-	-17	4
G14	3.062	5	12.5	120	75	15	0.22	0.012	1	0.1	-18	5
G15	3.062	5	12.5	120	75	15	0.22	0.012	1	0.1	-18	5
G16	3.062	5	12.5	120	75	15	0.22	0.012	1	0.1	-18	5
G17	3.062	5	12.5	120	75	15	0.22	0.012	1	0.1	-18	5
G18	3.062	5	12.5	120	75	15	0.22	0.012	1	0.1	-18	5
G19	1.8991	10	20	70	-	-	-	-	-	-	-11	4
G20	1.8991	10	20	70	-	-	-	-	-	-	-11	4

APPENDIX II: PUBLICATIONS AND PERMISSION TO REPRODUCE

List of publications

[1] S. Naderi, M. Javadi, M. Mazhari and C. Y. Chung, "A Machine Learning-Based Framework for Fast Prediction of Wide-Area Remedial Control Actions in Interconnected Power Systems," in *IEEE Transactions on Power Systems*, doi: 10.1109/TPWRS.2022.3165210.

[2] S. Naderi, M. Javadi, M. Mazhari and C. Y. Chung, "Data-driven approach for generator shedding prediction to prevent transient instability in power system using wide-area measurements," under preparation to be submitted to IEEE Access journal

Copyright permission letters from Co-Authors

To Whom It May Concern:

I, Chi Yung Chung, hereby grant permission to Mr. Soheil Naderi to include the following papers in his thesis titled “Machine learning-based framework for remedial control action prediction using wide-area measurements in interconnected power systems”.

[1] S. Naderi, M. Javadi, M. Mazhari and **C. Y. Chung**, "A Machine Learning-Based Framework for Fast Prediction of Wide-Area Remedial Control Actions in Interconnected Power Systems," in *IEEE Transactions on Power Systems*, doi: 10.1109/TPWRS.2022.3165210.

[2] S. Naderi, M. Javadi, M. Mazhari and **C. Y. Chung**, " Data-driven approach for generator shedding prediction to prevent transient instability in power system using wide-area measurements," under preparation to be submitted to IEEE Access.

I am aware that all University of Saskatchewan theses are also posted in the digital USask e-Commons thesis repository, making the thesis openly available on the internet.

Date:

Signature:

To Whom It May Concern:

I, Seyed Mahdi Mazhari, hereby grant permission to Mr. Soheil Naderi to include the following papers in his thesis titled “Machine learning-based framework for remedial control action prediction using wide-area measurements in interconnected power systems”.

[1] S. Naderi, M. Javadi, **M. Mazhari** and C. Y. Chung, "A Machine Learning-Based Framework for Fast Prediction of Wide-Area Remedial Control Actions in Interconnected Power Systems," in *IEEE Transactions on Power Systems*, doi: 10.1109/TPWRS.2022.3165210.

[2] S. Naderi, M. Javadi, **M. Mazhari** and C. Y. Chung, " Data-driven approach for generator shedding prediction to prevent transient instability in power system using wide-area measurements," under preparation to be submitted to IEEE Access.

I am aware that all University of Saskatchewan theses are also posted in the digital USask e-Commons thesis repository, making the thesis openly available on the internet.

Date:

Signature:

To Whom It May Concern:

I, Masoud Javadi, hereby grant permission to Mr. Soheil Naderi to include the following papers in his thesis titled “Machine learning-based framework for remedial control action prediction using wide-area measurements in interconnected power systems”.

[1] S. Naderi, **M. Javadi**, M. Mazhari and C. Y. Chung, "A Machine Learning-Based Framework for Fast Prediction of Wide-Area Remedial Control Actions in Interconnected Power Systems," in *IEEE Transactions on Power Systems*, doi: 10.1109/TPWRS.2022.3165210.

[2] S. Naderi, **M. Javadi**, M. Mazhari and C. Y. Chung, " Data-driven approach for generator shedding prediction to prevent transient instability in power system using wide-area measurements," under preparation to be submitted to IEEE Access.

I am aware that all University of Saskatchewan theses are also posted in the digital USask e-Commons thesis repository, making the thesis openly available on the internet.

Date:

Signature: